EPA-600/4-76-016d
May 1976

Environmental Monitoring Series

CONTINUED RESEARCH IN MESOSCALE AIR POLLUTION SIMULATION MODELING: Volume IV - Examination of the Feasibility of Modeling Photochemical Aerosol Dynamics

Environmental Sciences Research Laboratory
Office of Research and Development
U.S. Environmental Protection Agency
Research Triangle Park, North Carolina 27711

EPA 600/4-76-016 D
May 1976

CONTINUED RESEARCH IN MESOSCALE AIR POLLUTION SIMULATION MODELING: VOLUME IV - EXAMINATION OF THE FEASIBILITY OF MODELING PHOTOCHEMICAL AEROSOL DYNAMICS

by

T. N. Jerskey
J. H. Seinfeld

Systems Applications, Incorporated
950 Northgate Drive
San Rafael, California 94903

68-02-1237

Project Officer

Kenneth L. Demerjian
Meteorology and Assessment Division
Environmental Sciences Research Laboratory
Research Triangle Park, North Carolina 27711

U.S. ENVIRONMENTAL PROTECTION AGENCY
OFFICE OF RESEARCH AND DEVELOPMENT
ENVIRONMENTAL SCIENCES RESEARCH LABORATORY
RESEARCH TRIANGLE PARK, NORTH CAROLINA 27711

DISCLAIMER

This report has been reviewed by the Office of Research and Development, U.S. Environmental Protection Agency, and approved for publication. Mention of trade names or commercial products does not constitute endorsement or recommendation for use.

CONTENTS

DISCLAIMER ii

LIST OF ILLUSTRATIONS v

LIST OF TABLES vii

I INTRODUCTION 1

II PHYSICAL PROCESSES INFLUENCING THE DYNAMICS OF AEROSOLS IN PHOTOCHEMICAL SMOG 4

A. Sources and Observed Properties of Photochemical Aerosols 4

1. Sources of Aerosols in Los Angeles 4

2. Observations of Photochemical Aerosols 7

3. Summary 13

B. Physical Processes Influencing Aerosol Dynamics 15

1. Homogeneous Nucleation 15

2. Heterogeneous Condensation 20

3. Coagulation 33

4. Turbulent Diffusion 42

5. Gravitational Settling 43

6. Deposition of Particles on Surfaces 45

7. Rainout and Washout of Aerosols 49

C. Summary of Important Physical Processes in the Evolution of Photochemical Aerosols 51

1. Coagulation 54

2. Heterogeneous Condensation 55

3. Turbulent Diffusion 57

4. Gravitational Settling 57

5. Deposition of Particles on Surfaces 58

6. Washout of Aerosols 58

III CHEMICAL PROCESSES INFLUENCING THE FORMATION OF AEROSOLS IN PHOTOCHEMICAL SMOG 60

A. The Chemical Composition of the Los Angeles Aerosol . . 60

1. The Spatial Distribution of Sulfate and Nitrate . . 61

2. The Diurnal Patterns of Sulfate and Nitrate 63

3. The Sulfur, Nitrogen, and Carbon Composition of the Los Angeles Aerosol 67

4. Summary 70

B. Rates of Conversion of Sulfur, Nitrogen, and Carbon to Aerosol 73

1. Rates of Sulfur Conversion 76

2. Rates of Nitrogen Conversion 80

3. Rates of Carbon Conversion 84

C. Possible Chemical Reactions That Influence the Evolution of Photochemical Aerosols 88

1. Sulfate Formation 88

2. Nitrate Formation 98

3. The Generation of Organic Compounds of Low Volatility 105

4. The Role of Water in Photochemical Aerosols 111

D. Summary 114

IV MATHEMATICAL MODELING OF THE DYNAMIC BEHAVIOR OF PHOTOCHEMICAL AEROSOLS 119

A. The Status of Aerosol Emissions Inventories 119

B. The Basic Equations of an Aerosol Model 122

C. Application of the General Equation to Photochemical Aerosols 128

1. Mean Number Density Distribution Function 129

2. Total Mean Number Density 133

3. Total Mean Aerosol Volume 134

D. Alternative Forms of Aerosol Models 135

E. Summary 140

V RECOMMENDATIONS FOR FUTURE RESEARCH 142

REFERENCES 147

FORM 2220-1 156

ILLUSTRATIONS

1 Comparison of Surface and Volume Distributions for Background and Motor Vehicle Source-Enriched (Near the Harbor Freeway) Sites 9

2 Comparison of the Characteristics of Photochemical and Nonphotochemical Urban Aerosols 12

3 Development of the Volume Distribution with Time in Los Angeles on 3 September 1969 32

4 Collision Frequency Factors β_{BM} for Particles of Size D_{pi} and D_{pj} 37

5 The Normalized Frequency Factors $\beta_{BM_{ij}}/\beta_{BM_{ii}}$ as a Function of Normalized Particle Diameter D_{pj}/D_{pi} 39

6 Comparison of Different Collision Mechanisms in in the Los Angeles Aerosol 41

7 Equation (42) Fitted to the "Grand Average" Data of Blumenthal et al. (1974) 46

8 Deposition Velocity and Terminal Settling Velocity for Flow over Grass. 48

9 The Contribution of Various Sources to the Total Aerosol Mass in the Los Angeles Basin 62

10 Diurnal Variations for Sulfate and Selected Pollutants at West Covina on 23-24 July 1973 65

11 Diurnal Variations for Nitrate, Sulfate, and NO_x at West Covina on 23-24 July 1973 66

12 Diurnal Variations in Size Distributions for Sulfate and Nitrate at West Covina on 23-24 July 1973 68

13 Diurnal Variations in the Ratio of Particle to Gas Phase Sulfur 77

14 Scatter Diagram of the Sulfur Conversion Ratio in Particles Smaller Than 0.5 μm in Diameter and Ozone 81

15 The Sulfur Conversion Ratio as a Function of the Product of Gas Phase Ozone and Nonmethane Hydrocarbon Concentrations 82

16 Diurnal Variations in the Ratio of Particle Phase to Gas Phase Nitrogen ($N_{NO} + N_{NO_2}$) 83

17 Scatter Diagram of the Ratio of Particle to Gas Phase Nitrogen as a Function of Ozone Level 85

18 Hourly Variations of b_{scat}, Organic Distribution Factors (f_c), Ozone, Total Particulate Matter (TP), Gaseous Hydrocarbons (GRH), and Organics 87

19 Pathways for Formation of Nitrate Aerosols 100

20 Extrapolation of the Vapor Pressure of Adipic Acid to the Ambient Temperature 109

21 The Light-Scattering Coefficient as a Function of Liquid Water Content 113

22 Diurnal Patterns of Waterometer Data for Pomona--4-5 October 1972 115

23 Diurnal Patterns of Waterometer Data for Pasadena--9 September 1972 116

24 Diurnal Patterns of Waterometer Data for Pasadena--20 September 1975 117

25 Diagram of the Relationship of the Emissions Inventory to the Total Aerosol Mass 120

TABLES

1 Physical Processes Affecting the Evolution of Aerosol Number Density Distributions 5

2 Source Contributions to Aerosol Samples from Pasadena, California (3 September 1969). 8

3 Comparison of the Physical Properties of Photochemical and Nonphotochemical Aerosols. 11

4 Comparison of Aerosol Samples Taken from Photochemical Smog and Other Urban and Nonurban Aerosols 14

5 Rates of Conversion of Vapor Phase H_2SO_4 Through Heterogeneous and Homogeneous Nucleation 17

6 Parameters Used in Evaluating the Relative Importance of Thermal Effects on Aerosol Growth by Heterogeneous Condensation 26

7 Thermodynamic Data for Calculating the Growth Rates and the Critical Sizes for Growth 33

8 Estimated Rates of Change of Aerosol Number Densities in the Urban Atmosphere. 53

9 ACHEX Data for Nitrate and Sulfate in the South Coast Basin, 1972 to 1973. 64

10 NASN Data for Nitrate and Sulfate in the South Coast Basin for 1968 64

11 Sulfate, Nitrate, and Solvent Extractable Organic Concentrations at Three Sites During 1972. 69

12 High-Volume Sample Concentrations Obtained on 4 October 1972 69

13 A Comparison of Theoretical and Experimental Ammonium Values. 71

14 Secondary Aerosol Organics Identified in the ACHEX 72

15 Pseudo-First-Order Rate Constants for the Los Angeles Basin. . . 79

16 Diurnal Variations of Total Particulates (TP)--in $\mu g\ m^{-3}$-- Organic Carbon Fraction (OCF), and Organic Carbon Distribution Factor (f_C) 86

17 Reactions in the SO_2-NO_x-Air System 91

18 SO_2 Oxidation Reactions in Photochemical Smog 94

19 Chemical Equilibria in the SO_2-NH_3-H_2O-CO_2 System 96

20 Major Homogeneous Reactions Involving Nitric Acid in Photochemical Smog 102

21 Aqueous Reactions of Nitrogen Oxides 104

22 Studies Reporting Aerosol Formation for Different Hydrocarbons upon Reaction with Ozone or Photolysis in the Presence of NO_x. 106

23 Ozone-Olefin Reaction Mechanisms. 110

24 Organic Aerosol Constituents Identified in Smog Chamber Studies. 111

25 Mechanisms for Reactions of Cyclohexane Leading to Difunctional Aliphatic Compounds. 112

26 Sources of Data for an Aerosol Emissions Inventory. 121

27 Significance of the Terms in the General Dynamic Equation [Eq. (67)] 130

28 Levels of Detail in the Representation of an Urban Aerosol Population. 131

29 Functional Dependences of the Mean Number Density Distribution Function 137

I INTRODUCTION

Since photochemical smog consists of both gaseous and particulate air pollutants, a mathematical description of its dynamic behavior should ultimately include both gaseous and particulate components. Such a description is inherently more difficult for atmospheric aerosols than for gaseous air pollutants because the specification of aerosols requires not only their chemical composition, but also their thermodynamic state and size. In addition, because aerosol growth is often linked strongly to gas phase species concentrations by nucleation or heterogeneous condensation processes, knowledge of the dynamic behavior of the gaseous species is generally required as a component of the description of dynamic aerosol behavior.

Although the total mass of particulate pollutants in an urban atmosphere is generally small compared with that of gaseous pollutants, aerosols can, nevertheless, contribute significantly to visibility degradation and health effects. Despite many years of investigation, the origins and evolution of urban air pollution aerosols remain poorly understood in comparison to gaseous pollutants. For this reason, virtually no studies have been published on the mathematical modeling of urban aerosol dynamics.

The objective of our study was to assess the feasibility of developing mathematical models for urban aerosol dynamics. For this analysis, it was necessary to review the current state of understanding of the physical and chemical processes responsible for aerosol properties, since the description of these processes is required for an urban aerosol model. The study focused on aerosols that occur in photochemical air pollution--that is, in the presence of oxides of nitrogen, hydrocarbons, and sulfur dioxide. The mathematical modeling of such aerosols poses perhaps the most comprehensive problem possible associated with urban aerosol behavior, for it

includes all of the major urban pollutants. Thus, the results of a study of the requirements for modeling photochemical smog aerosol can be applied to modeling problems associated with urban aerosols in general.

From the standpoint of air pollution control, a model of aerosol evolution in the atmosphere will relate gaseous and particulate emissions to the properties of the aerosol that are responsible for visibility impairment and health hazards. Laboratory studies have shown that the effect of suspended particulate matter on human health results from a complex process that is not fully understood. Apparently, the particles themselves may cause injury, as well as carrying volatile gases into the human respiratory system, which may also cause injury. The Task Group on Lung Dynamics (1966) reported that the most efficient penetration into the lungs was by particles having diameters less than 1 μm. Landahl (1959) found essentially a 100 percent retention of particles larger than 10 μm in the nose and a substantial retention of particles larger than 2 μm.

Measurements of light scattered by aerosols have shown very high correlation coefficients (∿0.9) with the total volumes of aerosols in the size range $0.1\ \mu m < D_p < 1.0\ \mu m$. Hence, a very good measure of visibility reduction can be derived from a calculation of the mass in this size range (Charlson et al., 1968, 1969; Charlson, 1969; Thielke et al., 1972; Samuels et al., 1973).

In the mathematical modeling of urban aerosol dynamics, the following processes must be considered:

> Emissions
  - Primary particulate (natural and anthropogenic)
  - Gaseous pollutant
  - Background levels of particles
> Aerosol formation and growth
  - Homogeneous nucleation
  - Heterogeneous condensation

- Coagulation
- Heterogeneous chemical reaction

> Atmospheric transport and diffusion
- Advection
- Turbulent and Brownian diffusion
- Settling
- Deposition on surfaces.

Chapters II and III discuss the current understanding of these processes as they pertain to photochemical aerosols. For convenience, we have divided the processes that influence the dynamics of urban aerosols into physical and chemical categories. Physical processes are those that influence the size distribution of the aerosol or its number concentration in a unit volume of air. Chemical processes are those that influence the chemical composition of individual particles. As we demonstrate later, heterogeneous condensation can be classified in either category; we have chosen to include a discussion of that phenomenon with physical processes. In Chapter II, we examine the physical processes--that is, those that result from the diffusional motion of particles, particle collisions, or gas-to-particle conversion. (Of course, a physical process, such as coagulation, may lead to a change in the chemical constituency of the resulting particle.) In Chapter III, we focus on homogeneous and heterogeneous chemical reactions that may influence aerosol behavior. Based on the discussions in Chapters II and III, Chapter IV presents our initial development of mathematical models of photochemical aerosol dynamics and discusses the status of the aerosol emission inventory for Los Angeles and the additional information required to validate the model.

II PHYSICAL PROCESSES INFLUENCING THE DYNAMICS OF AEROSOLS IN PHOTOCHEMICAL SMOG

Whereas the physical processes that can affect the dynamics of gaseous pollutants are limited to those that alter concentrations in a unit volume of air through atmospheric transport, those that influence particle behavior are much more diverse. The objective of this chapter is to identify the physical processes that are potentially important in aerosol dynamics and to assess the actual significance of each process for photochemical aerosols. Table 1 summarizes the physical processes that affect the evolution of the aerosol in a unit volume of atmosphere. Since the importance of each of the physical processes in Table 1 depends strongly on the size range of the aerosol, we must identify the observed sizes of photochemical aerosols before we can assess the significance of each process.

A. SOURCES AND OBSERVED PROPERTIES OF PHOTOCHEMICAL AEROSOLS

Atmospheric and laboratory measurements have both provided information on the size distribution of photochemical aerosols. Much of the atmospheric data were obtained during two major field studies sponsored by the State of California Air Resources Board: the 1969 Pasadena smog experiment (Hidy, 1972) and the 1972 to 1973 Aerosol Characterization Study, which is called ACHEX (Hidy et al., 1975).

1. Sources of Aerosols in Los Angeles

The sources of suspended particulate matter can be natural or anthropogenic, and the aerosol itself can be primary (emitted from sources as particles) or secondary (formed in the atmosphere as particles). Secondary aerosols result when gaseous pollutants (or naturally occurring hydrocarbons)

Table 1

PHYSICAL PROCESSES AFFECTING THE EVOLUTION OF AEROSOL NUMBER DENSITY DISTRIBUTIONS

Process	Definition	Important Features
Homogeneous nucleation of a gaseous species	Agglomeration of molecules to form a stable particle	Particles formed in this way are very small. High concentrations and low vapor pressures are required to initiate homogeneous nucleation.
Heterogeneous condensation	Growth of particles by diffusion of gaseous species to the particle surface followed by absorption or adsorption	The driving force for growth is the difference between the ambient partial pressure and the vapor pressure just above the surface of the particle. Because the vapor pressure over a curved surface is greater than that above a flat surface (the Kelvin effect), there is a critical size--on the order of 0.1μm diameter--below which a particle will not grow by heterogeneous condensation.
Coagulation	The process of collision of two particles to form a single particle	Since it is a second-order process (i.e., its rate is proportional to the square of the local number density), high concentrations are required for appreciable rates. Because large particles (over 1 μm in diameter) generally do not exist in concentrations high enough to produce appreciable rates, coagulation is most important for small particles. Different mechanisms can bring two particles together; the efficiencies of these mechanisms depend on the sizes of the two particles.

Table 1 (Concluded)

Process	Definition	Important Features
Brownian diffusion	Diffusion of particles as a result of collisions with gas molecules	Brownian diffusivity depends on particle size; it is most important for small particles.
Turbulent diffusion	Motion of particles with the turbulent airflow	Turbulent diffusion of aerosols can be treated analogously to that of gaseous species.
Gravitational settling	Settling of particles due to gravity	This is important only for large particles (over 10 μm in diameter); it is the mechanism primarily responsible for the cutoff of the aerosol size spectrum at the upper end of the particle size range.
Deposition	Loss occuring when particles cross streamlines and deposit on surfaces, such as grass	Deposition is primarily important for particles larger than 1 μm in diameter.
Rainout in clouds	Loss of particles through their role as condensation nuclei in clouds	
Washout under clouds	Scavenging of particles by falling raindrops	

form products that can homogeneously nucleate or heterogeneously condense at ambient temperatures.

Table 2 shows an approximate aerosol inventory for Los Angeles. Primary and secondary anthropogenic sources have been estimated to contribute nearly two-thirds of the total aerosol mass in Los Angeles. Half of the anthropogenic contribution has been estimated to result from gas-to-particle conversion. Hence, an "emission inventory" for photochemical aerosols must include an inventory of gaseous species potentially convertible to the particulate phase.

Of prime interest in this chapter are the size distributions associated with the aerosol sources. Figure 1 shows the surface area and volume distributions measured during 1972 at four sites in the Los Angeles area. The Hunter-Liggett site is characteristic of a remote land site; the Harbor Freeway, of a motor vehicle dominated site; Goldstone, of a remote desert location; and Pt. Arguello, of a site dominated by a marine aerosol. As Figure 1 shows, the differences in the size distributions of the aerosols at the four sites are clearly evident. The motor vehicle exhaust aerosol has large numbers of particles that have diameters less than 0.1 μm, whereas the marine and natural continental aerosol particles are concentrated in the size range larger than 1.0 μm diameter.

2. Observations of Photochemical Aerosols

Once the major sources of photochemical aerosols have been identified, one can infer information about the physical properties important in the evolution of the aerosol from its measured size distributions. As noted earlier, the richest source of data on the properties of photochemical aerosols are the 1969 and 1972 to 1973 Aerosol Characterization Study conducted in Los Angeles.

Table 2

SOURCE CONTRIBUTIONS TO AEROSOL SAMPLES
FROM PASADENA, CALIFORNIA (3 SEPTEMBER 1969)

Source	Percentage
Natural background	
Primary	
Sea salt	1.3%
Soil dust	11.4
Secondary	
Organic vapors from plants	Unknown
Ammonia	Unknown
Hydrogen sulfide	Unknown
Man-made	
Primary	
Automobile exhaust	8.2
Tire dust	0.8
Cement dust (roads and construction)	1.7
Fuel oil fly ash	0.1
Diesel exhaust	1.8
Aircraft exhaust	2.7
Industrial emissions	7.3
Secondary	
Sulfur dioxide → sulfate	>10
Nitrogen oxides → nitrate	∿ 0.1
Organic vapors → particulate	26.7
Total	>72.3%

Source: Friedlander (1973).

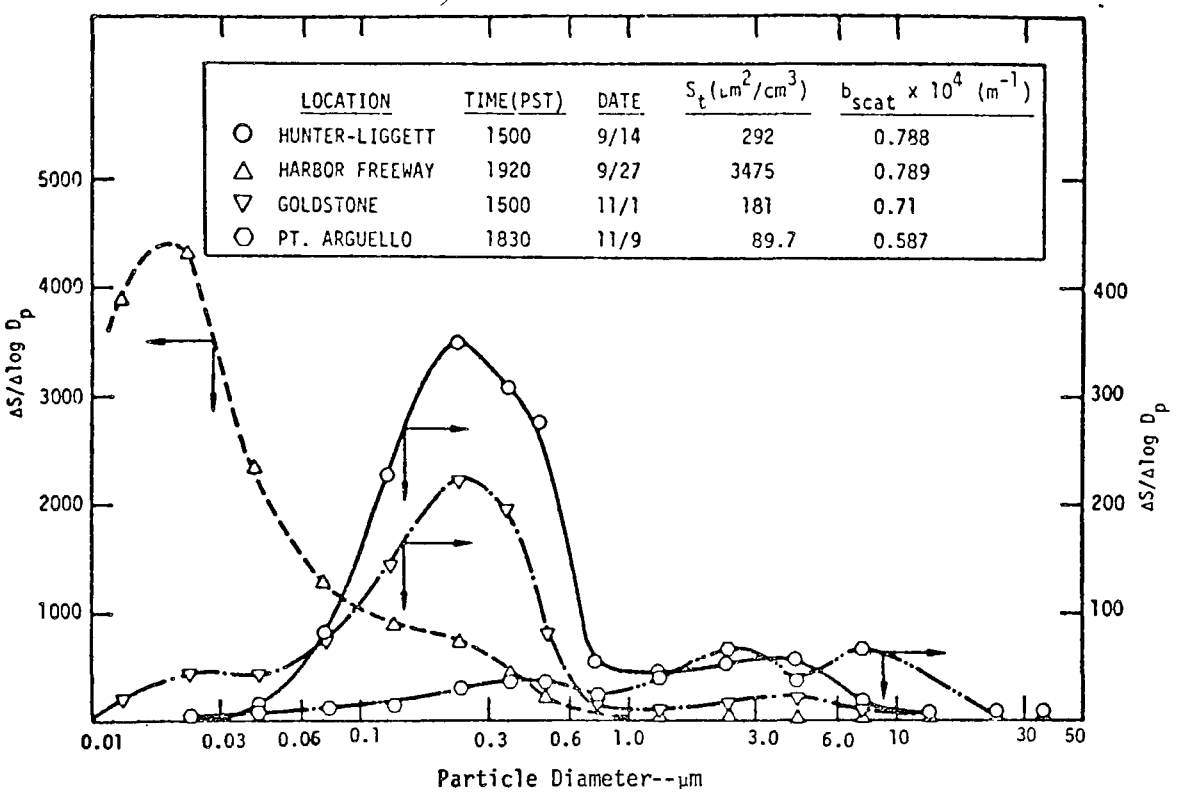

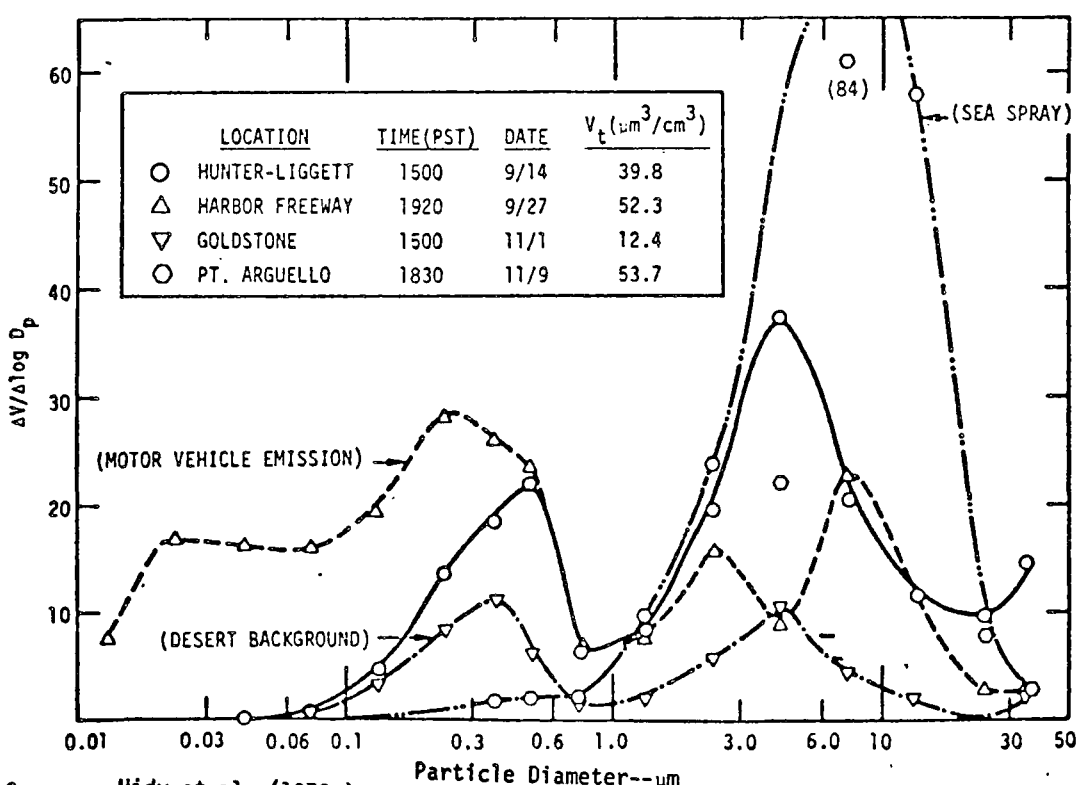

Source: Hidy et al. (1973a).

FIGURE 1. COMPARISON OF SURFACE AND VOLUME DISTRIBUTIONS FOR BACKGROUND AND MOTOR VEHICLE SOURCE-ENRICHED (NEAR THE HARBOR FREEWAY) SITES

Laboratory and field studies have elucidated certain differences between photochemical and nonphotochemical urban aerosols. Table 3 summarizes some of the conclusions based on available studies. Whitby et al. (1972) analyzed the number, surface area, and volume distributions of 342 size distributions measured during the 1969 study. The grand average number, surface area, and volume distributions, normalized to the total number, surface area, and volume, respectively, are shown in Figure 2(a). Figure 2(b) compares the volume distribution measured in Los Angeles with that measured in urban and rural locations where photochemical reactions were not expected to be important. The bimodel size distribution appears to be universal; however, the characteristics of the fraction in the size range $0.1 \leq D_p \leq 1.0$ μm indicate that these particles are apparently of a different origin in the Los Angeles aerosol than in the other aerosols studied. In Los Angeles, the peak in the submicron fraction occurs consistently around 0.25 μm diameter and reaches a maximum number density in phase with the peak in solar radiation. In contrast, the submicron fraction of the volume distribution in the Minneapolis aerosol is more skewed than that of the Los Angeles aerosol and peaks at about 0.8 μm at about 8 a.m. during the morning traffic. In all cases, the large particle fraction, with a peak above 1.0 μm, is attributable to local, naturally occurring particles, such as dust and sea spray.

The peak in the total particulate concentration in Minneapolis was nearly an order of magnitude larger than the peak in the Los Angeles aerosol. Husar et al. (1972) suggested the following reasoning: The probability that a particle whose diameter is less than 0.1 μm will collide with another the same size is less than that of collision with a particle in the size range $0.1 \leq D_p \leq 1.0$ μm. Therefore, the total number of particles in Los Angeles is less than that in Minneapolis because the Aitken nuclei produced by combustion and homogeneous nucleation are more effectively removed in Los Angeles through coagulation with the larger number of particles in the size range $0.1 \leq D_p \leq 1.0$ μm.

Table 3

COMPARISON OF THE PHYSICAL PROPERTIES
OF PHOTOCHEMICAL AND NONPHOTOCHEMICAL AEROSOLS

Property	Photochemical Aerosol (Los Angeles)	Nonphotochemical Aerosol (Minneapolis)
Average number density (Whitby et al., 1972)	1.14×10^5 cm^{-3}	$2.1\text{-}6.6 \times 10^4$ cm^{-3}
Daily peak number density	$\sim 2 \times 10^5$ cm^{-3}	$\sim 2 \times 10^6$ cm^{-3}
Volume arithmetic mean diameter (Whitby et al., 1972)	0.086 μm	0.09-0.11 μm

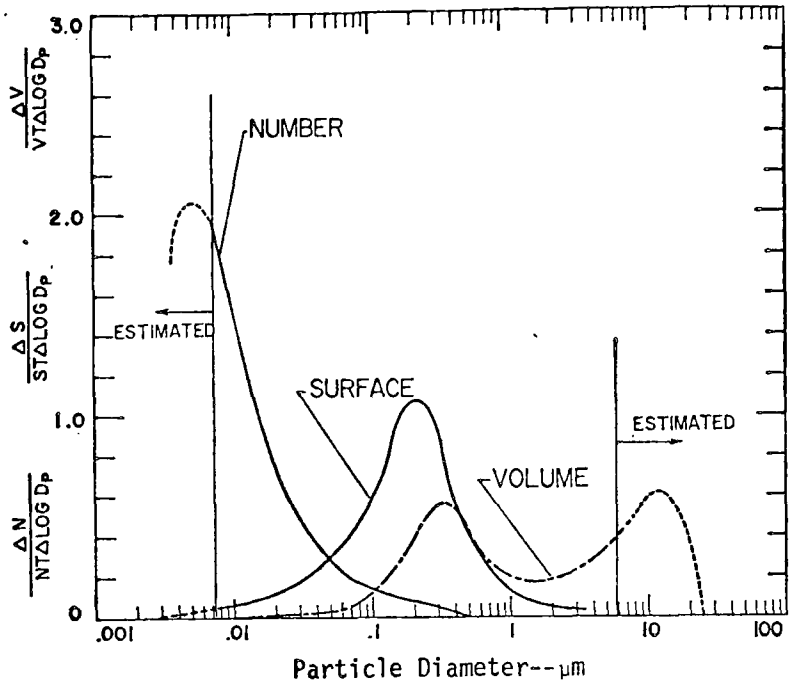

(a) Grand Average Number, Surface Area, and Volume Distribution of Los Angeles Smog

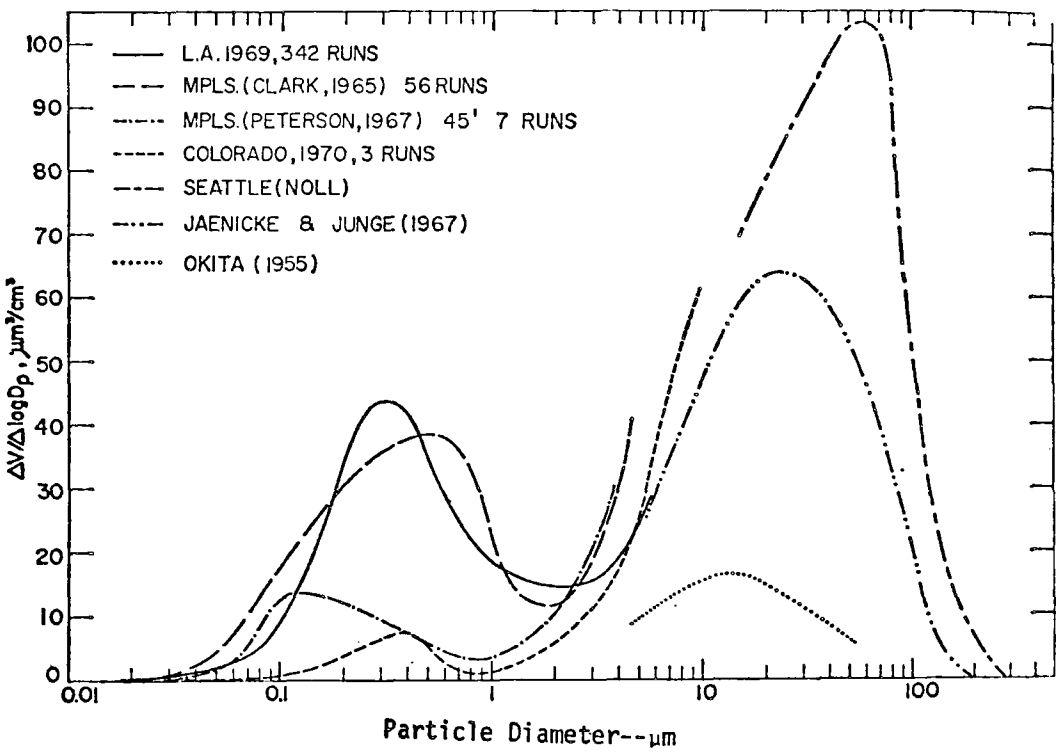

(b) Comparison of Volume Distributions Measured by Several Investigators in Different Locations

Source: Whitby et al. (1972).

FIGURE 2. COMPARISON OF THE CHARACTERISTICS OF PHOTOCHEMICAL AND NONPHOTOCHEMICAL URBAN AEROSOLS

The chemical composition of the Los Angeles aerosol also provides evidence that the physical mechanisms responsible for the evolution of the aerosol differ from those in areas where photochemistry was not expected to be important. Table 4 presents the concentrations of benzene-soluble organics, sulfates, and nitrates for 24-hour averaged aerosol samples obtained from the U.S. National Air Surveillance Network. The data indicate substantially larger concentrations of benzene-soluble organics and nitrates in the Los Angeles and Riverside aerosols than those observed in other areas. In the Riverside sample, the large nitrate concentration may be due to photochemical transformations of NO_x to nitrogen aerosol compounds or to sources of aerosols containing nitrogen compounds in the vicinity of the sampling site. For comparison, the fifth entry in the table is a sample taken from San Nicholas Island during Santa Ana conditions (meteorological conditions that place the island downwind of Los Angeles). In this sample, the nitrate and benzene soluble organic concentrations were higher than those normally found in samples taken from the island.

3. Summary

The sources and observations of photochemical aerosols can be summarized as follows:

> Sources of aerosols in Los Angeles are both natural and anthropogenic, but the largest fraction of aerosol mass is attributable to motor vehicle emissions.

> One-third to one-half of the aerosol mass has been attributed to gas-to-particle conversions in the atmosphere. The mass accumulates predominantly in the size range of 0.1 to 1.0 μm diameter.

> The maximum number density in the Los Angeles aerosol occurs in phase with solar radiation. In contrast, the concentration of nonphotochemical aerosols follows the diurnal pattern of the sources of particulate matter.

> The fraction of the aerosol that is composed of organics or nitrates is higher in the Los Angeles aerosol than in nonphotochemical aerosols, and it increases as the photochemical products in the atmosphere increase.

Table 4

COMPARISON OF AEROSOL SAMPLES TAKEN FROM PHOTOCHEMICAL SMOG AND OTHER URBAN AND NONURBAN AEROSOLS

Sample	Total Mass ($\mu g\ m^{-3}$)	Benzene Soluble		Sulfate		Nitrate		Reference
		$\mu g\ m^{-3}$	Percent	$\mu g\ m^{-3}$	Percent	$\mu g\ m^{-3}$	Percent	
Downtown Los Angeles (1968)	213	30.4	14.2%	16.0	7.5%	9.4	4.4%	Cadle (1966), Colucci et al. (1969)
Downtown Los Angeles (1966)	119	15.2	12.8	14.0	11.8	13.0	10.9	U.S. Public Health Service (1968)
Riverside, California (Summer-Fall 1968)	82	4.9	6.0	8.3	10.1	11.7	14.3	Lundgren (1969)
San Nicholas Island coastal and ocean (1956-1957)	69	3.6	5.2	8.4	12.2	2.8	2.9	Holzworth (1959)
San Nicholas Island (1956-1957) aged Los Angeles	110	10.1	9.2	9.3	8.4	5.4	4.9	Holzworth (1959)
Urban (1966-1967) 25 stations	102	6.7	6.6	10.1	9.9	2.4	2.4	Ludwig et al. (1970)
Nonurban (1966-1967) 15 stations	40.0	2.2	5.4	5.29	13.1	0.85	2.1	Ludwig et al. (1970)

B. PHYSICAL PROCESSES INFLUENCING AEROSOL DYNAMICS

In this section, we consider each of the processes listed in Table 1 to assess its importance to the rate of formation of photochemical aerosols. In Section II-C, we estimate the relative magnitude of the effect each process has on the aerosol size distribution and present sample calculations.

1. Homogeneous Nucleation

As indicated by estimates of gas-to-particle conversion in photochemical smog, secondary aerosols are responsible for a substantial fraction--as much as one-half--of the total aerosol mass. The conversion of gaseous species to the particulate phase can occur both in the absence and in the presence of foreign nuclei. Homogeneous nucleation refers to the spontaneous formation of stable nuclei from gas molecules. For a detailed treatment of the thermodynamics and kinetics of homogeneous nucleation of single species, we refer the reader to Hidy and Brock (1970). Stauffer et al. (1973) and Kiang et al. (1973) have reviewed the homogeneous nucleation of several species, which is called heteromolecular nucleation.

In cloud physics, it is generally assumed that even at the high supersaturations that occur in clouds, homogeneous nucleation of water vapor is negligible compared with condensation on preexisting particles. In photochemical smog, the primary candidates for heteromolecular nucleation are sulfuric acid, high-molecular-weight organic species, and water.

The importance of the conversion of SO_2 to sulfate aerosol in photochemical smog has long been recognized. In this conversion, the basic process appears to be the homogeneous oxidation of SO_2 to SO_3, followed by a rapid reaction of SO_3 with water, producing a molecule of sulfuric acid. The sulfuric acid molecule then participates in either of two processes: (1) Water molecules may homogeneously nucleate around the sulfuric acid molecule, at an observed ratio of about five molecules of water per molecule of H_2SO_4, or (2) the H_2SO_4 molecule may diffuse to an existing stable

particle and heterogeneously condense. Since sulfuric acid is supersaturated in the concentration range of parts per hundred billion, it thus rapidly follows one of these two paths. Rates of photooxidation of SO_2 in air have been measured by Hall (1953), Gerhard and Johnstone (1955), Renzetti and Doyle (1960), and Quon et al. (1971). Quon et al. measured a pseudo-first-order rate constant of 5×10^{-6} sec^{-1}. At SO_2 levels typical of air pollution episodes (0.65 ppm), the rate of formation of sulfuric acid by photooxidation of SO_2 (in the absence of hydrocarbons and NO_x) is 3×10^{-3} ppb sec^{-1}, or 1.31×10^{-4} g cm^{-3} sec^{-1} of sulfuric acid.

Table 5 shows comparisons of the rates of mass conversion of H_2SO_4 by homogeneous nucleation and by diffusion to the surface of 0.1 μm diameter particles at a particle concentration of 10^5 cm^{-3} for various concentrations of sulfuric acid vapor. The homogeneous nucleation rates are those calculated for various concentrations of H_2SO_4 vapor by Doyle (1961). To obtain these rates, we multiplied the nuclei formation rates obtained by Doyle by the number of molecules of H_2SO_4 per nuclei and the weight of a molecule of H_2SO_4.

A detailed discussion of solutions to the kinetic equations for homogeneous nucleation has been given by Hidy and Brock (1970). In the classical theory of particle generation by nucleation, the rate of formation of clusters of k molecules is assumed to be dominated by collisions between single molecules and clusters of molecules and by the evaporation of single molecules from the clusters. The interaction of particles is assumed to be negligible.

No general analytic solution to the differential equations for the rate of change of clusters in the presence of a saturated vapor has been obtained, but solutions have been found for the steady-state distribution of clusters of k molecules. In this case, the rate of nucleation is given by an equation of the form

$$I = I^{o} \exp\left(\frac{-\Delta G^{*}}{kT}\right) \quad ,$$

Table 5

RATES OF CONVERSION OF VAPOR PHASE H_2SO_4 THROUGH HETEROGENEOUS AND HOMOGENEOUS NUCLEATION*

H_2SO_4 Gas Phase Concentration (pbb)	Molecules per Nucleus	Mole Fraction of H_2SO_4	Homogeneous Rate ($gsec^{-1}$ cm^{-3})	Heterogeneous Rate ($gsec^{-1}$ cm^{-3})
1.3	5	0.357	4.3×10^{-8}	1.6×10^{-11}
0.13	11	0.320	1.7×10^{-11}	1.6×10^{-12}
1.3×10^{-2}	18	0.280	3.6×10^{-15}	1.6×10^{-13}
1.3×10^{-3}	41	0.248	8.1×10^{-23}	1.6×10^{-14}
1.3×10^{-4}	118	0.220	4.6×10^{-40}	1.6×10^{-15}
1.3×10^{-5}	298	0.186	1.64×10^{-60}	1.6×10^{-16}

*Homogeneous nucleation rates were calculated by Doyle (1961) for a binary system of H_2SO_4 and water vapor at 25°C and 50 percent relative humidity.

where ΔG^* is the free energy of formation of the nucleus and I^o is a function that depends on the properties of the molecular species comprising the clusters and the concentrations of their vapors.

Doyle (1961) adapted the model of Reiss (1950) for the determination of self-nucleation rates in binary systems to determine the rate of formation of nuclei in the sulfuric acid and water system. To calculate the rate of formation, I, at given concentrations of sulfuric acid vapor and water vapor, Doyle first determined the location of the activation barrier (that is, the minimum number of molecules for which an aggregate of molecules is stable). The activation barrier can be found by determining the free energy for which an aggregate of ${}^2n_1$ moles of H_2O and ${}^2n_2$ moles of H_2SO_4 is stable as follows:

$$\Delta G = {}^2n_1\left({}^2\mu_1 - {}^1\mu_1\right) + {}^2n_2\left({}^2\mu_2 - {}^1\mu_2\right) + \pi\gamma D_p^2 \quad ,$$

where

${}^2n_1$ and ${}^2n_2$ = the number of moles of H_2O and H_2SO_4, in the liquid phase, respectively,

${}^2\mu_1$ and ${}^2\mu_2$ = the chemical potentials of H_2O and H_2SO_4, respectively,

γ = the surface tension of the droplet,

D_p = the droplet diameter.

From the expression obtained by Reiss (1950), Doyle calculated the function I^o, which is a function of the properties of the two components of the system and the size of and surface energy of the embryo. The homogeneous nucleation rates given in Table 5 are uncertain by three or four orders of magnitude because of the inadequate data for partial pressures of sulfuric acid over its aqueous solution. Additional uncertainties in the results can be attributed to the model used.

In computing the heterogeneous condensation rates in Table 5, we assumed that the rate of condensation is controlled by the rate of diffusion of gaseous H_2SO_4 to the particles. The maximum rate of diffusion occurs when the concentration of the condensing material in the aerosol is negligible. In such a case, the rate of mass transfer of H_2SO_4 per unit volume of atmosphere to a monodispersed aerosol of diameter D_p and number density N in an atmosphere with a partial pressure p_∞ of H_2SO_4 is

$$\frac{dm}{dt} = \frac{2\pi D_p M p_\infty D N}{R T_\infty} \quad , \qquad (1)$$

where

M = the molecular weight of the condensing species,
D = the molecular diffusivity of the condensing species in air,
R = the gas constant,
T_∞ = the ambient temperature.

We computed the rates shown in Table 5 on the basis of the following values: $D_p = 10^{-5}$ cm, $D = 0.5$ cm^2 sec^{-1}, $M = 98$ g mole^{-1}, $T_\infty = 298^\circ$K, and $N = 10^5$ cm^{-3}.

Note that at H_2SO_4 concentration levels below about 0.1 ppb, the rate of loss of H_2SO_4 by heterogeneous condensation exceeds that of homogeneous nucleation. At the clean air photooxidation rate of SO_2 of 1.3×10^{-14} g cm^{-3} sec^{-1} reported earlier, if we assume that this rate is balanced by heterogeneous condensation, the contribution of homogeneous nucleation to the rate of loss of H_2SO_4 is completely negligible. Under these conditions, the concentration of H_2SO_4 in the gas phase would be about 10^{-3} ppb.

In general, at typical H_2SO_4 levels in the urban atmosphere ($\sim 10^{-3}$ ppb), homogeneous nucleation can be neglected, compared with heterogeneous condensation, as a mechanism for the conversion of gases to the particulate phase. If SO_2 concentrations were to reach values in the range of 60 ppm, as they do in concentrated plumes, then homogeneous nucleation of the H_2SO_4 formed might be expected to become important; otherwise, homogeneous nucleation can be neglected in the formulation of an urban-scale dynamic model for aerosols.

2. Heterogeneous Condensation

Growth by heterogeneous condensation is thus an important mechanism in photochemical aerosol dynamics. In fact, that part of the aerosol mass attributable to gas-to-particle conversion processes is basically the result of heterogeneous condensation. The theory of the growth of multicomponent liquid droplets by vapor diffusion is reasonably well developed (Fukuta and Walter, 1970). In applying the theory to photochemical aerosols, the major problem is that the physical state and chemical composition of the aerosols are often unknown. It is possible that some photochemical smog aerosols exist as solid particles, for example, containing high-molecular-weight organics that are solids at normal atmospheric temperatures and pressures. At present, there are no adequate theories to explain the growth of particles of this type, and the available experimental data on the true physical state of these particles are so scarce that it is not clear what the theoretical needs are. Therefore, in this section, we consider the theoretical aspects of growth of liquid droplets only. In this discussion, we cite some empirical results obtained experimentally by Heisler and Friedlander (1974).

a. Theoretical Relations for Diffusion-Controlled Heterogeneous Condensation

When the growth of a particle is controlled by diffusion of a single gaseous condensing species to the particle surface, the rate of change of particle volume is given by

$$\frac{dv}{dt} = \frac{2\pi D D_p M}{\rho_L R T_\infty} (p_\infty - p_s) \quad , \qquad (2)$$

where ρ_L is the density of the droplet and p_s is the partial pressure of the condensing species in the vapor just above the droplet surface. The critical parameter controlling droplet growth is p_s at given values of D_p and p_∞. The partial pressure of the condensing species at the droplet surface differs from that for the pure liquid species at T_∞ for several reasons:

> The temperature at the droplet surface is higher than T_∞ because of the heat released by condensation of the vapor. Since $T_s > T_\infty$, p_s is greater than the vapor pressure at T_∞.

> The surface tension associated with a curved surface increases the amount of energy required to form that surface from the vapor phase. The particle curvature has the effect, therefore, of increasing the vapor pressure of the species over a curved surface beyond that over a flat surface. The phenomenon is known as the Kelvin effect.

> The droplet may consist of several species, in which case p_s is the vapor pressure of the condensing species over a solution. The effect is that the vapor pressure over the solution is lower than that over the pure condensing species. This phenomenon is called the solute effect.

To estimate their possible importance in controlling the rate of growth of aerosol particles by heterogeneous condensation, we briefly consider each of these effects below.

Assuming that the droplet is at temperature T_s, the rate of loss of energy from the droplet to the atmosphere is given by*

$$\frac{dq}{dt} = L' \frac{dm}{dt} = 2\pi k D_p (T_s - T_\infty) \quad , \tag{3}$$

where L' is the latent heat of condensation (in solution) and k is the thermal conductivity of air. From Eqs. (2) and (3), the surface temperature can be related to the partial pressure by

$$T_s - T_\infty = \frac{DML'}{RT_\infty k} (p_\infty - p_s) \quad . \tag{4}$$

if the heat of condensation of the pure species, L, is approximately constant over the temperature range T_∞ to T_s, the Clausius-Clapeyron equation can be integrated to give

$$\frac{p_s(T_s)}{p_s(T_\infty)} = \exp\left[\frac{LM}{R}\left(\frac{1}{T_\infty} - \frac{1}{T_s}\right)\right] \quad . \tag{5}$$

If the exponent is small and $T_s T_\infty \cong T_\infty^2$, then

$$\frac{p_s(T_s)}{p_s(T_\infty)} \cong 1 + \frac{LM}{RT_\infty^2} (T_s - T_\infty) \quad . \tag{6}$$

The Kelvin-Gibbs relation for the vapor pressure at equilibrium over a curved surface of a pure component is

$$p_s = p_s^o \exp\left(\frac{4\sigma V_L}{RT_\infty D_p}\right) \quad , \tag{7}$$

where p_s^o is the vapor pressure over a flat surface of pure species at T_s, σ is the surface tension, and V_L is the molar volume of the species in the liquid.

---

*In writing this relationship, we assume that the characteristic time for the conduction of heat in the droplet is much shorter than that for changes in ambient conditions. The characteristic time is estimated as $t = D_p^2/\alpha$, where $\alpha = k_L/\rho_L C_{p_L}$ is the thermal diffusivity of the droplet. A typical value of t is 10^{-6} sec for a 015 μm diameter drop of water

The vapor pressure over a solution can be related to that of the pure component at the same temperature by Raoult's law:

$$p_s = \gamma_i x_i p_{s_i} \quad , \tag{8}$$

where γ_i is the activity coefficient of species i, x_i is the mole fraction of species i in the solution, and p_{s_i} is the vapor pressure of the pure species i.

Equations (2), (4), (6), (7), and (8) can be combined to give the following expression for the rate of growth of a two-component droplet by diffusion of one component, species i, to the droplet:

$$\frac{dv}{dt} = \frac{2\pi D_p}{\rho_L}\left[\frac{S - \gamma_i x_i \exp\left(\frac{4\sigma V_L}{RT_\infty D_p}\right)}{\frac{RT_\infty}{DMp_s^o(T_\infty)} + \frac{LL'M}{kRT_\infty^2}\gamma_i x_i \exp\left(\frac{4\sigma V_L}{RT_\infty D_p}\right)}\right] \quad , \tag{9}$$

where $S = p_\infty(T_\infty)/p_s^o(T_\infty)$ is the saturation ratio. We note that in deriving Eq. (9) we assumed that the Kelvin effect is not altered in the presence of a solution; that is, that Eq. (7) holds for the vapor pressure over a solution droplet as well as for a droplet of pure species i.

We note from Eq. (9) that growth ceases when

$$S \leq \gamma_i x_i \exp\left(\frac{4\sigma V_L}{RT_\infty D_p}\right) \quad , \tag{10}$$

or, alternatively, when

$$D_p \leq \frac{4\sigma V_L}{RT_\infty \ln\left(\frac{S}{\gamma_i x_i}\right)} \quad . \tag{11}$$

Thus, there is generally a critical particle size below which growth does not occur. We also note that two phenomena act in opposite directions in governing the rate of condensation. The Kelvin effect increases the vapor pressure over that of the flat solution, whereas the solute effect decreases the vapor pressure over that of the pure solution. Growth does not occur if D_p is too small or if $\gamma_i x_i$ is sufficiently large.

The foregoing development can be extended to include multicomponent droplets. If there are K condensing species, the rate of change of the mass of a particle is the sum of the contributions from the K species:

$$\frac{dm}{dt} = \sum_{i=1}^{K} \frac{dm_i}{dt} \quad , \tag{12}$$

where

$$\frac{dm_i}{dt} = \frac{2\pi D_p D_i M_i}{RT_\infty} \left(p_{i_\infty} - p_{i_s}\right) \quad . \tag{13}$$

The derivation of the expression for $p_{i_s}(T_s)$ is analogous to that for $p_s(T_s)$ for the single component system, except that the vapor pressure of species i depends on the concentrations of the other N-1 species in the particle. The resulting relation is

$$p_{i_s}(T_s) = \gamma_i x_i \exp\left(\frac{4\sigma_i V L_i}{RT_\infty D_p}\right)\left[1 + \frac{L_i M_i}{kR^2 T_\infty^3} \sum_{j=1}^{K} L_j' D_j M_j \left(p_{j_\infty} - p_{j_s}\right)\right] p_{i_s}(T_\infty) \quad . \tag{14}$$

Equations (9), (12), (13), and (14) are general expressions for condensation growth relations that involve all three effects cited earlier (the Kelvin effect, the solute effect, and energy transport due to the latent

heat of condensation). The next step in the analysis of the growth of aerosols by condensation is to estimate the relative importance of each effect on the overall rate of growth of a typical atmospheric aerosol. We consider thermal effects first.

Thermal effects are embodied in the second term of the denominator of Eq. (9). Thus, the relative sizes of the two terms in the denominator provide an indication of the importance of thermal effects in relation to diffusive transport. Data typical of organic acids (see Table 6) indicate that the magnitude of the first term in the denominator of Eq. (9) is about a factor of 10^5 larger than the second term. Thus, it appears that thermal effects are unimportant in governing aerosol growth rates by heterogeneous condensation; that is, the particle can be considered to be at a temperature of T_∞. In that case, Eq. (9) becomes

$$\frac{dv}{dt} = \frac{2\pi D_p D M p_s(T_\infty)}{\rho_L R T_\infty}\left[S - \gamma_i x_i \exp\left(\frac{4\sigma V_L}{R T_\infty D_p}\right)\right] \quad . \tag{15}$$

The analogous relation for a multicomponent droplet is

$$\frac{dv}{dt} = \frac{2\pi D_p}{\rho_L}\sum_{i=1}^{K}\frac{M_i D_i p_{i_s}(T_\infty)}{R T_\infty}\left[S_i - \gamma_i x_i \exp\left(\frac{4\sigma_i V_{L_i}}{R T_\infty D_p}\right)\right] \quad . \tag{16}$$

b. <u>Theoretical Relations for Reaction-Controlled Heterogeneous Condensation</u>

The alternative to heterogeneous condensation growth controlled by vapor diffusion is growth controlled by heterogeneous chemical reaction.

Table 6

PARAMETERS USED IN EVALUATING THE RELATIVE IMPORTANCE OF THERMAL EFFECTS ON AEROSOL GROWTH BY HETEROGENEOUS CONDENSATION

Parameter	Value	Remarks
k	2.62×10^3 ergs cm^{-1} sec^{-1} $^oK^{-1}$	
T_∞	300^oK	
D	0.07 cm^2 sec^{-1}	Estimated value typical of organic acids (Dreisbach, 1959)
σ	26.25 dyne cm^{-1}	Estimated for organic acids
R	8.31×10^7 ergs $mole^{-1}$ $^oK^{-1}$	
L,L'	6.8×10^9 ergs g^{-1}	Value typical of organic acids (Dreisbach, 1959)
V_L	150 cm^3 $mole^{-1}$	Estimate
D_p	10^{-5} cm	
$p_s^o(T_\infty)$	2.6×10^{-2} dyne cm^{-2}	Adipic acid

In this case, vapor diffusion is rapid compared with the rate of consumption of the condensing species by chemical reaction in the particle, and the overall rate of heterogeneous condensation is equal to the heterogeneous reaction rate. We can develop the general form of a growth law as follows.

Let c denote the concentration of the diffusing gaseous species. Then, in the steady state, c is governed by

$$\frac{d^2c}{d\rho^2} + \frac{2}{\rho}\frac{dc}{d\rho} = 0 \quad , \tag{17}$$

where ρ is the radial position in the vapor ($\rho = 0$ is the particle center and $\rho = D_p/2$ is the particle radius). The boundary conditions on c are

$$\begin{aligned} c &= c_\infty \quad , \quad \rho \to \infty \quad , \\ -D\left.\frac{dc}{d\rho}\right|_{\rho=D_p/2} \pi D_p^2 &= \frac{\pi}{6} D_p^3 kc \quad , \quad \rho = D_p/2 \end{aligned} \tag{18}$$

The second boundary condition states that the flux of the condensing species at the particle surface is equal to the rate of consumption of the species by first-order reaction in the volume of the particle (k is the first-order rate constant). Thus, this problem describes the case in which the rate of condensation is controlled by a volume reaction in the particle.

The rate at which the vapor species condenses on the particle is

$$\text{Rate} = \frac{\pi}{6} D_p^3 \left(\frac{1}{1-\phi}\right) kc_0 \quad , \tag{19}$$

where $\phi = kD_p^2/12D$. When reaction controls the rate, we expect $\phi << 1$. This rate is directly related to the rate of change of the particle volume. Thus, in this case,

$$\frac{dv}{dt} \sim D_p^3 \quad , \tag{20}$$

in contrast to the case of vapor diffusion controlling in which, as we have already seen,

$$\frac{dv}{dt} \sim D_p \quad . \tag{21}$$

If a surface reaction controls the rate of growth, the above boundary condition at $\rho = D_p/2$ is replaced by

$$-D \left.\frac{dc}{d\rho}\right|_{\rho=D_p/2} = k'c \quad , \tag{22}$$

where k' is a surface reaction rate constant. In that case, it can be shown that the growth law is of the form

$$\frac{dv}{dt} \sim D_p^2 \quad . \tag{23}$$

c. Experimental Studies of Heterogeneous Condensation Growth of Photochemical Aerosols

There are two sources of data on the growth of aerosols by heterogeneous condensation: laboratory investigations and ambient field studies. In this subsection, we briefly summarize some of the available data from both sources

In a laboratory study, Heisler and Friedlander (1974) compared experimentally observed rates of growth with theoretical aerosol growth laws. The objective of their study was to determine whether it is possible to infer the dominant mechanism of growth from experimentally observed aerosol growth. In analyzing their data, Heisler and Friedlander assumed that the basic multicomponent growth law was

$$\frac{dv}{dt} = \frac{2\pi D_p}{\rho_L} \sum_{i=1}^{K} \frac{M_i D_i p_{i_s}(T_\infty)}{RT_\infty(1 + \ell Kn)} \left[S_i - \gamma_i x_i \exp\left(\frac{4\sigma_i V_{L_i}}{RT_\infty D_p}\right)\right] \quad , \qquad (24)$$

where

$$\ell = \frac{1.333 + 0.71 Kn^{-1}}{1 + Kn^{-1}} \qquad (25)$$

and where $Kn = 2\lambda/D_p$--the particle Knudsen number--is the ratio of the mean free path of the gas to the particle radius. In the limit as $Kn \to 0$, Eq. (24) reduces to Eq. (16). The factor $(1 + \ell Kn)$ in Eq. (25) is the result of an attempt to extend empirically the validity of Eq. (16) to the regime of the intermediate Knudsen number.

The main objective of the Heisler and Friedlander study was to determine whether the growth relation given by Eq. (24) was capable of representing experimentally observed growth rates. In particular, the investigators wanted to see if experimental growth rates were proportional to D_p (rather than D_p^2, indicating a surface reaction, or D_p^3, indicating a volume reaction). If these rates were found proportional to D_p, the growth rate would then indicate a diffusion-controlled mechanism. For the purposes of analyzing their data and determining whether $dv/dt \sim D_p$, Heisler and Friedlander assumed that the mole fraction of species i remained constant in time and that the saturation ratio remained constant and near unity. By expanding the exponential in Eq. (24), they obtained the following approximate growth relation:

$$\frac{dv}{dt} = \frac{A}{1 + \ell Kn} (D_p - D_p^*) \quad , \qquad (26)$$

where A is a function of particle composition and saturation ratio but is assumed to be constant.

Heisler and Friedlander made a linear least-square fit of their data plotted in the form of $(1 + \ell Kn)(dv/dt)$ versus D_p. Their results indicate that a growth law of the form of Eq. (26) is capable of representing the data and that it predicts a minimum particle size for growth of about 0.25 μm If we assume that the condensing species are primarily hydrocarbons, then we can use Eq. (11) and the data given in Table 6 to show that

$$\ell n\left(\frac{S}{\gamma_i x_i}\right) \leq 2.5 \times 10^{-2}$$

for the experimental conditions reported by Heisler and Friedlander. Hence, in this experiment, the gaseous species that diffused to the particles were only slightly supersaturated and were very likely unsaturated (since $\gamma_i x_i$ is less than 1, in general).

The assumptions invoked to reduce Eq. (24) to Eq. (26) lead to a fundamental change in the nature of the growth law. Equation (26) predicts that as long as $D_p > D_p^*$ a particle will grow, whereas Eq. (24) predicts that if a particle continues to grow, a point will be reached when growth will cease. This cessation occurs when the partial pressure of the dissolved species above the particle equals the ambient vapor pressure of that species:

$$S_i = \gamma_i x_i \exp\left(\frac{4\sigma_i V_{L_i}}{RT_\infty D_p}\right) \quad . \tag{27}$$

If we assume that the mole fraction of the condensing species in the particle is small and that S_i is always near unity, then the equilibrium size predicted by Eq. (27) will not be reached, and a growth law similar to Eq. (26) will be obtained. Therefore, the following is an important question: In the description of photochemical aerosol growth by condensation, is it necessary to account for the change in composition of the particle, and hence in the vapor pressure over the surface of the particle, with time, or is it

acceptable to neglect this change? The resolution of this question requires a comparison of theoretical predictions with experimental observations. In a recent study, Heisler (1975) attempted to reproduce the size distribution of aerosols observed in the Los Angeles smog using a growth relationship of the form

$$\frac{dv}{dt} = \sum_{i=1}^{2} \frac{A_i}{1 + \ell Kn} \left(D_p - D_{pi}^* \right) \quad .$$

Good agreement with the data was found when $A_1 t_f = 0.236\ \mu m^2$, $D_{p1}^* = 0.055\ \mu m$, $A_2 t_f = 0.581\ \mu m^2$, $D_{p2}^* = 0.240\ \mu m$, where t_f represents the duration of aerosol growth. The growth relationship above represents the growth of two gaseous species onto the particulate phase. The smallest critical size ($D_{p1}^* = 0.055\ \mu m$) might result from the conversion of secondary sulfur, although the growth relationship of the form given by Eq. (26) has never been tested for sulfates.

It is interesting to compare the empirical constants with those calculated on the basis of thermodynamic data of the gaseous species which may be diffusing to the particles. If we assume the two species above to be sulfuric acid formed in the gas phase and the organic acid $C_8H_{18}COOH$ formed in the gas phase, then the data necessary to calculate the rate of particle growth and the critical size are given in Table 7. For sulfuric acid we calculate that $A_1 = 2.76 \times 10^{-3}\ \mu m^2 sec^{-1}$ and $D_{p1}^* = 1.91 \times 10^{-5}\ \mu m$ and for the organic acid $A_2 = 4.40 \times 10^{-2}\ \mu m^2 sec^{-1}$ and $D_{p2}^* = 2.86 \times 10^{-3}\ \mu m$. If the actual growth time was 5 hours in Heisler's model (Heisler, 1975) then $A_1 = 1.3 \times 10^{-5}\ \mu m^2 sec^{-1}$ and $A_2 = 3.2 \times 10^{-5}\ \mu m^2 sec^{-1}$. Hence, the theoretical values indicate a more rapid rate of growth than was measured and critical sizes which are much smaller than the values determined by Heisler.

The second source of aerosol data is atmospheric monitoring. Several volume distributions measured at various times on 3 September 1969 by Whitby et al. (1972) are shown in Figure 3. The diameter at which the mode of the volume distribution is located does not appear to vary appreciably, although

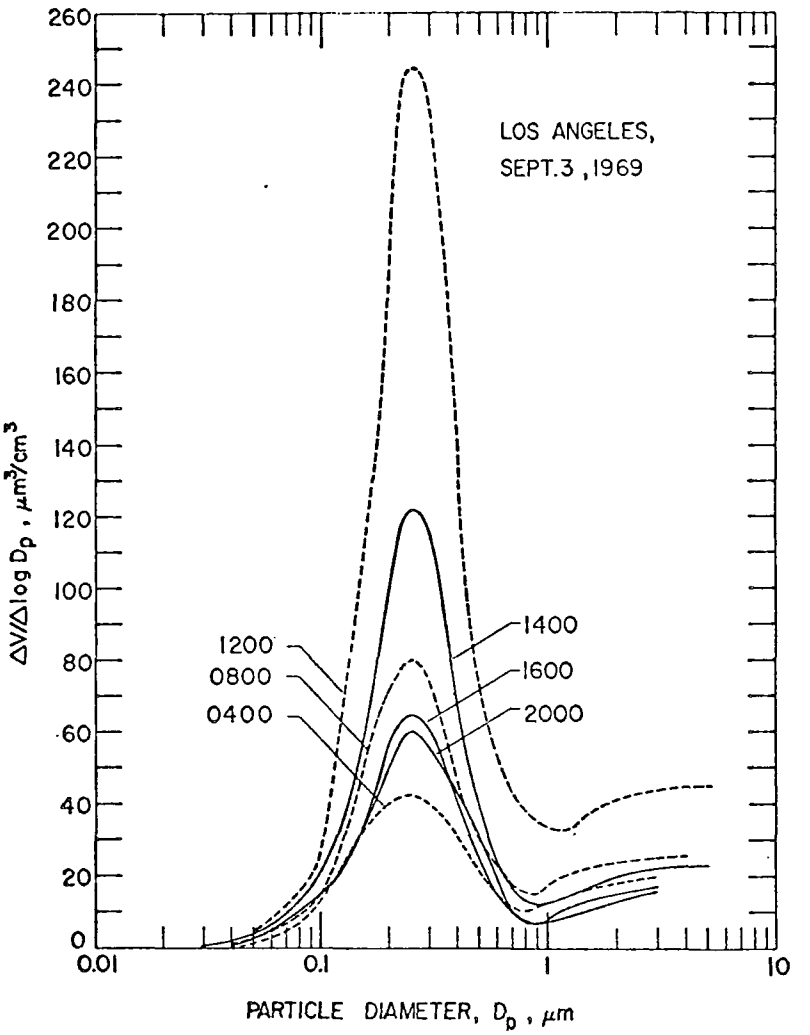

Source: Whitby et al. (1972).

FIGURE 3. DEVELOPMENT OF THE VOLUME DISTRIBUTION WITH TIME IN LOS ANGELES ON 3 SEPTEMBER 1969

Table 7

THERMODYNAMIC DATA FOR CALCULATING THE GROWTH RATES AND THE CRITICAL SIZES FOR GROWTH

Parameter	Value for H_2SO_4	Value for $C_8H_{18}COOH$
M_i	98 g $mole^{-1}$	159 g $mole^{-1}$
D_i	0.07 $cm^2 sec^{-1}$	0.07 $cm^2 sec^{-1}$
P_{i_s}	1.3×10^{-3} dynes cm^{-2}	5.92×10^{-1} dynes cm^{-2}
ρ_i	1.87 g cm^{-3}	0.94 g cm^{-3}
S_i	23	0.349
$\gamma_i X_i$	0.1	0.1
σ_i	52 dynes cm^{-1}	26.25 dynes cm^{-2}
$\bar{V}_{L_i}$	52.5 $cm^3 mole^{-1}$	169 $cm^3 mole^{-1}$

the total aerosol volume changes substantially during the day. Husar, Whitby, and Liu (1972) showed that diffusion-controlled growth (i.e., $\partial v/\partial t \sim D_p$) results in growth for which the location of the mode in the volume distribution does not change appreciably in time.

Although the results shown in Figure 3 are interesting, other data (in particular, the 1972 ACHEX data) do not support the symmetry or the consistent location of the mode in the volume distribution. There does not now appear to be sufficient evidence to characterize the structure of the mode of the volume distribution in the $0.1 < D_p < 1.0$ μm diameter size range. Certainly, the characteristics of this mode--in particular, its behavior with time--should provide evidence of the nature of the gas-to-particle conversion process occurring in the atmosphere.

3. Coagulation

Coagulation can result from any of several mechanisms that bring particles together: (1) Brownian motion, (2) turbulent shear, (3) gravitational settling, and (4) electrostatic attraction. The objective of this section is to assess the importance of each mechanism, and of coagulation in general, to the dynamics of photochemical aerosols.

In a spatially homogeneous aerosol, the size distribution function $n(D_p,t)$, is defined so that $n(D_p,t)dD_p$ is the number of particles with diameters in the range D_p to $D_p + dD_p$. The rate of disappearance of particles of diameter D_p as a result of collision with particles of diameter $\tilde{D}_p$ can be expressed in terms of the size distribution function as

$$\beta(D_p,\tilde{D}_p)\ n(D_p,t)\ n(\tilde{D}_p,t) \quad ,$$

where $\beta(D_p,\tilde{D}_p)$ is the collision frequency factor in ($cm^3\ sec^{-1}$). Thus, the rate of change of the size distribution function at diameter D_p due to collision with all other particles is

$$\int_0^\infty \beta(D_p,\tilde{D}_p)\ n(D_p,t)\ n(\tilde{D}_p,t)\ d\tilde{D}_p \quad .$$

The different mechanisms of coagulation are reflected in the functional form of $\beta(D_p,\tilde{D}_p)$. If we define $N_j(D_{pj},t)$ as the number density of particles $N_j(D_{pj},t)$ in the discrete size range D_{pj} to $D_{pj} + \Delta D_{pj}$

$$N_j(D_{pj},t) = \int_{D_{pj}}^{D_{pj}+\Delta D_{pj}} n(D_p,t)\ dD_p \quad ,$$

then the rate of disappearance of particles in the size range D_{pi} to $D_{pi} + \Delta D_{pi}$ due to collision with particles in another size range D_{pj} to $D_{pj} + \Delta D_{pj}$ can be estimated by

$$L_i = \beta(D_{pi},D_{pj})\ N_i(D_{pi},t)\ N_j(D_{pj},t) \quad . \tag{28}$$

[Note that $n(D_p,t)$ is a size distribution function expressed in units of $\mu m^{-1}\ cm^{-3}$, whereas $N_i(D_p,t)$ is a number density in cm^{-3}.] We can use Eq. (28) to estimate the rate of disappearance of particles in certain size ranges due to coagulation once β has been specified. Note that L_i is expressed in units of $cm^{-3}\ sec^{-1}$.

a. Coagulation Due to Brownian Motion

In Brownian coagulation, the particle collisions result from the random particle motions induced by collisions with molecules of the gas. The manner in which motion is imparted to a particle depends on the size of the particle relative to the mean free path of the gas, i.e. on the particle Knudsen number, $Kn = 2\lambda/D_p$.

When the particle Knudsen number is small, $Kn \leq 0.1$, the particle is in the so-called continuum regime, where the particle is large enough relative to the mean free path of the gas that the gas appears as a continuum to the particle. Assuming that particles are hard spheres, the collision frequency factor can be written as

$$\beta_{BM} = 2\pi M_{ij} D_{ij} D_{pij} \quad , \tag{29}$$

where D_{ij} is the sum of the Brownian diffusivities of particles of diameters D_{pi} and D_{pj}; $D_{pij} = D_{pi} + D_{pj}$; and M_{ij} is the symmetry number, defined as

$$M_{ij} = \begin{cases} \frac{1}{2} & , i = j \quad , \\ 1 & , i \neq j \quad . \end{cases}$$

Using the Stokes-Einstein diffusivity for a particle of diameter D_{pi},

$$D_i = \frac{kT}{3\pi\mu D_{pi}}$$

where k is Boltzman's constant and μ is the viscosity of the gas, we obtain the collision frequency factor for coagulation in the continuum regime

$$\beta_{BM} = \frac{2}{3}\frac{kT}{\mu}\,(D_{pi} + D_{pj})\left(\frac{1}{D_{pi}} + \frac{1}{D_{pj}}\right) M_{ij} \tag{30}$$

In this regime both particles must be larger than about 0.5 μm diameter.

When both particle Knudsen numbers are large ($Kn \geq 10$, or $D_p \leq 0.01$ μm), then the particles are in the so-called free molecular regime. In the

transition regime, when $K_n \approx 1$, the approaching particles are engaged in gas-particle collisions but not frequently enough for the diffusion equation to be applicable, as in the continuum regime. Husar (1969) has summarized the form of the collision frequency factor covering the range from the continuum regime to the free molecule regime. The collision frequency factor for arbitrary Kn may be expressed in the form,

$$\beta_{BM} = 2\pi M_{ij} D_{ij} D_{pij} \gamma_{ij} \tag{31}$$

where the correction factor,

$$\gamma_{ij} = \frac{1}{1+\lambda Kn_{ij}}$$

and where the collision Knudsen number is defined as

$$Kn_{ij} = \frac{2\lambda_{ij}}{D_{pij}}$$

The effective mean free path λ_{ij} should be calculated from

$$\lambda_{ij} = \frac{3D_{ij}}{\bar{V}_{ij}}$$

where $\bar{V}_{ij} = \sqrt{\bar{v}_i \bar{v}_j}$, where $\bar{v}_i$ and $\bar{v}_j$ are the mean molecular velocities.

The parameter λ in γ_{ij} is called the linear extrapolation distance. Tabulated values of λ as a function of Kn are given by Husar based on the work of Sahni. The tabulated values can be fit by the following relations:

$$\lambda = \begin{cases} 0.515\ Kn + 0.71 & 0 < Kn < 0.30 \\ 0.153\ \ell n\ Kn + 1.043 & 0.30 \leq Kn < 2.0 \\ 1.33 - 0.355\ Kn^{-1} & 2.0 \leq Kn < \infty \end{cases} \tag{32}$$

The collision frequency factors obtained from Eq. (31) are shown in Figure 4 for the size range 0.002 μm < D_p < 10 μm. The bottom heavy line in Figure 4 represents the collision frequency factor for equal size particles and exhibits a rather weak size dependence over the entire range of particle sizes. In the free molecule regime the collision frequency factor

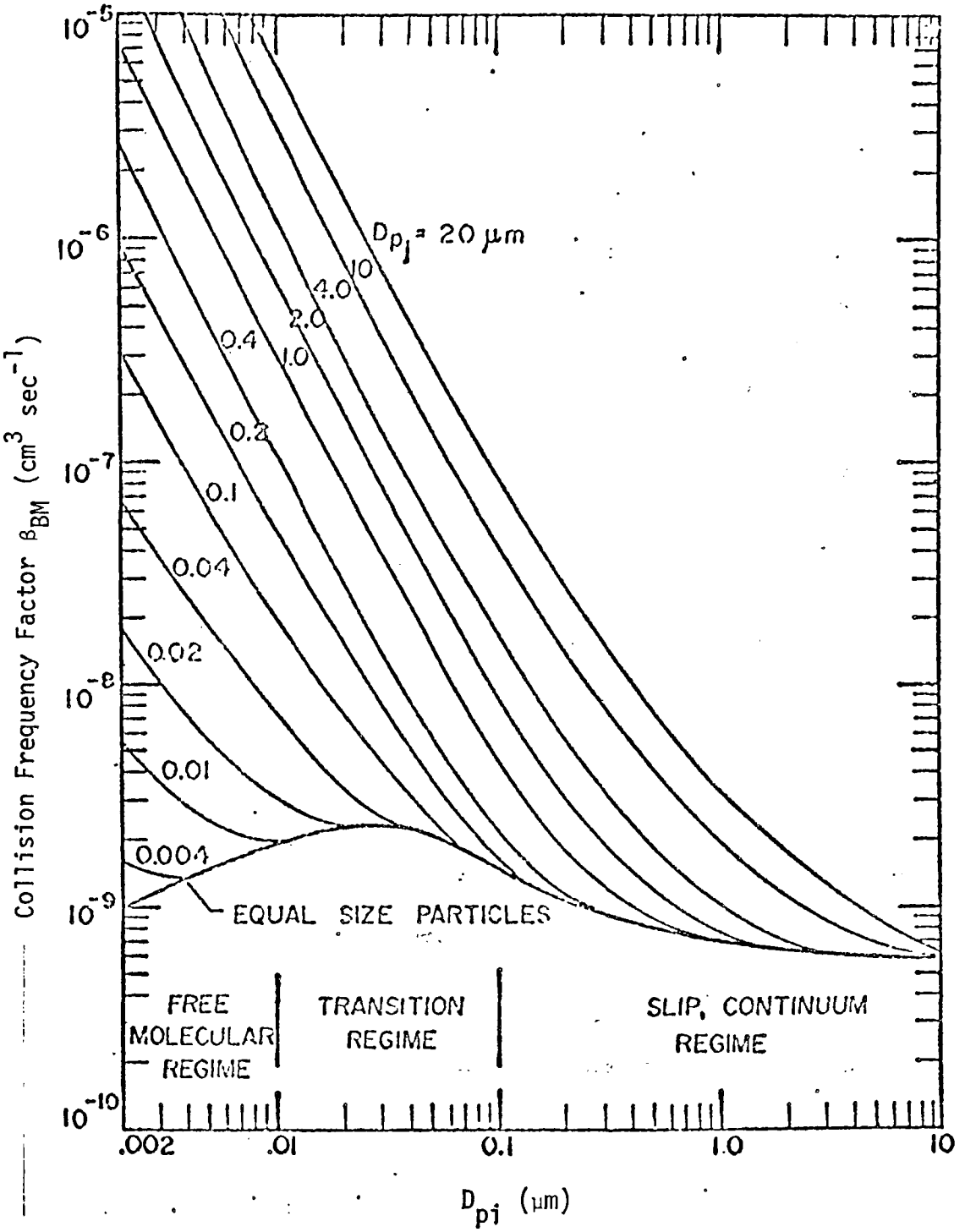

FIGURE 4. COLLISON FREQUENCY FACTORS β_{BM} FOR PARTICLES OF SIZE D_{pi} AND D_{pj}

Source: Husar (1971).

depends strongly on the ratio of the sizes of the two particles, D_{pi}/D_{pj}. To illustrate this dependence further, Figure 5 shows the normalized collision frequency factor,

$$\beta'_{BM} = \beta_{BM_{ij}}/\beta_{BM_{ii}}$$

versus the particle size ratio, D_{pi}/D_{pj}. In the continuum regime β'_{BM} increases roughly linearly with D_{pi}/D_{pj}, whereas in the free molecule regime, β'_{BM} approaches a quadratic dependence on D_{pi}/D_{pj}. The collision regime for two unequal size particles is determined essentially by the size of the larger particle.

b. Coagulation Due to Turbulent Shear

When particles exist in a turbulent fluid, the motion of fluid eddies brings particles in contact with each other. If the characteristic length scale of the eddies is larger than a characteristic particle size (which is always the case in the atmosphere), the following two processes can be responsible for collisions between particles:

> Spatial variations of the fluid velocities result in different velocities of neighboring particles.
> Particles--because of their inertia--may not follow fluid streamlines.

In the first case, collisions can occur between particles of equal or unequal size, whereas the second mechanism is restricted to different sized particles, since particles of equal size in close proximity have equal inertia in the same direction.

Saffman and Turner (1956) formulated a theory of coagulation due to turbulent shear. They derived an expression for the collision frequency factor in the form

$$\beta_{TS} = \frac{1.3}{8}(D_{pi} + D_{pj})^3\left(\frac{\varepsilon}{\nu}\right)^{1/2} , \qquad (33)$$

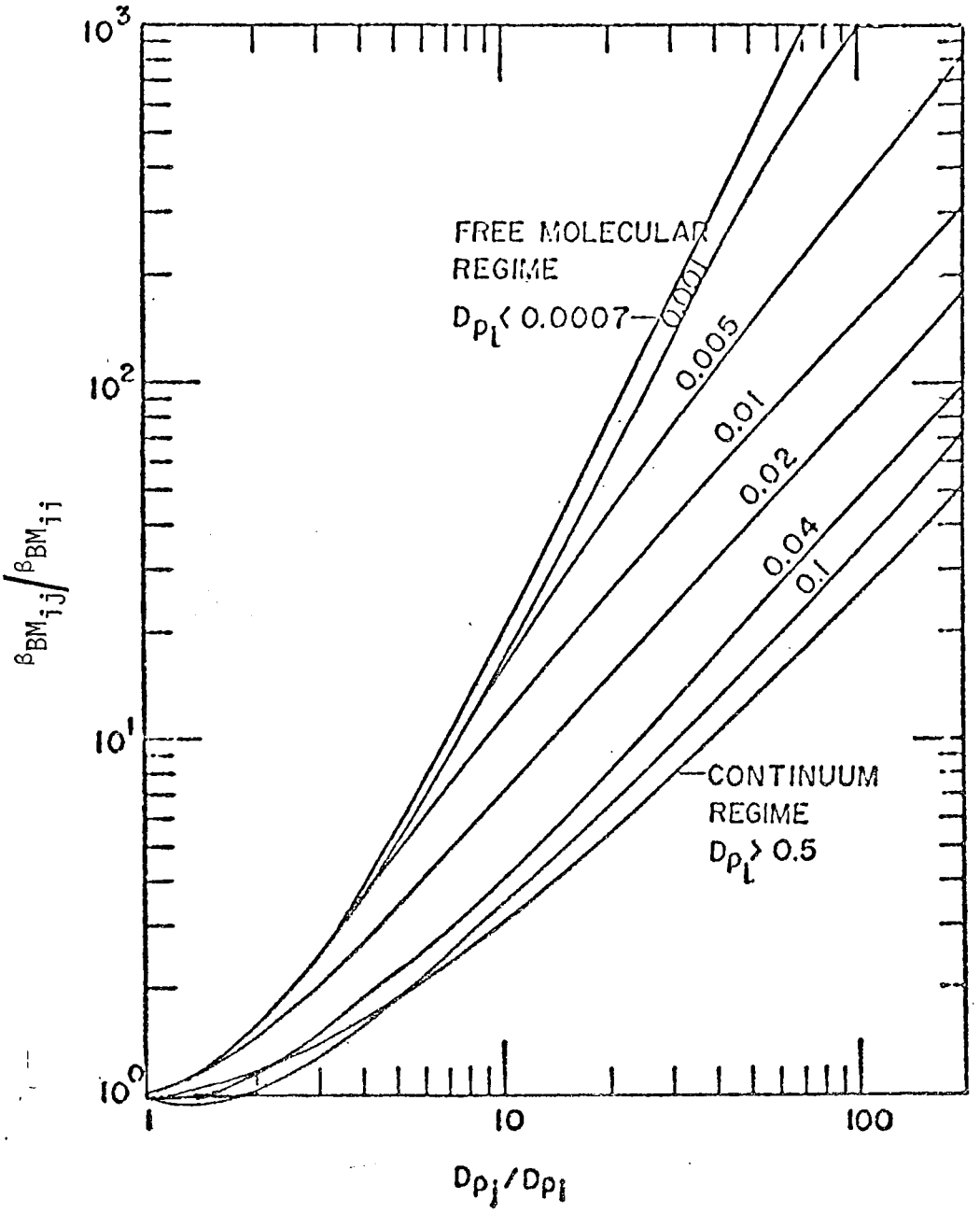

Source: Husar (1971).

FIGURE 5. THE NORMALIZED FREQUENCY FACTORS $\beta_{BM_{ij}}/\beta_{BM_{ii}}$ AS A FUNCTION OF NORMALIZED PARTICLE DIAMETER D_{pj}/D_{pi}

where ε is the local rate of energy dissipation in the small-scale turbulence and ν is the kinematic viscosity of the fluid. In this derivation, they neglected the effect of the particles on the velocity field.

c. Coagulation Due to Sedimentation

Coagulation can occur when particles of different masses are settling at their terminal velocities. The collision frequency factor in the limit as $D_{pi}/D_{pj} \rightarrow 0$ can be written as (Friedlander, 1964)

$$\beta_S = \frac{\pi D_{pi}^2}{8} \left| q_{s_j} - q_{s_i} \right| \quad , \tag{34}$$

where q_{s_j} is the terminal settling velocity of particle j:

$$q_{s_i} = \frac{\rho g D_{pi}^2}{24\pi\mu} \quad . \tag{35}$$

In this equation, ρ is the particle density. At 20°C,

$$\beta_s = \frac{\pi}{32} (1.3 \times 10^9) \, D_{pi}^2 \left| D_{pj}^2 - D_{pi}^2 \right| \quad . \tag{36}$$

In Eqs. (34) through (36), we assume that $D_{pi}^2 >> D_{pj}^2$.

d. Coagulation Due to Electrostatic Attraction

The effect of electrostatic forces on coagulation rates is difficult to assess, but we do not expect it to be significant in urban atmospheres.

e. Summary

The calculated collision parameters for the three mechanisms described above for the collisions of a 2 μm (from Hidy, 1973b) and a 0.2 μm diameter particle with particles of size D_{pj} are plotted in Figure 6. It is apparent that in the submicron size range collisions are dominated by the relative

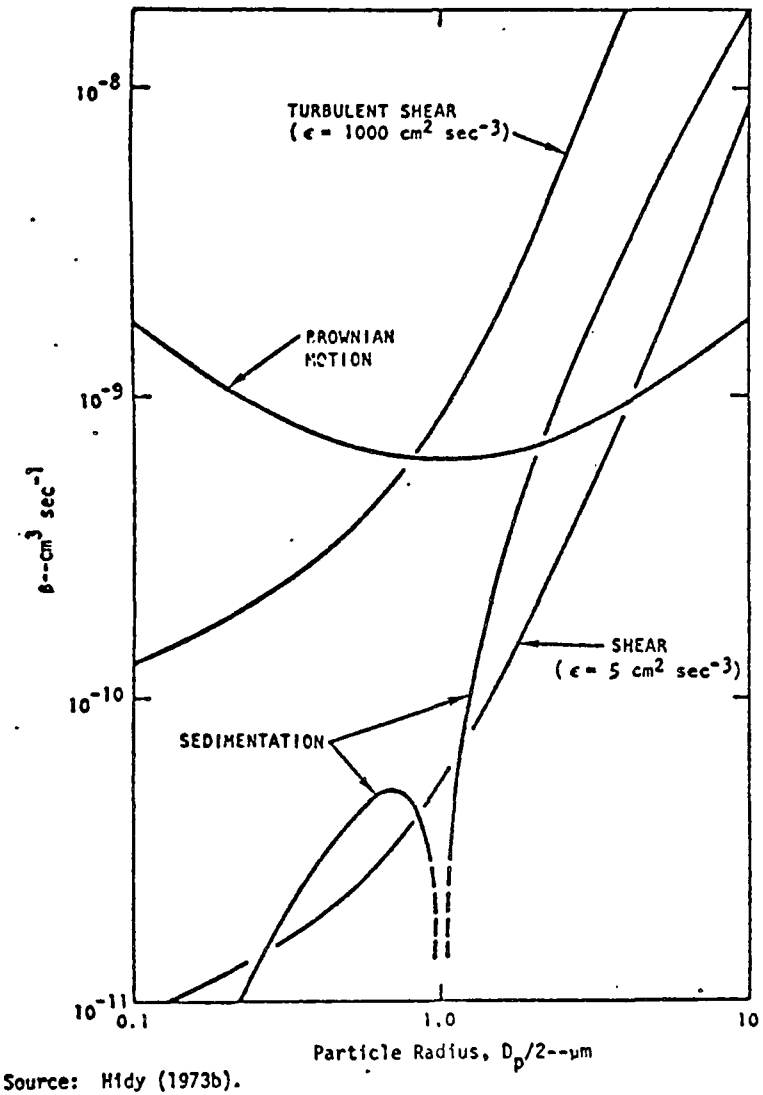

Source: Hidy (1973b).

(a) Collision of a Particle Whose Diameter is 2 μm with Particles of Various Sizes

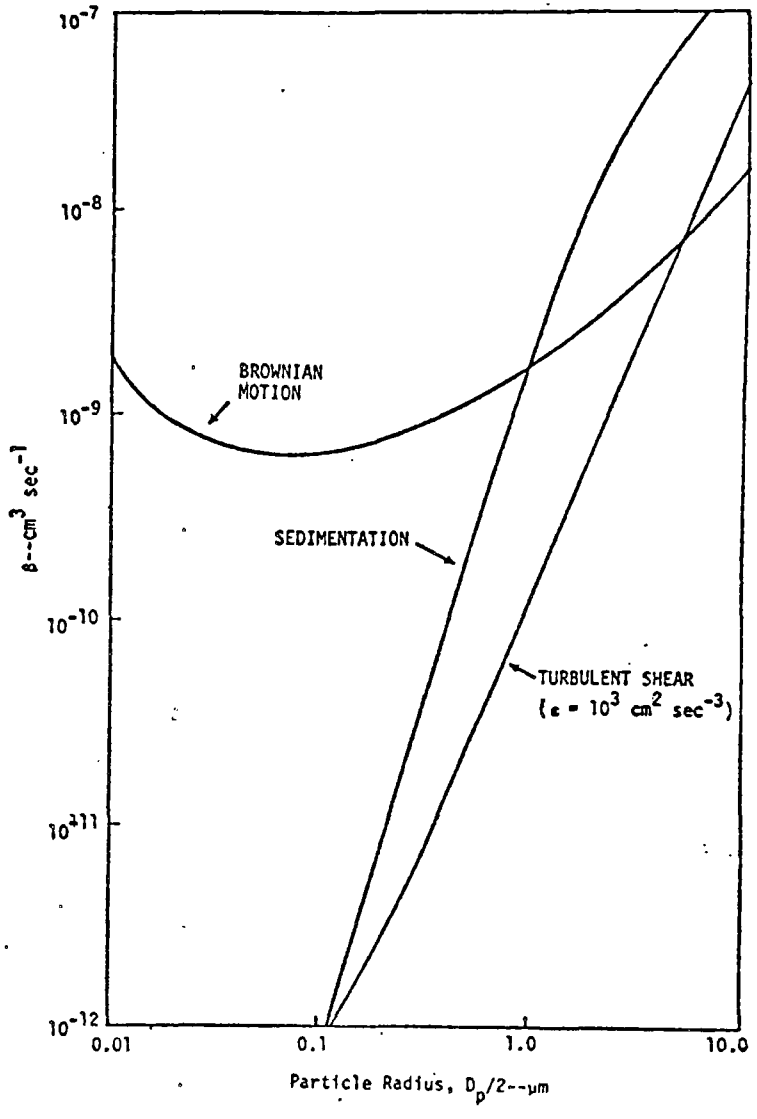

(b) Collision of a Particle Whose Diameter is 0.2 μm with Particles of Various Sizes

FIGURE 6. COMPARISON OF DIFFERENT COLLISION MECHANISMS IN THE LOS ANGELES AEROSOL

motion of particles due to their thermal velocities. For energy dissipation rates typical of ground-level atmospheric turbulence (ε = 1000 cm^2 sec^{-3}), turbulent coagulation becomes important for particles whose diameters are larger than 1 μm. An overall assessment of the role of coagulation in the atmosphere follows at the end of this chapter.

4. Turbulent Diffusion

We expect to find that turbulent diffusion is an important process shaping the distribution of particles found in the atmosphere. In particular, the mixing of emissions from the ground, both the gaseous emissions and primary particulate emissions, probably depends upon the stability of the atmosphere and the intensity of the turbulence in the mixed layer of the atmosphere.

Turbulent diffusion transports particles in all three coordinate directions. In the lowest layer of the atmosphere, turbulent diffusion in the vertical (z) direction is of primary interest. If we use an eddy diffusivity, K_{zz}, to characterize vertical turbulent diffusion, then the rate of change of the total particle number density in a unit volume of air can be written as

$$L_{TD} = K_{zz} \frac{\partial^2 N}{\partial z^2} \quad , \tag{37}$$

where, for the purpose of estimation, we assume that K_{zz} is constant. In the atmosphere, the turbulent diffusivity may range from 10^2 to 10^5 cm^2 sec^{-1}, depending on the proximity to the ground and the local hydrostatic stability. To calculate L_{TD}, we need an estimate of $\partial^2 N/\partial z^2$.

In the following subsection, we discuss the formulation of an expression for N(z) using a simple model and field data on the distribution of particle concentrations with height. We then use this expression for N(z) to calculate $\partial^2 N/\partial z^2$ in Eq. (37).

5. Gravitational Settling

Sedimentation, which is expected to be unimportant for particles whose diameters are less than 10 μm, provides an effective cutoff of the spectrum for particles larger than 50 μm in diameter. The rate of loss of particles per unit volume and time can be expressed as

$$L_{GS} = -q_s \frac{\partial N}{\partial z} \quad , \tag{38}$$

where q_s is the settling velocity and N is the total number density in the size range of interest. Assuming the Stokes law for the terminal velocity, we find that Eq. (38) becomes

$$L_{GS} = -0.32 \times 10^6 \, D_p^2 \frac{\partial N}{\partial z} \tag{39}$$

for particles of unit density in air at 20°C.

To calculate the rate of loss of particles from a unit volume of atmosphere by sedimentation, we must determine the gradient of the particle concentration in Eq. (39). Data are available that give the variation of particle concentration with altitude (Blifford and Ringer, 1969; Weickmann, 1955; Meszaros, 1969; Blumenthal et al., 1974). The fluctuations in the measurements from point to point and with altitude make it difficult to calculate a meaningful distribution of the particle number density from these field data. We therefore seek a simple way of estimating the particle density as a function of height in the atmosphere for use in estimating L_{GS} and L_{TD}.

Hidy (1972) has proposed a simple model of the height distribution of total particle number density in the atmosphere. In his formulation, the following assumptions were required to obtain the distribution:

> A quasi-stationary state exists in the particle distribution, that is, $\partial N/\partial t = 0$.
> The dominant physical processes affecting the distribution are turbulent diffusion and Brownian coagulation.
> The turbulent diffusivity has a constant value through the mixed layer.

These assumptions lead to the following differential equation for the particle distribution with height:

$$\frac{d^2x}{dy^2} - \gamma^2 x^2 = 0 \quad , \tag{40}$$

where

$x = N/N_0$,
$y = z/H$,
N, N_0 = the particle number densities at any height z and at z = 0, respectively,
H = a characteristic vertical length scale,
γ = an empirically determined constant that depends on the meteorological parameters and the ground-level concentration.

To formulate boundary conditions on Eq. (40), Hidy assumed that the concentration approaches a constant value as the distance from the ground becomes large. If one assumes that the concentration at the ground is constant, N_0, then the boundary conditions become

$$x = 1 \quad \text{at } y = 0$$

and (41)

$$\frac{dx}{dy} = 0 \quad \text{as } y \to \infty$$

A simple analytic solution to Eq. (40) with the boundary conditions given by Eq. (41) is

$$\frac{N}{N_0} = (1 + \gamma' z)^{-2} \quad , \tag{42}$$

where $\gamma' = \gamma/H$.

The assumptions made in obtaining Eq. (42) represent a gross oversimplification of the dynamics of urban aerosols. However, one might expect coagulation and turbulent diffusion to be the dominant mechanisms controlling the concentration of particles near the ground, particularly in source-enriched areas. Equation (42), with the adjustable parameter γ', can approximate the vertical distribution of particulate matter in the lower 1000 to 2000 feet of the atmosphere quite well. In Figure 7, we fitted the "grand average" distribution of condensation nuclei measured by Blumenthal et al. (1974) over El Monte, California. Below 2000 feet, Eq. (42) approximates the distribution of the condensation nuclei quite well. Thus, we use Eq. (42) to estimate $\partial N/\partial z$ and $\partial^2 N/\partial z^2$.

6. Deposition of Particles on Surfaces

The deposition of particles can occur through sedimentation, Brownian diffusion, or impaction. Impaction occurs when, because of its inertia, a particle is unable to follow the streamlines of air around an obstacle and is intercepted by the object. The removal of particles through impaction on an object can be defined in terms of a pseudo-deposition velocity q_g. The loss of particles per unit surface area of the object per unit time can then be expressed as

$$L_D^A = -q_g N \quad , \tag{43}$$

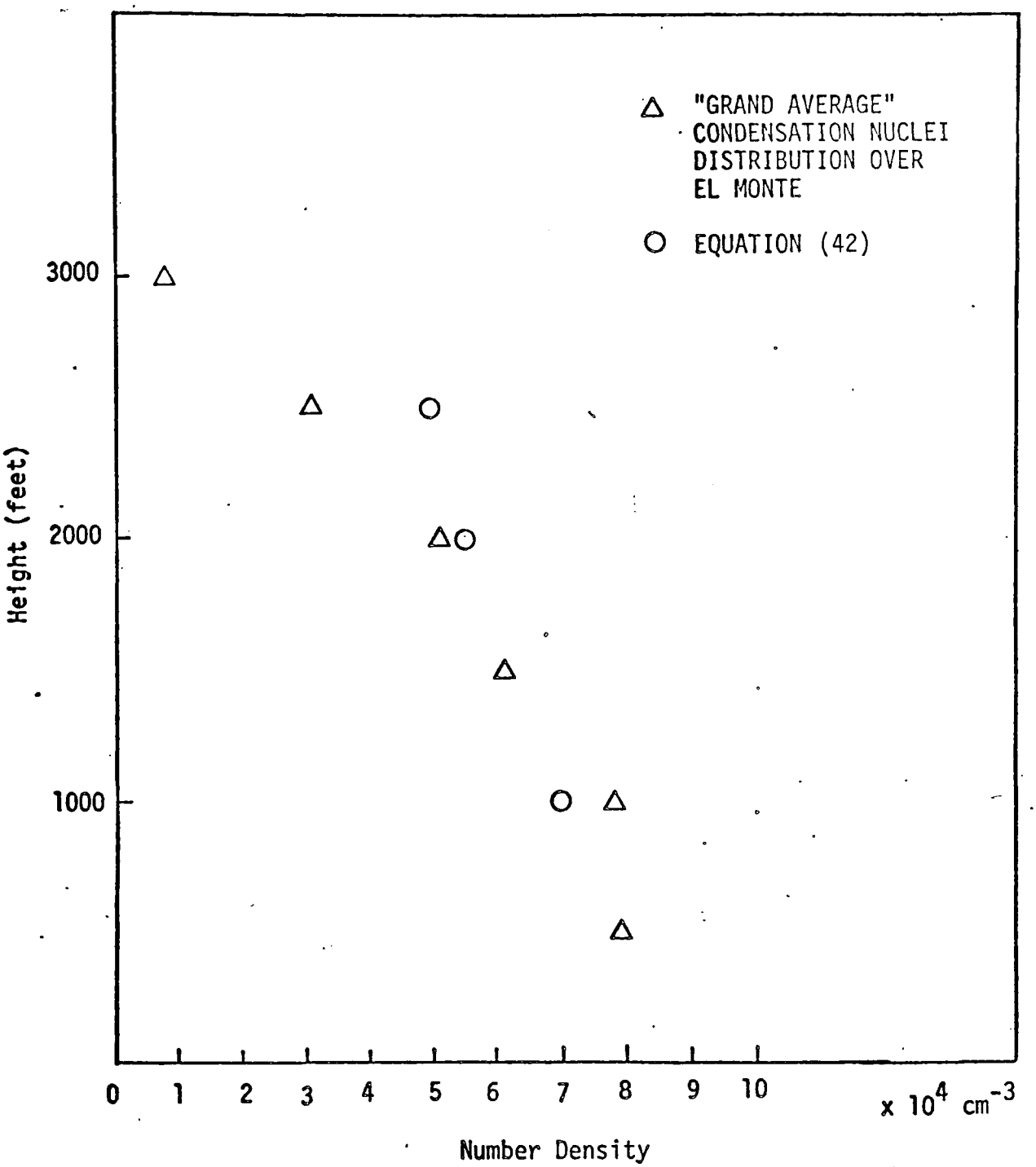

FIGURE 7. EQUATION (42) FITTED TO THE "GRAND AVERAGE" DATA OF BLUMENTHAL ET AL. (1974)

where N is the number density of particles in the size range corresponding to the deposition velocity q_g.

The transfer of aerosol particles from the turbulent atmosphere to an underlying bcundary depends upon the flow near the surface, as well as upon the nature of the surface itself. Particles are transferred through a turbulent boundary layer whose transport properties depend on the eddy motion of the turbulence. Near the surface, the particles move through a laminar sublayer, where the thermal motion of the particles becomes important.

Figure 8 presents values of q_g measured in a wind tunnel over a flat surface roughened with grass. In this figure, the terminal velocity of particles of unit density falling through air at 20°C has also been included to illustrate that the pseudo-deposition velocity of a particle is generally larger than the sedimentation velocity of a particle of the same size. The increase in q_g for particles smaller than 0.1 μm diameter might be expected from the increased mobility of small particles in the laminar sublayer.

Other factors, such as electrical charge and reentrainment of particles that have deposited on a surface, affect the magnitude of q_g. The relative importance of inertial effects, electrical charging, and reentrainment has been examined in a series of wind tunnel experiments with single conifer needles and conifer trees (Langer, 1965; Rosinski and Nagamoto, 1965). Langer (1965) observed no detectable effect of electrical charge on deposition losses for 2 μm diameter ZnS particles in simulated winds of 1.2 to 1.6 m sec^{-1}. In addition, Rosinski and Nagamoto (1965) observed that the rate of deposition on surfaces depends on the amount of material previously deposited on the surface; that is, the cohesive properties of the depositing material have a strong influence on the pseudo-deposition velocity.

It is apparent that the particle losses due to deposition strongly depend on the particle composition, the properties of the surface on which

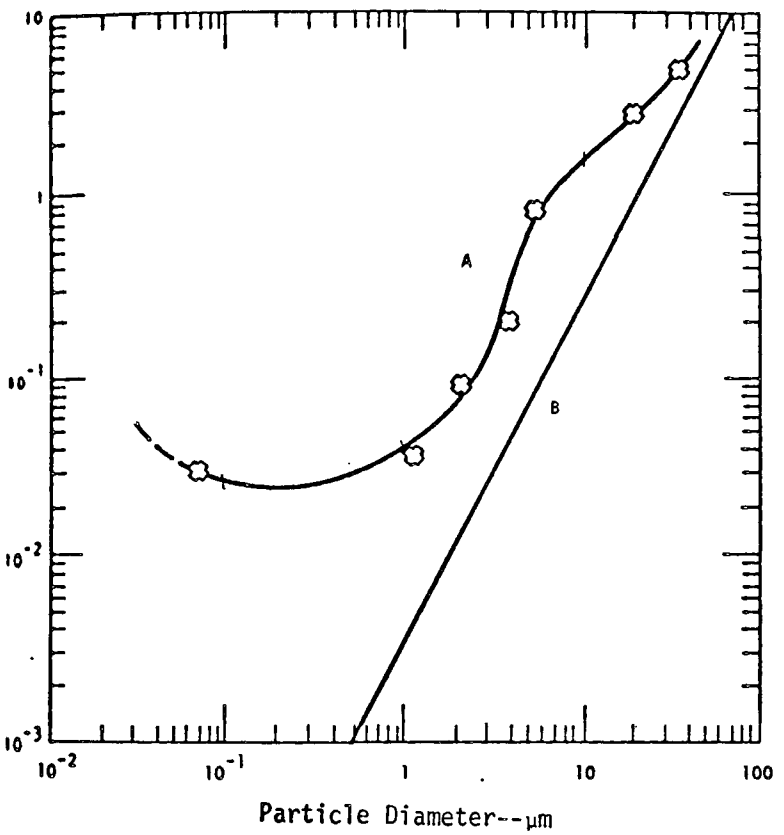

Source: Chamberlain (1967).

FIGURE 8. DEPOSITION VELOCITY AND TERMINAL SETTLING VELOCITY FOR FLOW OVER GRASS

material deposits, the surface roughness, and the wind speed. Hence, for the purposes of an order-of-magnitude estimate of deposition rates, we use below the results of Chamberlain (1967) to estimate q_g.

To compare the rate of loss from a unit volume of atmosphere due to the deposition of particles on a surface with other loss mechanisms, we must calculate the total loss on the surface boundary of the volume of interest. That is, the loss of particles by deposition per unit time per unit volume is given by

$$L_D = L_D^A \left(\frac{A}{V}\right) \quad , \tag{44}$$

where A denotes the surface area of obstacles bounding the volume, V, of interest. It is apparent then that the relative importance of depositional losses depends upon the buildings and the vegetation present in the modeling region.

7. Rainout and Washout of Aerosols

Precipitation can remove aerosols by two methods. Rainout involves the various processes taking place within a cloud that lead to the formation of raindrops. Washout refers to the removal of aerosols below the cloud by falling hydrometeors. In general, rainout is not an important process for the removal of urban aerosols because cloud formation takes place at elevations above the urban polluted layer.

The efficiency of removal of aerosols by washout depends on the size distributions of the aerosol and the raindrops, the solubility of the aerosol in water, and the total rainfall. The rate of removal of particles by collision with raindrops can be written as (Hidy, 1973b)

$$L_W = -n(D_{pi}) \int_0^\infty \frac{\pi}{4} (D_{pi}^2 + D_r^2)\, q_s(D_r)\, E_r(D_{pi}, D_r)\, g_r(D_r)\, dD_r \quad , \tag{45}$$

where $g_r(D_r)$ is the size distribution function for the raindrops and E_r represents the collection efficiency of aerosol particles in the size range D_{pi} to $D_{pi} + dD_{pi}$ with raindrops in the size range D_r to $D_r + dD_r$.

Langmuir and Blodgett (1946) obtained theoretical expressions for the collection efficiency of point masses flowing around spheres for the potential flow regime by incorporating the solution of Lamb (1932) for the potential flow around a sphere. If we assume that the raindrop is at rest and consider the flow around the droplet, the efficiency of collection of point mass aerosol particles by the raindrop is

$$E_r \approx \frac{(Stk)^2}{(Stk + 0.25)^2} \tag{46}$$

for $Stk \geq 0.2$, where the Stokes number, Stk, is equivalent to the ratio of the stop distance to the characteristic radius of the collecting sphere, defined by

$$Stk = \frac{q_{sr}\, \rho D_{pi}^2}{9\mu D_r} \quad . \tag{47}$$

Here, q_{sr} is the terminal velocity of the falling raindrop, μ is the viscosity of air, and ρ is the density of the aerosol particle.

Simple corrections to Eq. (46) are possible for aerosol particles of a finite diameter for two extreme cases: (1) when the inertia of a particle is so large that it moved in a straight line ($Stk >> 1$) and (2) when a particle possesses no inertia and moves along a streamline ($Stk = 0$). For the former case, one must consider the increase in the classical cross section for particle collisions, that is (Fuchs, 1964),

$$\Delta E_r = \frac{(D_{pi} + D_r)^2}{D_r^2} - 1 \quad ,$$

and the corrected collision efficiency becomes

$$E_r = \frac{(Stk)^2}{(Stk + 0.25)^2} + \left(\frac{D_{pi}}{D_r}\right)^2 + 2\left(\frac{D_{pi}}{D_r}\right) \quad . \tag{48}$$

If the terminal velocity of the raindrop is on the order of 4m sec^{-1}, the restriction Stk $\geq$ 0.2 limits the application of Eq. (48) to $D_p > 1.0$ μm if $D_r = 0.05$ cm and the aerosol particles have unit density. For small particles that diffuse to the raindrop, Slinn (1967) calculated the collection efficiency to be

$$E_r \simeq \frac{D}{q_{sr}D_r} \simeq \frac{4kT}{3\pi q_{sr}\mu D_r D_p} \quad , \tag{49}$$

where k denotes Boltzmann's constant, μ is the viscosity of air, and T is the temperature.

C. SUMMARY OF IMPORTANT PHYSICAL PROCESSES IN THE EVOLUTION OF PHOTOCHEMICAL AEROSOLS

In this chapter, we have discussed the importance of the following physical processes to the dynamics of photochemical aerosols:

- Homogeneous nucleation
- Heterogeneous condensation
- Coagulation
- Turbulent diffusion
- Gravitational settling
- Deposition on surfaces
- Washout.

With respect to homogeneous nucleation and heterogeneous condensation, the number density of particles in the atmosphere is sufficient to accommodate the condensation of supersaturated gaseous species; thus, homogeneous nucleation can be neglected relative to heterogeneous condensation.

Observations of the Los Angeles aerosol indicate that the aerosol volume in the diameter size range 0.1 μm < D_p < 1.0 μm grows at the rate of 10 to 40 $\mu m^3\ cm^{-3}$-hr (Husar, Whitby, and Liu, 1972). Two possible mechanisms responsible for this growth are heterogeneous condensation and coagulation. Coagulation of particles in the size range 0.1 to 1.0 μm diameter with particles of size 0.05 μm at respective number densities of 10^2 and 10^5 cm^{-3} and at a collision frequency factor of $10^{-1}\ cm^3\ sec^{-1}$ would transfer mass into the 0.1 to 1.0 μm size range at a rate of only 0.25 $\mu m^3\ cm^{-3}\ hr^{-1}$. Thus, coagulation cannot be responsible for the observed rate of volume increase of photochemical aerosols; heterogeneous condensation is the primary growth mechanism for photochemical aerosols.

For the purposes of formulating a model of the evolution of the particle number density distribution, $n(D_p,t)$, we would like to know the relative order of magnitude of the processes that remove or add particles from the infinitesimal size range D_p to $D_p + dD_p$ containing the infinitesimal number of particles $dN = n(D_p,t)dD_p$. To estimate the rate at which particles are transferred into and out of these size ranges, we divided the particle size spectrum into three size ranges: D_p < 0.1 μm, 0.1 < D_p < 1.0 μm, and D_p > 1.0 μm, in which the number densities were assumed to be:

D_p < 0.1 μm	0.1 < D_p < 1.0 μm	D_p > 1.0 μm
$10^5\ cm^{-3}$	$10^2\ cm^{-3}$	$10^{-1}\ cm^{-3}$

For each of these broad size ranges, we assumed that the particle sizes were (for the purposes of these calculations) 0.05 μm, 0.5 μm, and 5.0 μm, respectively. Table 8 summarizes the results of these calculations.

Table 8

ESTIMATED RATES OF CHANGE OF AEROSOL NUMBER DENSITIES IN THE URBAN ATMOSPHERE

(In Particles per Cubic Centimeter per Second)

Process	Size Range		
	$D_{pi} < 0.1$ μm*	0.1 μm $\leq D_{pi} \leq 1.0$ μm†	$D_{pi} > 1.0$ μm§
Heterogeneous condensation** (Sulfate)			
50 percent conversion	10^4	1	10^{-5}
10 percent conversion	10^3	0.1	10^{-6}
1 percent conversion	10^2	0.01	10^{-7}
Heterogeneous†† condensation (hydrocarbons)	10^3	0.01	10^{-7}
Coagulation			
Brownian	1	10^{-4}	10^{-6}
Turbulent ($\varepsilon = 10^3$ cm^2 sec^{-3})	10^{-3}	10^{-3}	10^{-4}
Sedimentation ($D_{pj} = 10$ μm)	10^{-4}	10^{-8}	10^{-9}
Turbulent diffusion ($D_T = 10^5$ cm^2 sec^{-1})	1	10^{-3}	10^{-6}
Gravitational settling	10^{-5}	10^{-6}	10^{-7}
Deposition on surfaces□	10^3 (A/V)	(A/V)	10^{-1} (A/V)
Washout△	10^{-4}	10^{-8}	10^{-4}

* Assuming that $D_{pi} = 0.05$ μm for all particles and that the number density is 10^5 cm^{-3}.

† Assuming that $D_{pi} = 0.5$ μm for all particles and that the number density is 10^2 cm^{-3}.

§ Assuming that $D_{pi} = 5$ μm for all particles and that the number density is 10^{-1} cm^{-3}.

** Percentage conversions of 0.3 ppm SO_2.

†† Rate of condensation of 5 ppb of adipic acid.

□ The quantity (A/V) represents the ratio of the obstacle surface area and the volume of interest (A/V has the units cm^{-1}).

△ Assuming that the raindrops are 1 mm in diameter at a number density of 10^{-3} cm^{-3}.

Because of the approximations made in estimating the order of magnitude of the physical processes listed in Table 8, some care must be taken in drawing conclusions from the results included in this table. The assumptions we made to determine the order of magnitude of the turbulent diffusion term should give lower values than expected (we discuss this subsequently). We conclude from these results that for the length scales and the time scales for which an aerosol model will be developed, heterogeneous condensation and turbulent diffusion are the mechanisms that play dominant roles in the evolution of the spatial and size distribution of the aerosol. In the following subsections, we summarize the equations and numbers used in the calculation of the values in Table 8.

1. Coagulation

We used Eq. (28) to calculate the loss rate of particles of sizes ranging from D_{pi} to $D_{pi} + dD_{pi}$ that collide with others in the size range D_{pj} to $D_{pj} + dD_{pj}$ for collisions due to Brownian motion, turbulent shear, or differential sedimentation.

a. Brownian Coagulation

Since most particles are in the size range $D_p < 0.1$ μm, the rate of transfer of particles into or out of the size range D_p to $D_p + dD_p$ due to collisions with other particles is greatest for collisions with particles of radius less than 0.1 μm. For each size range, we used Eqs. (28) and (32) to calculate the rate of transfer through Brownian coagulation with $\mu = 1.83 \times 10^{-4}$ g cm^{-1} sec^{-1}, $k = 1.38 \times 10^{-16}$ ergs $^{\circ}$K^{-1}, T = 300°K, and

$D_p < 0.1$ μm	0.1 μm $< D_p < 1.0$ μm	$D_p > 1.0$ μm
$D_{pi} = D_{pj} = 0.05$ μm	$D_{pi} = 0.5$ μm	$D_{pi} = 0.05$ μm
$N_i = N_j = 10^5$ cm^{-3}	$D_{pj} = 0.05$ μm	$D_{pj} = 5$ μm
	$N_i = 10^2$ cm^{-3}	$N_i = 10^{-1}$ cm^{-3}
	$N_j = 10^5$ cm^{-3}	$N_j = 10^5$ cm^{-3}

b. Turbulent Shear

Similarly, collisions due to turbulent shear occur primarily with particles of diameter $D_p < 0.1$ μm. We used Eq. (33) for the calculation with Eq. (28). The local rate of energy dissipation in the small-scale turbulence had the value 1000 cm^2 sec^{-3} and $\nu = 0.1$ cm^2 sec^{-1}. The particle diameters and the number density were the same as those used for the calculation of Brownian coagulation.

c. Differential Sedimentation

We used the collision parameter in Eq. (36) in Eq. (28) to calculate the loss due to differential sedimentation. Because of the rapid increase in collision rate with particle diameter ($\sim D_p^4$), we assumed that $D_{pj} = 10$ μm for this calculation and that $N_j = 10^{-1}$ cm^{-3}. The values of the particle diameter and number density in each size range were the same as those used in the previous calculations.

2. Heterogeneous Condensation

To calculate the rate of loss of particles from a given size range due to gas-to-particle conversion, we assumed that the loss rate is proportional to the rate of change of particle size in each size range and the number of particles in the size range. We calculated the loss rate due to condensation on particles in the size range D_{pi} to $D_{pi} + dD_{pi}$ from

$$L_c = N_i \frac{1}{D_{pi}} \frac{dD_{pi}}{dt} \quad , \tag{50}$$

where we obtained the rate of particle growth from Eq. (15). The loss rate from a given size range by condensation is then

$$L_c = \frac{4DMp_s^o(T_\infty)\, N_i}{\rho_L R T_\infty D_{pi}^2} \left[S - \gamma x \exp\left(\frac{4\sigma V_L}{R T_\infty D_{pi}} \right) \right] \quad . \tag{51}$$

for the growth of a binary droplet.

We calculated the order of magnitude of the loss for the conversion of sulfuric acid and adipic acid as indicated in Table 8. The three numbers listed for H_2SO_4 represent the conversion of 50, 10, and 1 percent of a 0.3 ppm concentration of SO_2. The other values used in the calculation were:

$D = 0.07\ cm^2\ sec^{-1}$,
$M = 98\ g\ mole^{-1}$,
$p_s^o(T_\infty) = 1.3 \times 10^{-3}$ dynes cm^{-2} (Doyle, 1961),
$\rho_L = 1.87\ g\ cm^{-3}$,
$T_\infty = 300\ ^oK$,
$\gamma x = 1$,
$\sigma = 52$ dynes cm^{-1} [International Critical Tables (1928)].

We also calculated the rate of loss of particles due to diffusion of adipic acid to the surface of the particle. Because adipic acid does not appear to be saturated for reasonable gas phase concentrations, we calculated a maximum value for the rate of diffusion; that is, we assumed that the concentration of adipic acid in the droplet was zero, $x = 0$. We assumed a concentration of adipic acid of 5 ppb, corresponding to roughly a 10 percent conversion of all reactive hydrocarbons. The values of the other quantities used in the calculation were

$D = 0.07\ cm^2\ sec^{-1}$,
$M = 150\ g\ mole^{-1}$,
$p_s^o(T_\infty) = 2.6 \times 10^{-2}$ dynes cm^{-2},
$\rho_L = 0.94\ g\ cm^{-3}$,
$T_\infty = 300\ ^oK$.

3. Turbulent Diffusion

We calculated the values listed in Table 8 for the removal rate of particles from a unit volume of atmosphere due to turbulent diffusion at $z = 0$ from Eqs. (37) and (42) with $K_{zz} = 10^5$ cm^2 sec^{-1} and $\gamma' = 5 \times 10^{-6}$ cm^{-1}. Unfortunately, the technique we employed to calculate the order of magnitude of the turbulent diffusion term relies on a smoothed function of time-averaged data. In the real atmosphere, the distribution of the particle concentration is not monotonic as we represented it, and the transport of mass due to diffusion from one volume element to another is far greater than our calculations indicate. Therefore, in formulating a model, we will retain the turbulent diffusion term along with the diffusion-controlled growth term.

4. Gravitational Settling

We calculated the order of magnitude of losses from a unit volume of atmosphere by gravitational settling for particles of unit density in air at 20°C using Eq. (39). To compute the gradient of the particle number density, we used Eq. (47) and the concentration data reported by Blumenthal et al. (1974). For the data shown in Figure 7, we found the parameter γ' to be 5×10^{-6} cm^{-1}.

The data actually apply only to sizes smaller than 0.1 μm, the size range that contains most of the number density. However, there are little reliable data on the vertical distribution of larger particles; therefore, for the purposes of this calculation, we assumed that Eq. (42) can also be applied to larger particles. We calculated the loss of particles from a unit volume of air due to sedimentation from Eqs. (39) and (42) at $z = 0$ or

$$L_{GS} = 3.2\ D_p^2 N_0 \tag{52}$$

using values of D_p and N_0 given previously for each size range.

5. Deposition of Particles on Surfaces

To calculate the losses of particles per unit volume per unit time due to deposition, we used Eqs. (43) and (44). From the data of Chamberlain (1967), we computed the following deposition velocities:

$$D_p = 0.05\ \mu m \quad , \quad q_g = 2.7 \times 10^{-2}\ cm\ sec^{-1} \quad ,$$

$$D_p = 0.5\ \mu m \quad , \quad q_g = 4 \times 10^{-2}\ cm\ sec^{-1} \quad ,$$

$$D_p = 5.0\ \mu m \quad , \quad q_g = 1.0\ cm\ sec^{-1} \quad ,$$

It is apparent from the results of our calculations that losses due to deposition on surfaces are important only when the obstacle surface area is large. Such situations might arise in forested areas or in urban areas where buildings are tall and closely spaced. However, in general, for the modeling regions of interest, $A/V << 1\ cm^{-1}$, and deposition losses can be neglected in comparison with other processes shaping the aerosol concentration in the atmosphere.

6. Washout of Aerosols

To calculate the effect of washout on the concentration of particles of diameter D_p in the atmosphere, we assumed that we can consider the properties of all droplets to be given by the properties of an average size droplet of diameter $\overline{D}_r = 0.05$ cm. Under this assumption, for $\overline{D}_r >> D_p$, we can rewrite Eq. (45)

$$L_W = -N(D_{pi})\ \frac{\pi}{4}\ \overline{D}_r^2\ q_{sr}(\overline{D}_r)\ E_r\left(\frac{D_p}{\overline{D}_r}\right)\int_0^\infty g(D_r)\ dD_r \quad ,$$

where all functions outside of the integral are evaluated for the raindrop of mean diameter $\overline{D}_r$. For the purposes of the calculations presented in Table 8, we assumed that the total concentration of raindrops was 10^{-3} cm^{-3} and that the terminal velocity of the raindrops was approximated by $q_{sr}(\overline{D}_r) = 4m\ sec^{-1}$. For submicron aerosol particles, we calculated the collection efficiency from Eq. (49); and for aerosol particles with diameters greater than 1.0 μm, we calculated the collection efficiency from Eq. (48). We used the molecular viscosity of air at 20°C in Eqs. (47) and (49), and we assumed that the density of the aerosol particles was that of water.

III CHEMICAL PROCESSES INFLUENCING THE FORMATION OF AEROSOLS IN PHOTOCHEMICAL SMOG

The physical processes that influence photochemical aerosols mainly determine the size distribution of the aerosol. Although heterogeneous condensation could equally well be classified as a chemical process, we chose to include it in the discussion of physical processes because of its strong influence on the aerosol size distribution. In this chapter, we briefly consider those aspects of aerosol chemistry which are important in the study of photochemical aerosols. Our main objective in this examination is to summarize what is currently known and to indicate what is unknown about the chemistry of photochemical aerosols. This discussion is intended not as an exhaustive survey of photochemical aerosol chemistry, but rather as an analysis of the chemical information ultimately required in formulating a dynamic model for photochemical aerosols.

We first summarize experimental measurements of the chemical composition of the Los Angeles aerosol, with particular emphasis on compounds of sulfur, nitrogen, and carbon. Then we discuss the apparent rates of conversion of gaseous sulfur, nitrogen, and carbon to the corresponding particulate forms. Finally, we speculate on the homogeneous and heterogeneous reaction mechanisms that might account for the observed rates of atmospheric conversion and the species found in the particulate phase.

A. THE CHEMICAL COMPOSITION OF THE LOS ANGELES AEROSOL

The 1969 and 1972 to 1973 Los Angeles aerosol characterization studies provided considerable data on the chemical composition of aerosols in photochemical smog [see, for example, Hidy and Friedlander (1971), Miller et al. (1972), Friedlander (1973), Hidy et al. (1975)]. On the basis

of the data from these studies, one can represent the composition of typical photochemical aerosols in a π diagram as in Figure 9. This pie diagram represents the collected aerosol mass equilibrated to air at less than 50 percent relative humidity based on 1969 and earlier results. The upper half of the figure shows secondary constituents, and the lower half, primary constituents. Although this figure indicates that nitrate comprises only about 2 percent of the aerosol mass, most data now indicate a nitrate concentration of 10 to 20 percent. Thus, roughly one-half of the aerosol mass is a result of secondary conversions of gaseous species. In addition, compounds of sulfur, nitrogen, and carbon are of prime importance in the secondary fraction of photochemical aerosols.

In this section, we summarize recent data on the composition of the Los Angeles aerosol, focusing particular attention on compounds of sulfur, nitrogen, and carbon. The objective of the summary is to ascertain typical aerosol constituencies and, thus, to provide background for a discussion of chemical processes important in aerosol dynamics.

1. The Spatial Distribution of Sulfate and Nitrate

Sulfur oxide emissions in the Los Angeles basin basically originate from the following:

Source	Percent
Stationary sources (power plants)	49%
Sulfur recovery plants	20
Transportation	15
Petroleum refining	12

Although sulfur oxide emissions appear almost totally as SO_2, in the atmosphere SO_2 can be oxidized to sulfate ($SO_4^{=}$). Measured annual averages indicate that sulfate levels are rather uniformly distributed over the Los Angeles basin and that they range from 9 to 15 $\mu g\ m^{-3}$. Average ambient $SO_2/SO_4^{=}$ ratios vary from about 3 or 4 in coastal areas to about 1.5 to 2 in the inland areas. Since the concentration of $SO_4^{=}$ is relatively uniform

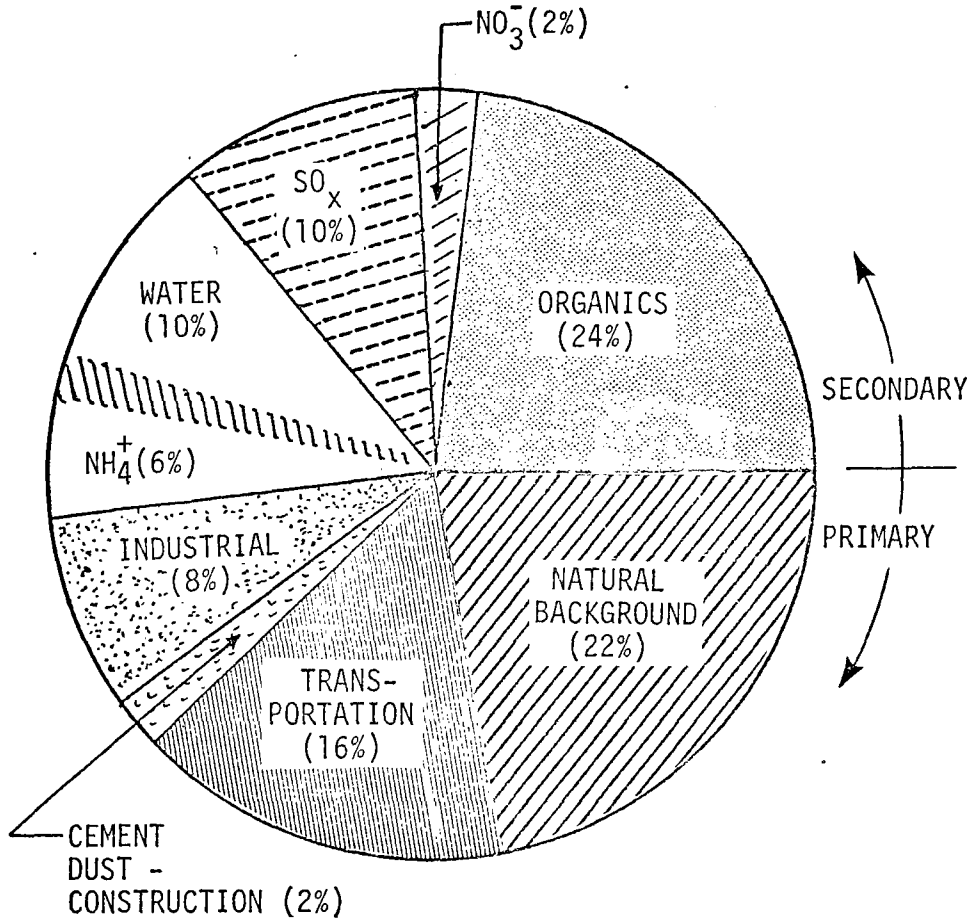

Source: Hidy et al. (1975).

FIGURE 9. THE CONTRIBUTION OF VARIOUS SOURCES TO THE TOTAL AEROSOL MASS IN THE LOS ANGELES BASIN

spatially, this variation in ratio probably reflects the fact that most of the SO_2 sources are located in the coastal regions and that SO_2 is diluted and dispersed as it is carried eastward. The uniformity of $SO_4^{=}$ levels probably indicates a general balance between dilution effects and the oxidation of SO_2 to $SO_4^{=}$. The average sulfate background level in Los Angeles has been estimated as 4 μg m^{-3}. Thus, of the typical 9 to 15 μg m^{-3} annual average sulfate, only about 5 to 11 μg m^{-3} originate from man-made sources.

Table 9 shows 24-hour average high-volume sample data from the ACHEX obtained at different times during the 1972 to 1973 period. Table 10 shows similar data, obtained from the National Air Surveillance Network (NASN) in 1968, based on 26 sampling periods at each location. These data tend to confirm the following (Appel et al., 1974):

> Nitrate and sulfate together often comprised more than 15 percent of the total aerosol mass in Los Angeles on a 24-hour average basis.

> Twenty-four-hour average values of sulfate and nitrate in Los Angeles were on the order of 15 μg m^{-3} and 10 μg m^{-3}, respectively.

2. The Diurnal Patterns of Sulfate and Nitrate

Figure 10 shows the diurnal pattern of sulfate, total carbon, ozone, and SO_2 at West Covina on 23-24 July 1973. The diurnal behavior of sulfate parallels that of the other pollutants shown. Figure 11 shows the diurnal variation of sulfate, nitrate, and NO_x for the same location and time period. In contrast to sulfate, the diurnal behavior of total nitrate mass typically exhibits its maximum in the morning, close to the maximum in NO_x. At first glance, this observation seems inconsistent with the observation that nitrate levels increase as the air travels eastward. However, an examination of the diurnal behavior of the size distributions of sulfate and nitrate provides some insight into this problem.

Table 9

ACHEX DATA FOR NITRATE AND SULFATE IN THE SOUTH COAST BASIN
1972 TO 1973

(24-Hour Average Values)

Sampling Location	No. of Episodes	Nitrate		Sulfate	
		$\mu g\ m^{-3}$	Percent of Mass	$\mu g\ m^{-3}$	Percent of Mass
Harbor Freeway	2	6.3	5.6%	5.7	5.1%
Dominguez Hills	2	4.1	3.1	17.8	13.6
Pasadena	6	6.5	9.0	7.0	9.7
West Covina	5	8.2	4.5	21.8	12.0
Pomona					
1972	5	19.8	14.6	9.6	7.1
1973	2	7.9	4.8	11.5	7.0
Rubidoux	3	31.5	12.5	10.7	4.2
Riverside	9	15.2	13.4	7.7	6.8

* Analyses of high-volume samples collected on Whatman-41 filters during July to October periods.

Source: Appel et al. (1974).

Table 10

NASN DATA FOR NITRATE AND SULFATE
IN THE SOUTH COAST BASIN FOR 1968

(Annual 24-Hour Average Values*†)

Sampling Location	Nitrate		Sulfate	
	$\mu g\ m^{-3}$	Percent of Mass	$\mu g\ m^{-3}$	Percent of Mass
Long Beach	5.7	5.0%	12.7	11.1%
Los Angeles	7.7	6.0	10.2	7.9
Ontario	9.1	7.9	9.0	7.8
Riverside	10.2	8.8	8.3	7.2

* From air quality data for 1968 obtained by the National Air Surveillance Network and contributing state and local networks, EPA, Research Triangle Park (1972).

† Data were based on the geometric mean of 26 24-hour sampling periods.

Source: Appel et al. (1974).

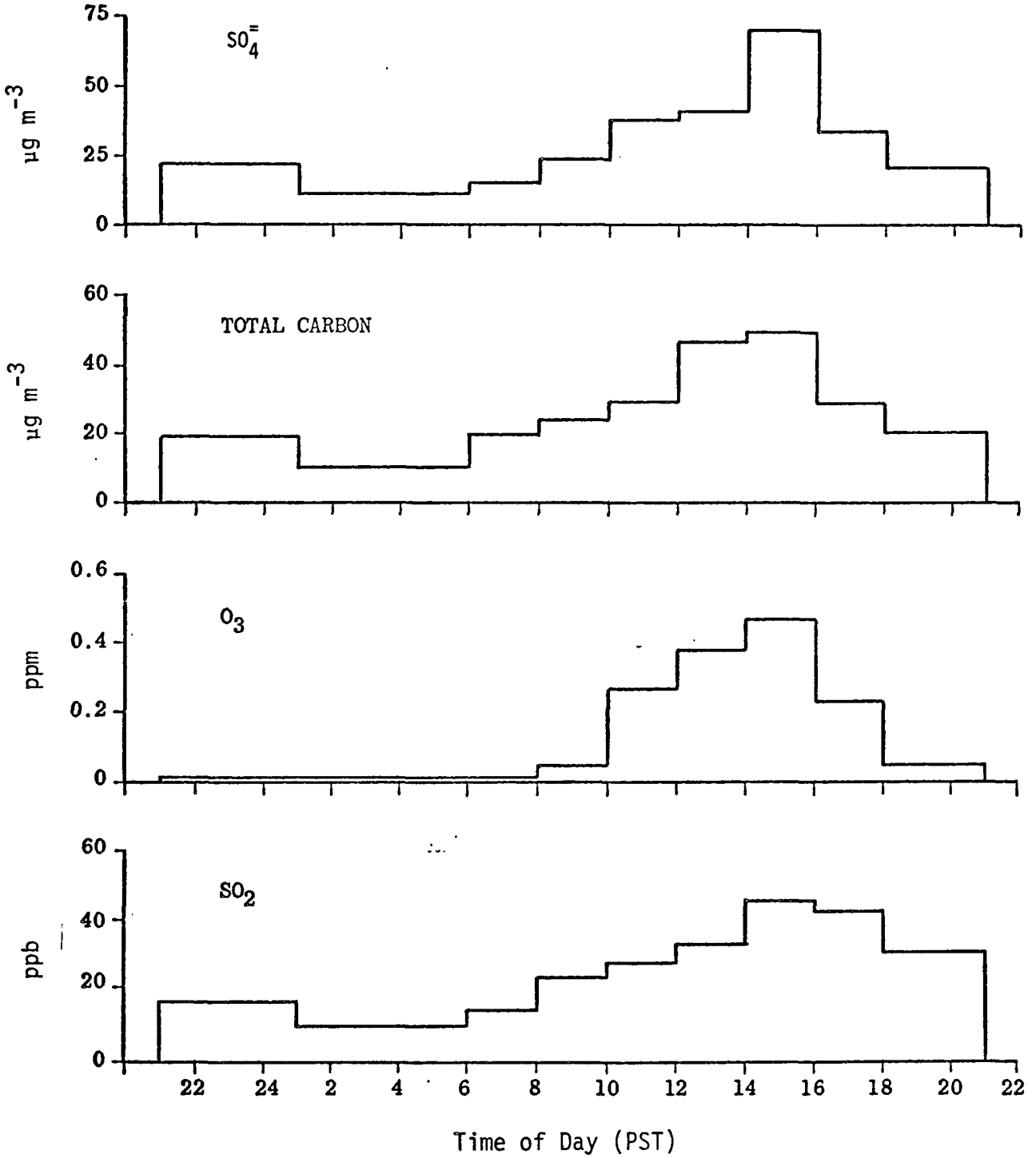

Source: Appel et al. (1974).

FIGURE 10. DIURNAL VARIATIONS FOR SULFATE AND SELECTED POLLUTANTS AT WEST COVINA ON 23-24 JULY 1973

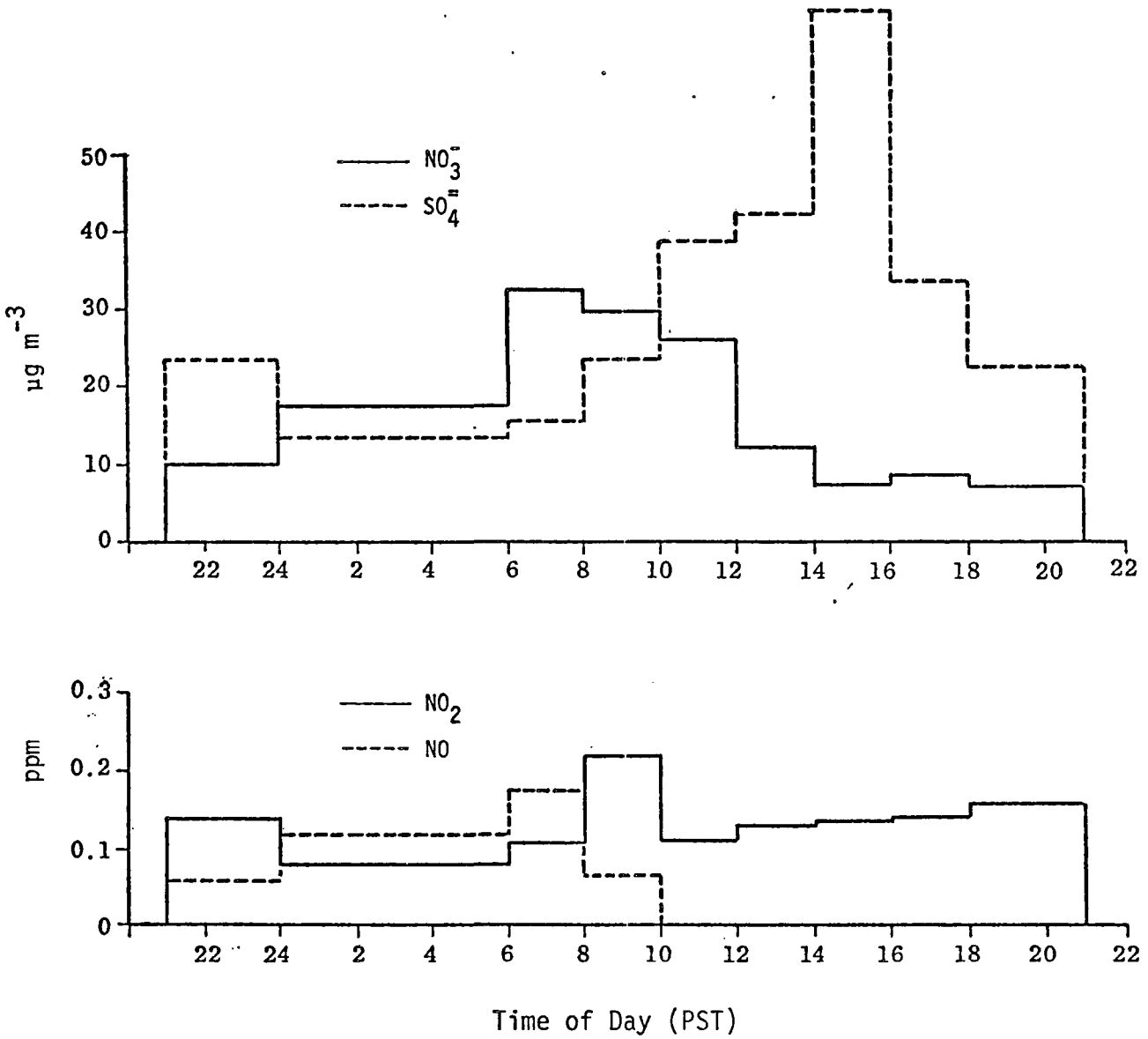

Source: Appel et al. (1974).

FIGURE 11. DIURNAL VARIATIONS FOR NITRATE, SULFATE, AND NO_x AT WEST COVINA ON 23-24 JULY 1973

Figure 12 shows the diurnal variations in concentration of the total nitrate and sulfate masses and of only those particles less than 0.5 μm in diameter at West Covina on 23-24 July 1973. The total sulfate level reached a maximum at about 1600 hours, probably as a result of the transport to West Covina of particles produced earlier in the day in the western regions of the basin. The increased fraction of sulfur contained in particles whose diameters were less than 0.5 μm reflects the fact that freshly produced sulfate is generally associated with particles smaller than 0.5 μm. From the curves for total nitrate mass concentration and nitrate mass concentration of particles smaller than 0.5 μm in diameter, it is clear that the early morning nitrate peak was associated mainly with particles larger than 0.5 μm. The decrease in the total nitrate mass concentration was due to transport away from the site. Although the peak in the curve for nitrate particles smaller than 0.5 μm is not pronounced, during the late morning and afternoon the fraction of nitrate particles that are smaller than 0.5 μm increased substantially. Apparently, later in the day nitrate is produced on particles smaller than 0.5 μm. The implication is that there may exist two nitrate-forming mechanisms: one in the early morning associated with particles larger than 0.5 μm and one later in the day associated with particles smaller than 0.5 μm. The sulfate and nitrate size distributions in aged aerosols are rather similar, even though the original mechanisms of incorporation may be quite different.

Mass median particle diameters determined during the ACHEX for sulfate and nitrate fall in the ranges of 0.3 to 0.4 μm and 0.6 to 1.2 μm, respectively.

3. Sulfur, Nitrogen, and Carbon Composition of the Los Angeles Aerosol

Table 11 summarizes sulfate, nitrate, and solvent extractable organic concentrations at three sites in the South Coast air basin during 1972. Table 12 shows additional data obtained from an analysis of 24-hour average high-volume filter samples during the 1972 program.

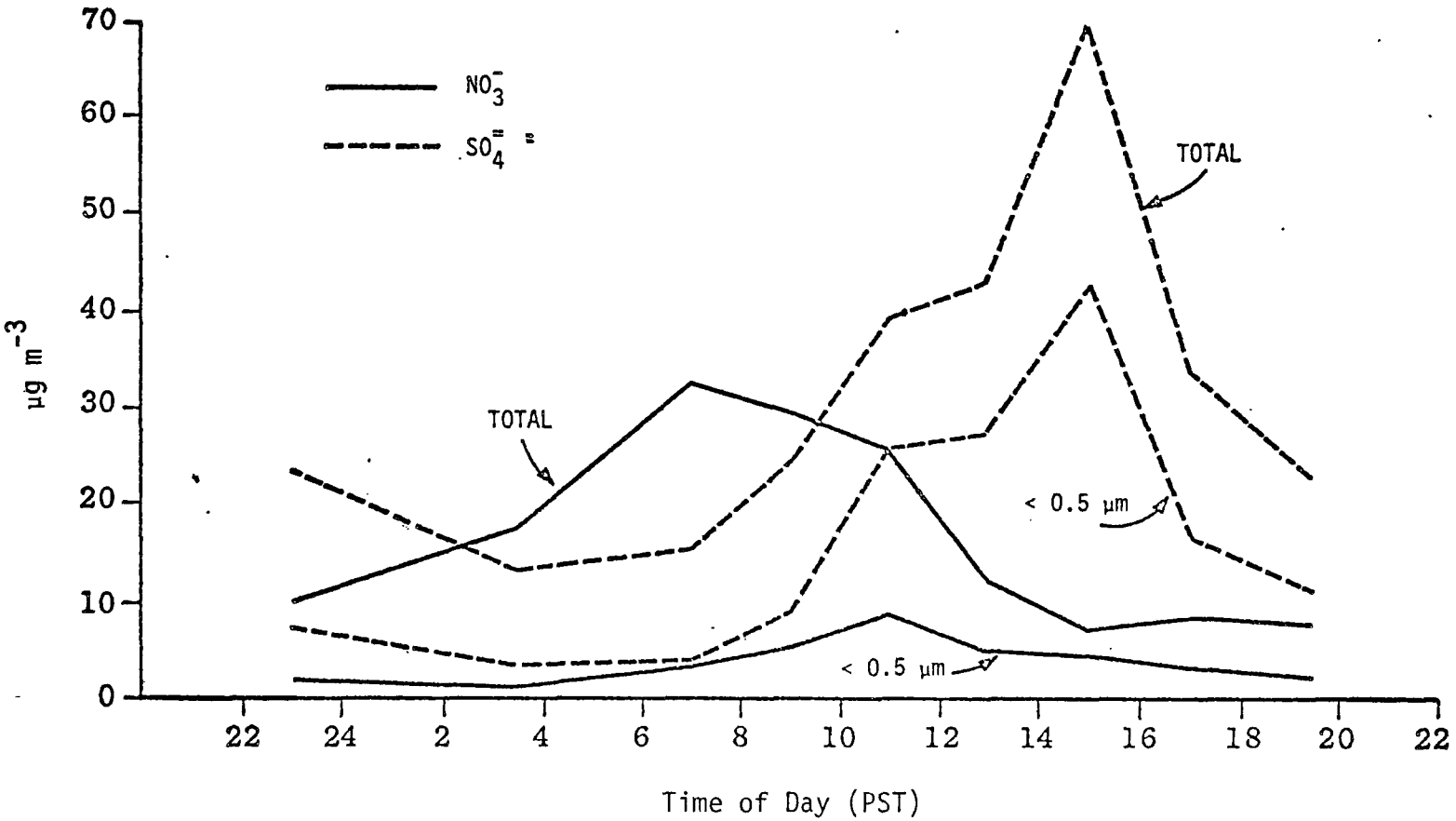

Source: Appel et al. (1974)

FIGURE 12. DIURNAL VARIATIONS IN SIZE DISTRIBUTIONS FOR SULFATE AND NITRATE AT WEST COVINA ON 23-24 JULY 1973

Table 11

SULFATE, NITRATE, AND SOLVENT EXTRACTABLE ORGANIC CONCENTRATIONS AT THREE SITES DURING 1972

(In $\mu g\ m^{-3}$)

Site	Total	Sulfate	Nitrate	Solvent Extractable Organic*
Pasadena				
April 1972	80	9.45 ± 1.41	0.69 ± 0.097	
Summer/Fall 1972	69.1 ± 7.7	6.11 ± 1.6	5.76 ± 0.44	3.3 ± 0.2
Riverside				
April 1972	154 ± 5	11.2 ± 1.7	0.486 ± 0.075	5.79 ± 0.58
Summer/Fall 1972	110 ± 12.7	8.22 ± 2.1	16.6 ± 1.4	4.7 ± 0.2
Pomona				
October 1972	126.4 ± 14.4	9.71 ± 2.9	18.0 ± 1.6	5.4 ± 0.4

* Cyclohexane extractable.

Source: Hidy, et al. (1975)

Table 12

HIGH-VOLUME SAMPLE CONCENTRATIONS OBTAINED ON 4 OCTOBER 1972

(In $\mu g\ m^{-3}$)

Sample	Pasadena	Pomona	Riverside
NO_3^-	7.19 ± 0.54	13.1 ± 1.4	15.4 ± 1.2
SO_4^{-2}	3.9 ± 0.1	6.2 ± 1.5	5.8 ± 1.4
CEO*	3.1 ± 0.2	4.8 ± 0.4	4.8 ± 0.2
NH_4^+	4.17 ± 0.4	6.39 ± 0.32	6.61 ± 0.33
$(NO_3^- + SO_4^=)/NH_4^+$	2.7 (3.2)	3.0 (3.2)	3.2 (3.2)
Mass	69.5 ± 7.6	137.0 ± 15.0	134.0 ± 15.0
NO_3^-/Pb	4.73	7.66	8.7
SO_4^{-2}/Pb	2.56	3.63	3.28
NO_3^-/mass	0.103	0.096	0.115
SO_4^{-2}/mass	0.056	0.044	0.043

* Cyclohexane extractable organics.

Source: Hidy, et al. (1975)

In the ACHEX, investigators found that the predominant compounds of sulfate and nitrate are $(NH_4)_2SO_4$ and NH_4NO_3, respectively (Appel et al, 1974).* Table 13 compares the observed levels of NH_4^+ in the aerosol with the amounts calculated, assuming that all the sulfate and nitrate were present as ammonium salts. For the South Coast air basin, the observed NH_4^+ ranged from 62 to 103 percent of the calculated values, with an average of 85 percent. These data suggest that, except near important sources of sulfate, ammonium salts are the predominant sulfate and nitrate compounds. The general level of NH_4^+ is about 10 $\mu g\ m^{-3}$. The main source of gaseous NH_3 in Los Angeles is feed-lot emissions. For the data in Table 12, the measured NH_4^+ is roughly equivalent stoichiometrically to that needed to balance $SO_4^=$ and NO_3^- for ammonium salts.

Aerosol organics were identified in the ACHEX (Hidy et al., 1975). Table 14 summarizes organic compounds identified at Pasadena on 22 September 1975 and at West Covina on 24 July 1974. The organics can be classified according to difunctional aliphatic compounds, monofunctional aromatic compounds and oxygenated compounds derived from terpenes. The compounds listed in Table 14 represent secondary organics (not listed). Grosjean and Friedlander (1975) estimated that secondary organics contribute 80 percent--and in some cases as much as 95 percent--of the total aerosol organics. Subsequently, we discuss mechanisms that might explain the occurrence of many of the compounds in Table 14.

4. Summary

In this section, we have summarized some available data relating to the chemical composition of the Los Angeles aerosol. Although a great deal concerning the composition of photochemical aerosols is still unknown, several general conclusions can be drawn on the basis of the data obtained to date.

---

* Craig et al. (1974) identified seven separate chemical species of sulfur in aerosol samples from California: SO_3, $SO_4^=$, SO_2, $SO_3^=$, S^0, and two kinds of sulfides. However, sulfates were generally the dominant species.

Table 13

A COMPARISON OF THEORETICAL AND EXPERIMENTAL AMMONIUM VALUES*

Sampling Location	No. of Samples	Expected NH_4^+ Based on NO_3^- and $SO_4^=$ Present†	Observed NH_4^+ as Percent of Expected
Harbor Freeway	2	4.0	103%
Pasadena	6	4.0	82
West Covina	4	10.3	76
Pomona			
1972	5	8.9	94
1973	2	6.6	75
Riverside	7	7.9	93
Rubidoux	3	15.5	73
Dominguez Hills	2	7.9	62

* Analyses of high-volume samples collected on Whatman-41 filters.

† Assuming the composition $(NH_4)_2SO_4$ and NH_4NO_3.

Source: Appel et al. (1974).

Table 14

SECONDARY AEROSOL ORGANICS IDENTIFIED IN THE ACHEX

Difunctional Aliphatic Compounds

(1) $X - (CH_2)_n - Y$, $n = 3, 4, 5$

X	Y
COOH	CH_2OH
COOH	COH
COOH	COOH
COOH	CH_2ONO
or	
COH	CH_2ONO_2
COH	CH_2OH
COH	COH
COOH	COONO
or	
COH	$CONO_2$
COH	COONO
COOH	$COONO_2$
COOH	CH_2ONO_2

(2) Others

$CH_2OH - CH = C(COOH)CHO$

$CH_2OH - CH_2 - CH = C(COOH) - CHO$

$CHO - CH = CH - CH(CH_3)CHO$

$CH_2OH - CH = CH - CH = C(CH_3)CHO$

Monofunctional Aromatic Compounds

(1) $C_6H_5 - (CH_2)_n - COOH$, $n = 0, 1, 2, 3$

(2) $C_2H_5CH_5OH$

C_2H_5CHO

Sources: Hidy et al. (1975).
Schuetzle et al. (1973).

About 50 percent of the aerosol mass can be attributed to gas-to-particle conversion processes. Of the fraction of the aerosol that is secondary material, the important constituents are sulfate, nitrate, and organics. Since there are no major primary sources of sulfate and nitrate, except possibly for motor vehicles, the quantities in the aerosol are the result of gas-to-particle conversions. It is more difficult to estimate the relative contributions of primary and secondary sources to particulate carbon, although Grosjean and Friedlander (1975) estimated that organics resulting from conversion of photochemical products represent about 80 percent, and sometimes as high as 90 to 95 percent, of the total particulate carbon (in the submicron size range). Under the assumption that NO_3^- and $SO_4^=$ are present as ammonium salts, the NH_4^+ level can be calculated. Measurements indicate that ammonium salts may account for as much as 90 percent of the nitrate and sulfate. Considerably less is known about the species comprising the organic particulate fraction than about sulfate and nitrate.

A profile of a "typical" submicron photochemical aerosol particle might show the following composition:

> Ammonium sulfate $(NH_4)_2SO_4$
> Ammonium nitrate NH_4NO_3
> Oxygenated organic species
> Water
> Primary material (e.g., lead, salt).

B. RATES OF CONVERSION OF SULFUR, NITROGEN, AND CARBON TO AEROSOL

In representing the rates of conversion of sulfur, nitrogen, and carbon to the particulate phase, it is useful to define a measure of the relative amounts of the species in the gaseous and particulate phases at any time and location. Two ways of representing this distribution between gaseous and particulate phases have been used. The first is the so-called <u>distribution factor</u>, which is the ratio of the mass of the species in the particulate phase to the total mass of the species in the gaseous

and particulate phases. For example, one can define the distribution factors for sulfur, nitrogen, and carbon as follows (Grosjean and Friedlander, 1975):

> Sulfur distribution factor

$$f_S = \frac{[SO_4^{=}]}{[SO_2] + [SO_4^{=}]} ,$$

where

$[SO_4^{=}]$ = particulate sulfate concentrations, expressed as SO_2, in $\mu g\ m^{-3}$,
$[SO_2]$ = gas phase SO_2 concentrations, in $\mu g\ m^{-3}$.

> Nitrogen distribution factor

$$f_N = \frac{[NO_3^-]}{[NO_x] + [NO_3^-]} ,$$

where

$[NO_3^-]$ = particulate nitrate concentration, expressed as NO_2, in $\mu g\ m^{-3}$,
$[NO_x]$ = gas phase $NO + NO_2$ concentration, expressed as NO_2, in $\mu g\ m^{-3}$.

> Carbon distribution factor

$$f_C = \frac{[C_p]}{[C_g] + [C_p]} ,$$

where

$[C_p]$ = particulate organic concentration, in $\mu g\ m^{-3}$, as carbon,

$[C_g]$ = gas phase reactive hydrocarbons, converted from ppm CH_4 to carbon in $\mu g\ m^{-3}$ = total hydrocarbons (including oxygenates), as CH_4 - $([CH_4] + [C_2H_2])$.*

(One might wish to restrict $[C_g]$ to only aerosol-forming hydrocarbons. However, available data, both on which hydrocarbons lead to aerosol formation and on the concentrations of these hydrocarbons, are incomplete.)

The alternative to using the distribution factor for representing the gaseous-particulate fractions of species is simply the ratio of the mass of the species in the particulate phase to that in the gaseous phase. For example, we can define the following ratios:

$$g_S = \frac{[SO_4^{=}]}{[SO_2]} \quad ,$$

$$g_N = \frac{[NO_3^{-}]}{[NO_x]} \quad ,$$

$$g_C = \frac{[C_p]}{[C_g]} \quad .$$

In g_S and g_N, the concentrations can be expressed in terms of SO_2 and NO_2, or simply sulfur and nitrogen. The mass ratios are related to the distribution functions by relations such as

$$f_S = \frac{g_S}{g_S + 1} \quad ;$$

* Grosjean and Friedlander did not measure the concentration of benzene, which is also unreactive, although if it were known, its concentration would also be subtracted from that of the total hydrocarbons.

thus, data reported in terms of g_S can be readily converted into f_S, and vice versa. If one is interested in the degree of chemical conversion, the distribution factor is a more revealing measure than the mass ratio.

There are two potential sources of data on the rates of conversion of sulfur-, nitrogen-, and carbon-containing species to the particulate phase: ambient monitoring and laboratory studies. In this section, we confine our attention to ambient monitoring data because there are virtually no available laboratory data available from which the desired ratio of conversion can be inferred.

1. Rates of Sulfur Conversion

Figure 13 shows the diurnal patterns of the ratio of particulate sulfur to total gas phase sulfur for four locations during four periods in 1973. The sites,which are presented in their order from west to east, include one source-enriched site (Dominguez Hills) and three receptor sites. Close to a strong SO_2 source, g_S was about 0.2, whereas at the receptor sites it reached values as high as 0.6. Ignoring SO_2 losses, we found that $g_S = 0.6$ corresponds to a conversion of gaseous SO_2 of about 35 percent. On the basis of the travel time from the source area to the receptor areas, one can estimate an approximate rate of conversion from data as those given in Figure 13.

Roberts and Friedlander (1974) estimated gas-to-particle conversion rates for sulfur on the basis of measurements of the particulate to gas phase sulfur ratio near major stationary sources and downwind of these sources along known air trajectories. They assumed that the conversion of SO_2 to particulate sulfate is a first-order process in SO_2 and that $[SO_2]/[S_T]$, where $[S_T]$ is the total concentration of sulfur, is independent of both height above the ground and time and depends only on distance along a trajectory. Then the first-order rate constant for the conversion of SO_2 could be estimated from the following equation:

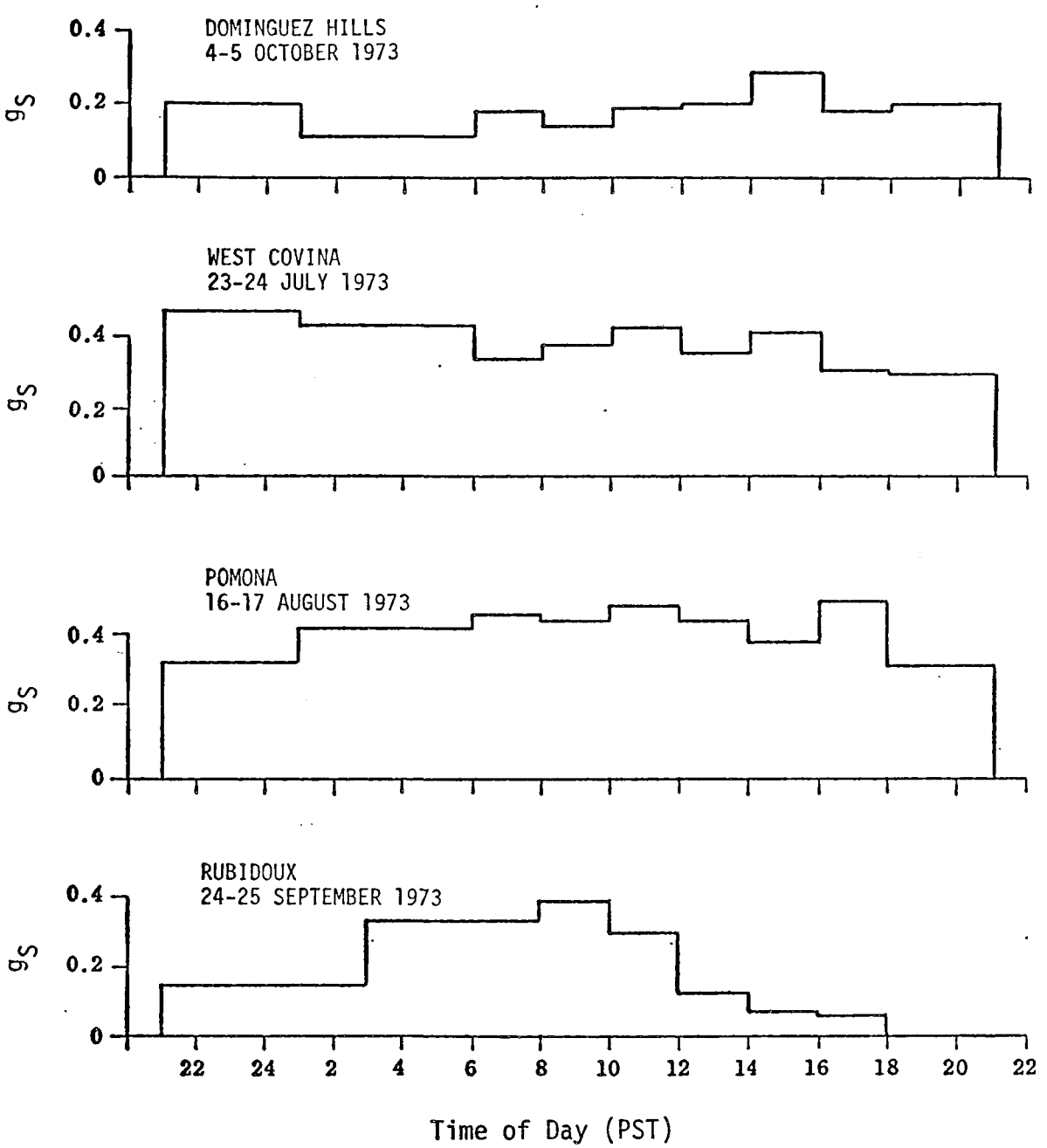

Source: Appel et al. (1974).

FIGURE 13. DIURNAL VARIATIONS IN THE RATIO OF PARTICLE TO GAS PHASE SULFUR

$$k = \frac{1}{\Delta T}\left\{ \ln \frac{[SO_2]}{[S_T]} \Bigg|_{\text{end}}^{\text{start}} + \int_{\text{start}}^{\text{end}} \left[\left(1 - \frac{[SO_2]}{[S_T]}\right)\left(\frac{v_a - v_g}{H} + \frac{W_{S_T}}{H[SO_2]}\right) - \frac{\alpha W'_{S_T}}{H[SO_2]} \right] dT \right. , \tag{53}$$

where

"start" and "end"	=	the beginning and termination, respectively, of an air trajectory,
ΔT	=	the duration of time of the trajectory,
v_a and v_g	=	the deposition velocities for loss of aerosol sulfur and SO_2, respectively, to the ground,
H	=	the mixing height,
W_{S_T}	=	the area source emission rate for total sulfur,
W'_{S_T}	=	the area source emission rate for motor vehicles only,
α	=	the ratio of aerosol sulfur to total sulfur in auto exhaust.

To determine the value of k for a particular trajectory, Roberts and Friedlander solved Eq. (53) iteratively by first assuming a value of k and using the hourly average measured values of $[SO_2]$ and $[S_T]$ to evaluate the integral and to compute $[SO_2]/[S_T]$ at the end of the trajectory. They then compared the calculated value of $[SO_2]/[S_T]$ at the end of the trajectory with the measured value and adjusted k until a match was achieved.

Table 15 shows the k values that Roberts and Friedlander calculated for three days in July 1973. The Alamitos Bay area contains two large power plants, and the El Segundo area has two power plants and a refinery. As indicated, an initial value of 0.97 was assumed for the $[SO_2]/[S_T]$ ratios

Table 15

PSEUDO-FIRST-ORDER RATE CONSTANTS
FOR THE LOS ANGELES BASIN*

Date (1973)	Time of Arrival at Pasadena (PST)	k (percent per hour)	Starting Location
July 10	1300	1.2	El Segundo
	1400	3.0	El Segundo
	1500	9.0	El Segundo
	1600	13.0	El Segundo
July 25	1400	12.8	Alamitos Bay
	1500	8.2	El Segundo
	1600	8.8	El Segundo
July 26	1200	4.3	Alamitos Bay
	1300	5.6	Alamitos Bay
	1400	7.6	Alamitos Bay
	1500	4.7	Alamitos Bay

* Assuming that

$$\frac{\partial[SO_2]}{\partial t} = -k[SO_2] \text{ and } \left.\frac{[SO_2]}{[S_T]}\right|_{start} = 0.97 \quad .$$

Source: Roberts and Friedlander (1974).

near these two sources. The calculated values of k vary considerably, indicating a dependence of k on other meteorological and chemical parameters in the atmosphere.

It is of interest to determine whether a correlation exists between the rate of conversion of SO_2 to sulfate and other quantities in the photochemical smog system. Since ozone is generally taken as a measure of the intensity of photochemical smog, one can examine the dependence of the conversion on ozone level. Figure 14 shows a plot of S_p/S_g versus O_3 for several sampling periods at three locations. In this figure, S_p refers only to particulate sulfur in particles smaller than 0.5 μm in diameter. As this figure indicates, an approximate correlation appears to exist between S_p/S_g and the O_3 level.

As we discuss in the next section, one path proposed for the oxidation of SO_2 is that of reaction with a product of the reaction of ozone and olefins. Assuming that the concentration of the product responsible for the oxidation is proportional to $[O_3][\text{Olefin}]$, the ratio of S_p (less than 0.5 μm) to S_g can be plotted as function of $[O_3][\text{Olefin}]$ for monitoring data. Because the total gas phase olefin concentration was not available, this correlation must be presented as S_p/S_g versus the product of the O_3 concentrations and the total nonmethane hydrocarbon concentration (assuming that olefin levels are proportional to total hydrocarbon levels). Figure 15 shows a correlation of this type prepared from the ACHEX study. The correlation does not appear to be superior to that constructed on the basis of O_3 alone.

2. Rates of Nitrogen Conversion

Figure 16 shows the diurnal patterns of the ratio of particulate nitrogen (N_p) to total gaseous nitrogen (N_g) at three locations on three days. The N_p/N_g ratios are generally lower than those of S_p/S_g, although on 5-6 September 1973 in Rubidoux, values of N_p/N_g exceeding 0.6 were observed. There appears to be a stronger variation of S_p/S_g with location in the basin; this is consistent with the observations of the spatial variation of the total particulate mass of sulfate and nitrate.

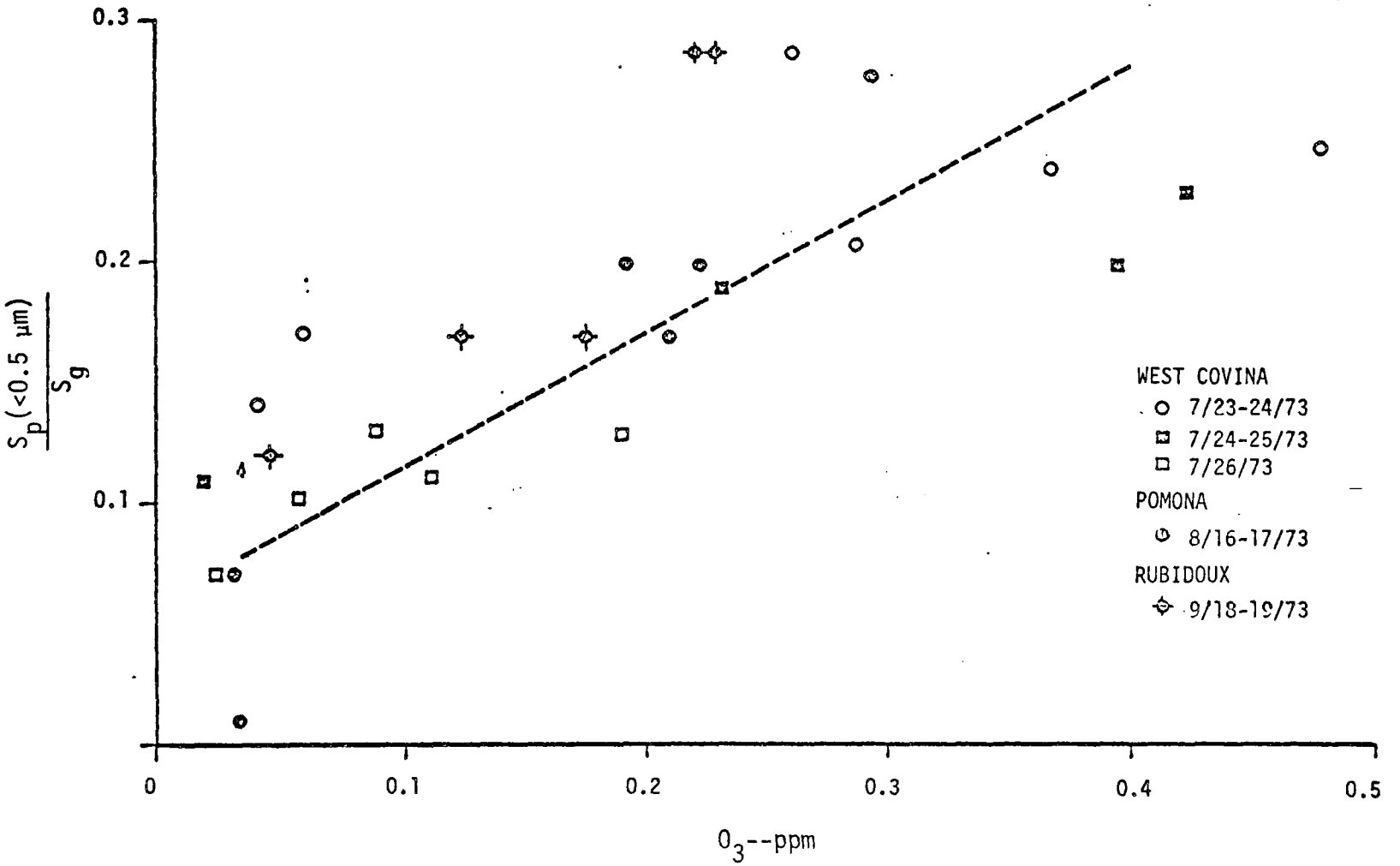

Source: Appel et al. (1974).

FIGURE 14. SCATTER DIAGRAM OF THE SULFUR CONVERSION RATIO IN PARTICLES SMALLER THAN 0.5 μm IN DIAMETER AND OZONE

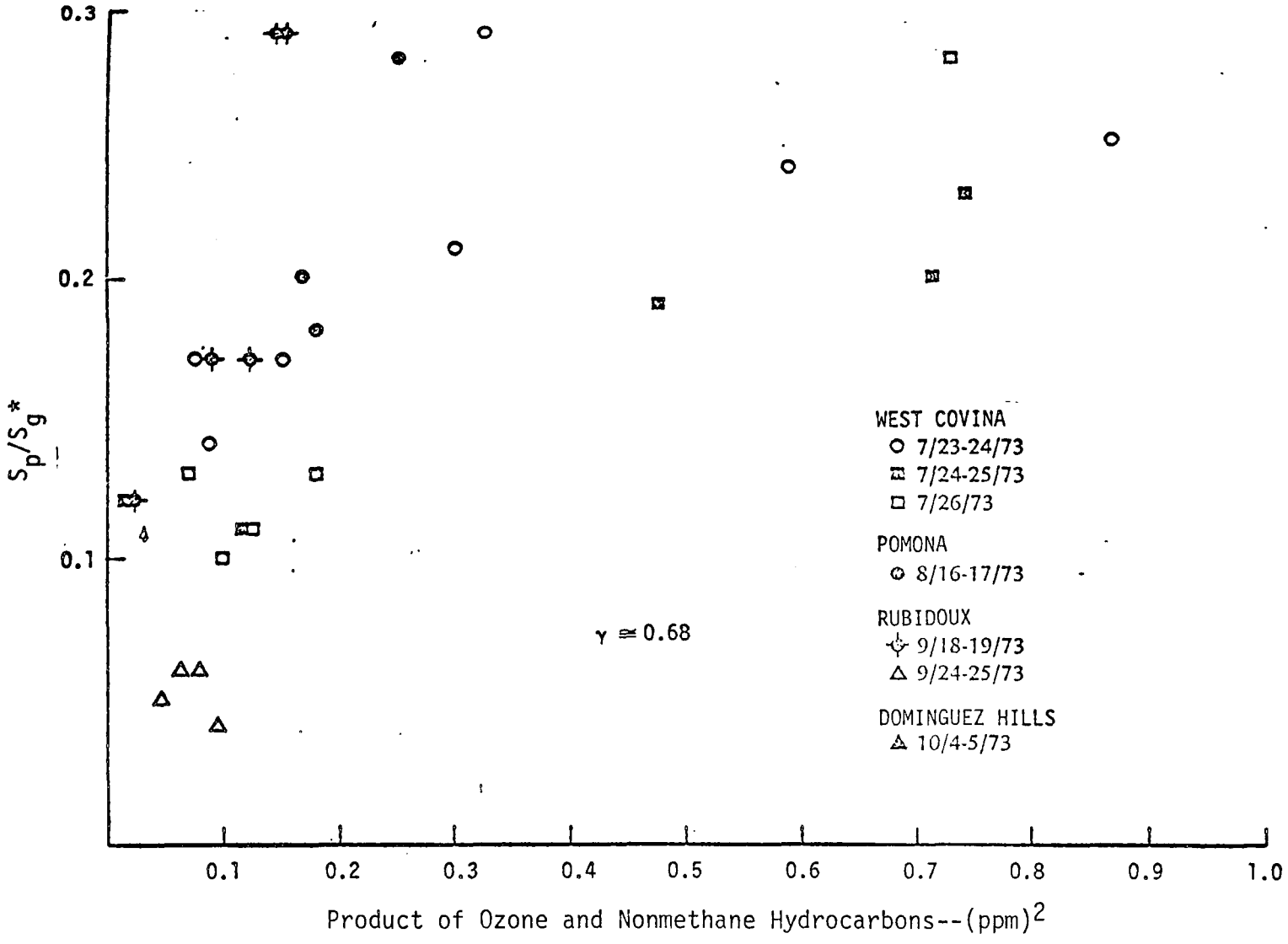

* S_p for particles smaller than 0.5 μm in diameter.

Source: Appel et al. (1974).

FIGURE 15. THE SULFUR CONVERSION RATIO AS A FUNCTION OF THE PRODUCT OF GAS PHASE OZONE AND NONMETHANE HYDROCARBON CONCENTRATIONS

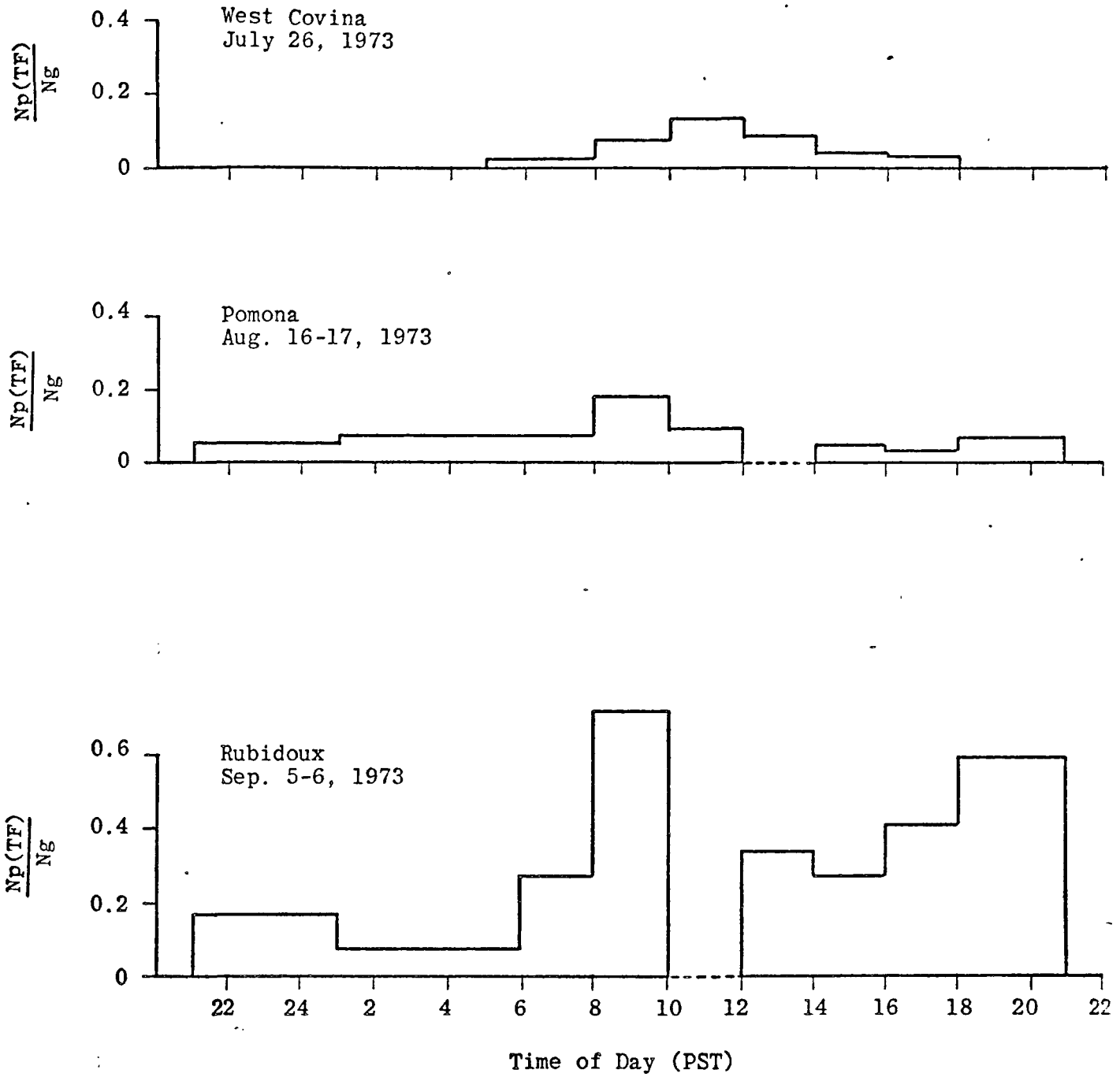

Source: Appel et al. (1974)

FIGURE 16. DIURNAL VARIATIONS IN THE RATIO OF PARTICLE PHASE TO GAS PHASE NITROGEN ($N_{NO} + N_{NO_2}$).

Less is known about the rate of conversion of NO_x to nitrate than about that of SO_2 to sulfate. Appel et al. (1974) explored the relationship between N_p/N_g and ozone levels at several locations during 1973; Figure 17 presents their results. Although a correlation is not evident, the overall trend of the data suggests that particulate nitrate levels may be inversely related to O_3 levels. The data in Figure 17 might be explained on the basis of a nitrate conversion mechanism that is most efficient when photochemical smog intensity is low. We have already seen that there appear to be two mechanisms for nitrate conversion: one for early morning and one for afternoon. The early morning mechanism, involving mainly particles larger than 0.5 μm in diameter, may involve absorption of NO_x into liquid droplets. The wide range of N_p/N_g values at the low O_3 levels of Figure 17 might reflect the effect of relative humidity and early morning absorption of gaseous NO_x.

3. Rates of Carbon Conversion

Table 16 presents total particulate concentrations, organic carbon fractions (the fraction of the total particulate weight due to organics), and the organic distribution factors (f_C) determined on six days in 1973 by Grosjean and Friedlander (1975). As indicated in this table, their results show that the measured organic carbon fractions (OCF) were always substantial, reaching a level as high as 0.43. Figure 18 presents the hourly variations of organics, total particulate matter, b_{scat}, f_C, $[O_3]$, and reactive hydrocarbons on 25 July 1973. Grosjean and Friedlander observed two maxima in the OCF and f_C curves. The second peak is closely related to $[O_3]$ and is probably the result of the conversion of gas phase hydrocarbons to aerosols. The first peak in OCF and f_C probably reflects a more direct conversion of primary emissions.

In summary, although only about 3 percent of the organic gases are converted to aerosols, this material comprises about 30 percent of the total aerosol mass. The estimated rates of conversion of total organic gases is thus less than 2 percent per hour. Since most of the secondary organic

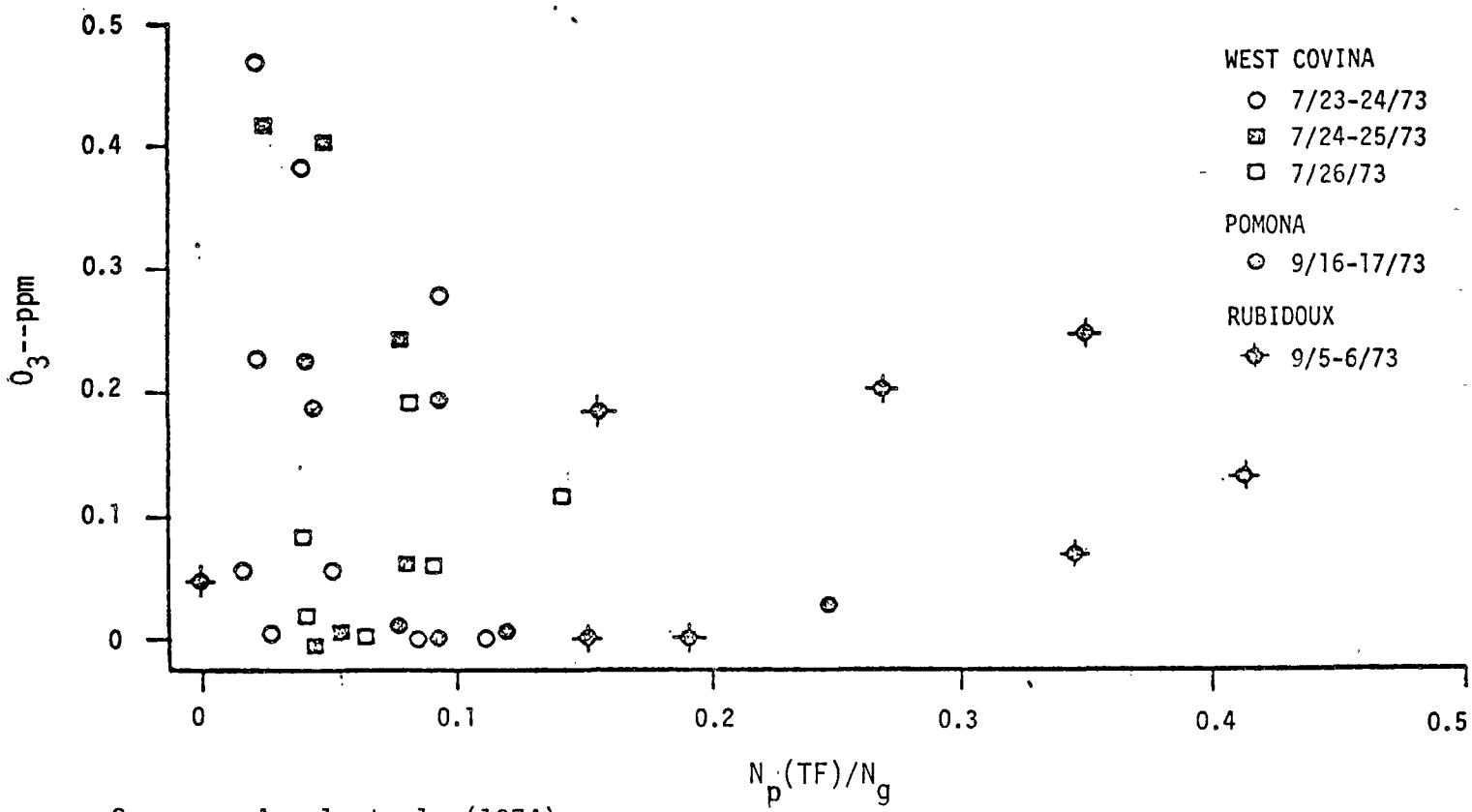

Source: Appel et al. (1974).

FIGURE 17. SCATTER DIAGRAM OF THE RATIO OF PARTICLE TO GAS PHASE NITROGEN AS A FUNCTION OF OZONE LEVEL

Table 16

DIURNAL VARIATIONS OF TOTAL PARTICULATES (TP)--IN $\mu g\ m^{-3}$--
ORGANIC CARBON FRACTION (OCF),
AND ORGANIC CARBON DISTRIBUTION FACTOR (f_C)

May 16			June 19			July 25		
TP	OCF	$f_C \times 10^2$	TP	OCF	$f_C \times 10^2$	TP	OCF	$f_C \times 10^2$
99	0.255	2.5	158	0.338	2.4	126	0.178	2.1
123	0.248	3.0	152	0.367	2.9	128	0.221	1.6
116	0.050	0.6	128	0.292	3.4	144	0.241	2.0
183	0.160	2.9	97	0.535	5.8	153	0.343	3.65
180	0.270	4.8	89	0.398	3.9	168	0.212	2.9
172	0.248	4.3	88	0.394	3.7	238	0.058	0.9
130	0.215	2.4	108	0.430	4.0	214	0.151	2.1
119	0.274	3.1	144	0.198	2.4	296	0.277	3.85
117	0.240	2.9	119	0.159	2.0	303	0.350	5.15
87	0.090	0.8	96	0.202	2.15	232	0.428	6.15
84	--	--				184	0.317	4.95
						131	0.158	2.0
						90	0.281	2.35
						46	0.141	0.6

July 10			July 12			October 17		
TP	OCF	$f_C \times 10^2$	TP	OCF	$f_C \times 10^2$	TP	OCF	$f_C \times 10^2$
225	0.266	3.3	106	0.154	1.4	52	0.229	0.42
179	0.221	2.35	148	0.182	2.35	103	0.112	0.79
149	0.164	1.55	154	0.123	1.75	192	0.156	2.05
136	0.220	2.1	116	0.267	3.0	61	0.177	0.88
104	0.131	1.0	101	0.205	2.1	53	0.108	0.66
			75	0.112	0.9			

Note: The sampling periods were as follows:

- May 16------1 hour, 7:00 to 18:00 (11 samples).
- June 19-----1 hour, 6:30 to 16:30 (10 samples).
- July 10-----1 hour, 12:30 to 17:30 (5 samples).
- July 12-----8:00 to 12:00, 12:00 to 14:00, 14:00 to 16:00, 16:00 to 18:00, 18:00 to 20:00, and 20:00 to 24:00 (6 samples).
- July 25-----0:00 to 6:30, then 1 hour, 6:30 to 17:30, 17:30 to 19:30, and 19:30 to 24:00 (14 samples).
- October 17--8:00 to 10:00, 10:00 to 12:00, 12:00 to 13:00, 13:00 to 15:00, and 15:00 to 17:00 (5 samples).

Source: Grosjean and Friedlander (1975).

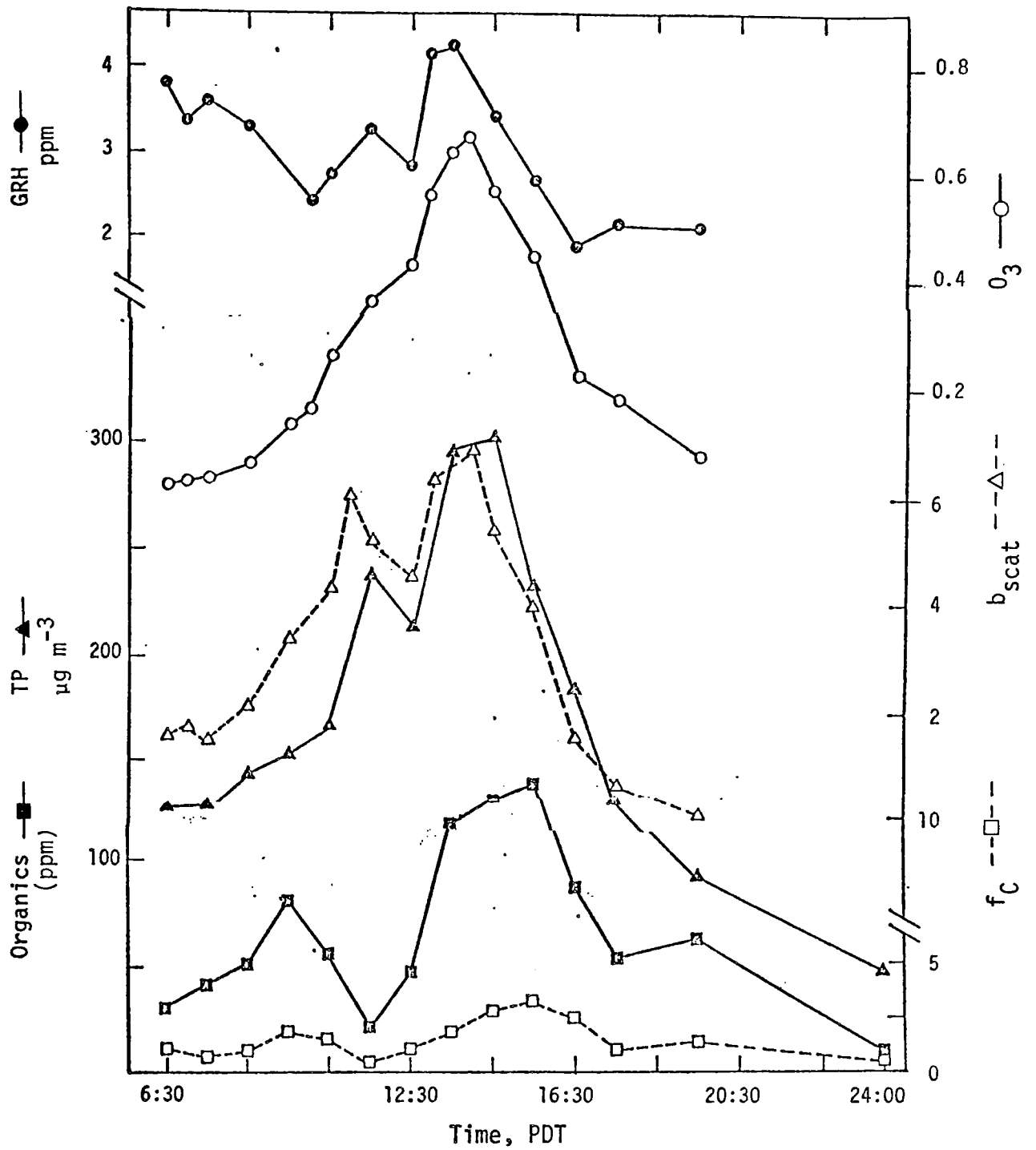

Source: Grosjean and Friedlander (1975)

FIGURE 18. HOURLY VARIATIONS OF b_{scat}, ORGANIC DISTRIBUTION FACTORS (f_c), OZONE, TOTAL PARTICULATE MATTER (TP), GASEOUS HYDROCARBONS (GRH), AND ORGANICS.

species identified in the aerosol are difunctional aliphatic and monofunctional aromatic compounds, it is possible to identify likely olefinic precursors, as discussed later.

C. POSSIBLE CHEMICAL REACTIONS THAT INFLUENCE THE EVOLUTION OF PHOTOCHEMICAL AEROSOLS

Up to this point, we have reviewed the observations made by several investigators on the chemical composition and rates of formation of photochemical aerosols. The objective of this review has been to provide a basis upon which to determine the chemical processes responsible for photochemical aerosol formation. In this section, we discuss the current understanding of these chemical processes. The treatment is divided into sulfate formation, nitrate formation, and the generation of organic compounds of low volatility.

1. Sulfate Formation

There are basically two paths by which SO_2 can be converted to particulate sulfate:

> Gas phase reactions lead to the formation of SO_3, which rapidly combines with water to give H_2SO_4. The H_2SO_4 formed in the gas phase can then dissolve in existing droplets or serve as embryonic nuclei for molecular clusters of water molecules.

> Sulfur dioxide dissolves in aerosol droplets, wherein it is subsequently oxidized to sulfate. The oxidation requires a catalyst, and two types of catalysts have been identified and studied--dissolved NH_3 and metal salts.

a. Gas Phase Formation of Sulfate

Surveys of gas phase atmospheric reactions involving SO_2 have been carried out by Urone and Schroeder (1969), Katz and Gale (1970), Bufalini (1971), Urone et al. (1971), and Calvert (1974). Compared with the wealth of available laboratory smog chamber data on hydrocarbon-NO_x systems, there are at present relatively few studies on irradiated mixtures of hydrocarbon-NO_x-SO_2 systems (Wilson and Levy, 1970; Wilson et al., 1971; Calvert, 1973; Smith and Urone, 1974). The lack of smog chamber studies involving SO_2 can apparently be attributed to two factors. First, investigators have generally felt that it is necessary to understand the chemistry of hydrocarbon-NO_x mixtures before proceeding to the more complex hydrocarbon-NO_x-SO_2 systems. Second, when SO_2 is added to hydrocarbon-NO_x systems, irradiation often results in pronounced aerosol formation, which has been viewed as undesirable in laboratory studies. Thus, even at this time, not enough laboratory data are available to test thoroughly proposed mechanisms for SO_2 photooxidation chemistry. Some uncertainty still exists as to the predominant paths for homogeneous oxidation of SO_2 in the atmosphere (Cox and Penkett, 1971; Sidebottom et al., 1972; Davis et al., 1974; Calvert, 1974; Wood et al., 1974).

It has been suggested that heterogeneous paths may account for the formation of most of the photochemical sulfate aerosol observed in the atmosphere under certain conditions (Goetz and Pueschel, 1967; Urone et al., 1968). However, if, as it is generally agreed, SO_3 is primarily responsible for the heterogeneous formation of sulfate, the homogeneous oxidation of SO_2 to SO_3 becomes a key step in the sulfate formation process. In addition, smog chamber experiments have shown that significant rates of SO_2 oxidation can be achieved in the absence of any apparent heterogeneous paths. Once SO_3 is produced, nuclei can be formed via the following reactions:

$$SO_3 + H_2O \rightarrow H_2SO_4 \quad ,$$

$$H_2SO_4 + H_2O \rightarrow H_2SO_4 \cdot H_2O \quad ,$$

$$\vdots$$

$$H_2SO_4 \cdot (n-1)H_2O + H_2O \rightarrow H_2SO_4 \cdot nH_2O \quad .$$

In the absence of foreign nuclei, the acid embryos represented as H_2SO_4-nH_2O are formed initially as very small particles, on the order of 10 Å in size. With other aerosol particles present, it is likely that molecules of H_2SO_4 will condense on existing particles as opposed to undergoing heteromolecular nucleation with water molecules.

The Photochemistry of SO_2. The photooxidation of SO_2 alone or in mixtures of SO_2 and oxygen proceeds slowly relative to observed atmospheric rates (Hall, 1953; Gerhard and Johnstone, 1955; Renzetti and Doyle, 1959; Rao et al., 1969; Okuda et al., 1969). We will not review the photochemistry of SO_2 here. The interested reader is referred to Rao et al. (1969), Okuda et al. (1969), and Bufalini (1971) for details.

SO_2-NO_x-Air Mixtures. The principal reactions occurring in the SO_2-NO_x-air system are listed in Table 17. Although Reaction 1 cannot compete with the primary ozone formation reaction $O + O_2 + M \rightarrow O_3 + M$ in the depletion of oxygen atoms, Reaction 1 is apparently the most important SO_2 oxidation reaction in SO_2-NO_x-air systems. Several investigators have suggested that Reactions 4-6 might be important SO_2 removal paths.

Although Jaffee and Klein (1966) reported a rate constant for Reaction 5 of 3.7×10^{-3} ℓ mole^{-1} sec^{-1} at 24°C, data reported by Boreskov and Illarionov (1940) indicates that the rate constant is almost six orders of magnitude smaller. Sidebottom et al. (1972) estimated that Reaction 5 should have a low activation energy and a high preexponential factor; however, more recent data of Daubendiek and Calvert (1974) set an upper limit on the rate constant at 25×10^{-5} ppm^{-1} min^{-1}. Daubendiek and Calvert (1973) also indicated that the rate constant of Reaction 6 is 1.7×10^{-8} ppm^{-1} min^{-1}. Reaction 7, suggested by Wilson and Levy (1972), has not been substantiated, although Urone and Schroeder (1971) obtained a white crystalline solid with empirical formula SNO_5 in their experiments with SO_2 and NO_2 in dry air. Rate constant data for reactions such as Reaction 7 are not available and would probably be difficult to estimate. In summary, Reactions 4 through 7 apparently play an unimportant role in the SO_2-NO_x- air system, judging by the current values of their rate constants.

Table 17

REACTIONS IN THE SO_2-NO_x-AIR SYSTEM

No.	Reaction	Rate Constant at 25°C, ppm^{-1} min^{-1}	Reference
1.	$O(^3P) + SO_2 + M \rightarrow SO_3 + M$	$3 \times 10^{-5*}$	Garvin and Hampson (1974)
2.	$O + SO_2 + {}^3SO_2 \rightarrow SO_3 + SO_2$	$1 \times 10^{-3*}$	Mulcahy et al. (1967)
3.	$O_3 + SO_2 \rightarrow SO_3 + O_2$	3×10^{-7}	Davis et al. (1974)
4.	$SO_2 + NO_2 \rightarrow SO_3 + NO$	9×10^{-14}	Boreskov and Illarionov (1940)
5.	$SO_2 + NO_3 \rightarrow SO_3 + NO_2$	25×10^{-5}	Daubendiek and Calvert (1973)
6.	$SO_2 + N_2O_5 \rightarrow SO_3 + N_2O_4$	1.7×10^{-8}	Daubendiek and Calvert (1973)
7.	$SO_2 + NO_x \rightarrow (SO_3)\ (NO_x)$ solid	--	
8.	$SO + O_3 \rightarrow {}^3SO_2 + O_2$	0.1	Levy et al. (1970)
9.	$SO + O_3 \rightarrow SO_2 + O_2$	110	Levy et al. (1970)
10.	$SO_3 + O \rightarrow SO_2 + O_2$	7.3×10^4	Garvin and Hampson (1974)

*ppm^{-2} min^{-1}

Reactions 8-10 participate in the reconversion of SO and SO_3 to SO_2. Urone and Smith (1974) observed a decrease in SO_2 oxidation rate at high initial NO_2 levels. Reaction 10 may be rapid enough to account for these observations.

<u>SO_2-Hydrocarbon-Mixtures.</u> The direct reaction of SO_2 and hydrocarbons has been studied since 1950 (Dainton and Ivin, 1950). Recently, Badcock et al. (1971) conducted a series of experiments on the SO_2-hydrocarbon system in which they used laser excitation to populate the excited triplet state of SO_2 (see also Sidebottom et al., 1971). They suggested that the SO_2-hydrocarbon reaction is either an insertion of the form

$$^3SO_2 + RH \rightarrow RSO_2H \qquad (11a)$$

or a free radical abstraction involving a hydrogen atom:

$$^3SO_2 + RH \rightarrow SO_2H + R \quad . \qquad (11b)$$

Badcock et al. (1971) and Sidebottom et al. (1971) determined the rate constants for Reactions (11a) and (11b) and for the collisional deactivation

$$^3SO_2 + RH \rightarrow SO_2 + RH \quad . \qquad (12)$$

Typical rate constant values for paraffins and olefins are $k_{11} = 512\ ppm^{-1}\ min^{-1}$ (ethane) and $2.08 \times 10^5\ ppm^{-1}\ min^{-1}$ (propylene).

A recent mass spectrometric study by Penzhorn et al. (1973) provides additional insight into the products of the SO_2-alkane reaction. In addition to the sulfinic and sulfonic acids identified by others (Dainton and

Ivin, 1950), a number of adducts, including RSO_2R, RSR, RSO_3R, and RSO_2SR, were found in the products. Penzhorn et al. suggested that an initiation step of the form of Reaction (11b) followed by

$$R\cdot + SO_2 \rightarrow RSO_2$$

and other propagation steps dominate the process.

<u>SO_2-NO_x-Hydrocarbon-Air Mixtures</u>. The main SO_2 oxidation reactions (in addition to those in Table 17) in the photochemical smog system are listed in Table 18. The products of the reactions in Table 18 are SO_3, $ROSO_2$, or RO_2SO_2. All of the reactions are exothermic and are favored thermodynamically. Most of the reactions in Table 18 have rates that are sufficiently rapid to account for observed rates of SO_2 oxidation in photochemical smog (Roberts, 1975).

It has been observed that SO_2 is efficiently oxidized in the presence of ozone and olefins (Cox and Penkett, 1971, 1972; McNelis, 1974). Reactions 18, 19a and 19b represent three possible reactions that might occur between SO_2 and initial products of ozone - olefin reactions. Based on the observations of Cox and Penkett and McNelis it is not possible to ascertain whether the SO_2 oxidation is due to reaction with the immediate ozone - olefin product or reaction with a subsequent decomposition product such as OH.

The radical addition products, such as $ROSO_2$, should react rapidly to generate sulfuric acid, peroxysulfuric acid, alkyl sulfates, and mixed intermediates such as $HOSO_2ONO_2$. All of these species can then ultimately lead to aerosol sulfate.

Table 18

SO_2 OXIDATION REACTIONS IN PHOTOCHEMICAL SMOG

No.	Reaction	Rate Constant at 25°C, $ppm^{-1}\ min^{-1}$	Reference
13	$SO_2 + OH \rightarrow HOSO_2$	2.65×10^3 (162°C)	Gordon and Niloc (1975)
14	$SO_2 + OH + M \rightarrow HOSO_2 + M$	1.3×10^3 (pseudo second-order)	Davis (1974)
15a	$SO_2 + HO_2 \rightarrow SO_3 + OH$	1.3	Payne et al. (1973)
15b	$SO_2 + HO_2 \rightarrow SO_2HO_2$	6.2×10^{-2}†	not measured
16a	$SO_2 + RO_2 \rightarrow SO_3 + RO$	1.5*	not measured
16b	$SO_2 + RO_2 \rightarrow SO_2RO_2$	6.2×10^{-2}	not measured
17	$RO + SO_2 \rightarrow ROSO_2$		
18	$CH_2\overset{O_3}{\diagup\diagdown}CH_2 + SO_2 \rightarrow SO_3 + 2CH_2O$		
19a	$CH_2OO + SO_2 \rightarrow SO_3 + CH_2O$		
19b	$CH_2{=}O{-}O + SO_2 \rightarrow SO_3 + CH_2O$		

† An estimate based on Calvert's suggestion that Reactions 15b and 16b should be about 1/8 as fast as Reactions 15a and 16a.

* An estimate based on the assumption that Reaction 16a should proceed about 30% faster than Reaction 15a at comparable concentrations.

b. Sulfate Formation in Solution

The catalytic oxidation of SO_2 in solution is known to be promoted by ammonium ions and metal ions, such as Fe^{+3} and Mn^{+2}. In such oxidation, the role of NH_4^+ is essentially to buffer the solution to permit effective absorption of SO_2 to form sulfurous acid and sulfite ions. The solution chemistry of this system seems to be reasonably well understood (Scott and Hobbs, 1967; Miller and dePena, 1971).

The important steps in the equilibrium chemistry of the SO_2-H_2O-NH_3 system are given in Table 19.

Sulfate forms according to:

$$SO_3^= + \frac{1}{2} O_2 \rightarrow SO_4^+ \quad . \tag{20}$$

Assuming that there is an excess of dissolved oxygen, we can represent the rate of formation of sulfate ion by

$$\frac{d\left[SO_4^=\right]}{dt} = k_{20}\left[SO_3^=\right] \quad .$$

Miller and dePena (1971) estimated that $k_{20} = 3.1 \times 10^{-3}$ sec^{-1}. Ammonia is important because it strongly governs the formation of $SO_3^=$. In Table 19 we present the chemical equilibria for the SO_2-NH_3-liquid water system, including CO_2 equilibria. Scott and Hobbs (1967) showed that as the concentration of $SO_4^=$ increases in a droplet, the concentration of hydrogen ions increases. The increase in $[H^+]$ causes $[SO_3^=]$ to decrease, and the rate of production of $SO_4^=$ thus decreases. This means that $[SO_4^=]$ approaches a limiting value as the reaction proceeds. Calculations performed by Scott and Hobbs indicate that for typical atmospheric conditions, the initial concentration of $SO_3^=$ is 500 times greater when NH_3 is present than when it

Table 19

CHEMICAL EQUILIBRIA IN THE SO_2-NH_3-H_2O-CO_2 SYSTEM

Reaction	Equilibrium Constant Expression	Value of the Equilibrium Constant at 25°C
$H_2O \rightleftarrows H^+ + OH^-$	$K_w = [H^+][OH^-]$	1.008×10^{-14}
$(SO_2)_g + H_2O \rightleftarrows SO_2 \cdot H_2O$	$K_{hs} = [SO_2 \cdot H_2O]/p_{SO_2}$	1.24
$SO_2 \cdot H_2O \rightleftarrows H^+ + HSO_3^-$	$K_{1s} = [H^+][HSO_3^-]/[SO_2 \cdot H_2O]$	0.0127
$HSO_3^- \rightleftarrows H^+ + SO_3^=$	$K_{2s} = [H^+][SO_3^=]/[HSO_3^-]$	6.24×10^{-8}
$(NH_3)_g + H_2O \rightleftarrows NH_3 \cdot H_2O$	$K_{ha} = [NH_3 \cdot H_2O]/p_{NH_3}$	57
$NH_3 \cdot H_2O \rightleftarrows NH_4^+ + OH^-$	$K_{1a} = [NH_4^+][OH^-]/[NH_3 \cdot H_2O]$	1.774×10^{-5}
$(CO_2)_g + H_2O \rightleftarrows CO_2 \cdot H_2O$	$K_{hc} = [CO_2 \cdot H_2O]/p_{CO_2}$	0.034
$CO_2 \cdot H_2O \rightleftarrows H^+ + HCO_3^-$	$K_{1c} = [H^+][HCO_3^-]/[CO_2 \cdot H_2O]$	4.45×10^{-7}
$HCO_3^- \rightleftarrows H^+ + CO_3^=$	$K_{2c} = [H^+][CO_3^=]/[HCO_3^-]$	4.68×10^{-11}

Source: Scott and Hobbs (1967).

is absent. Thus, based on Reaction 20 above, the initial rate of formation of $SO_4^{=}$ is also increased by a factor of 500 in the presence of NH_3. Not only does the presence of NH_3 increase the rate of formation of $SO_4^{=}$, but also the concentration of $SO_4^{=}$ formed after 24 hours in the presence of NH_3 is two orders of magnitude greater than in its absence.

Ozone is quite soluble in water. Thus, dissolved O_3 and SO_2 in water droplets might lead to enhanced oxidation rates of SO_2. Penkett (1972) found that oxidation of SO_2 in air at 7 ppb absorbed in water droplets, where ambient O_3 was at 5 pphm, was as fast as 13 percent per hour.

In studies in which NH_3 was added to a mixture of air, SO_2, and sulfuric acid embryos, Friend (1966) found a rapid production of large particles of ammonium sulfate. The following mechanism explains the experimental results:

$$H_2SO_4 \cdot nH_2O + NH_3 \rightarrow NH_4\,HSO_4 \cdot nH_2O \quad , \qquad (21)$$

$$NH_4HSO_4 \cdot nH_2O + NH_3 \rightarrow (NH_4)_2\,SO_4 \cdot nH_2O \quad , \qquad (22)$$

$$2NH_3 + SO_2 + H_2O + \frac{1}{2}\,O_2 \xrightarrow[\text{Catalyst}]{NH_4^+} (NH_4)_2SO_4 \quad . \qquad (23)$$

Reactions 21 and 22 represent the conversion of acid embryos to salt embryos. The solution present in the salt embryos is the medium necessary for the catalytic oxidation of SO_2 represented by Reaction 23.

Kiang et al. (1973) also considered the nucleation processes involved in aerosol formation and the possible chemical reactions associated with the formation of $(NH_4)_2SO_4$. They suggested that the gas phase reaction

$$NH_3 + SO_2 \xrightarrow{H_2O} NH_3 \cdot SO_2$$

is followed in the presence of water by a heteromolecular nucleation of gaseous $NH_3 \cdot SO_2$ and gaseous H_2O into an aqueous $NH_3 \cdot SO_2$ solution droplet:

$$NH_3 \cdot SO_2 + H_2O \rightarrow \text{Aerosol} \quad .$$

The solution droplets may form $(NH_4)_2SO_4$ after oxidation.

Stauffer et al. (1973) suggested that in a system of low volatility gases--such as H_2SO_4, $NH_3 \cdot SO_2$, NH_4Cl, NH_4NO_3, and organic acids--in equal concentrations and in the presence of water vapor, the gaseous substance with the lowest volatility nucleates first and the critical sized droplets then act as surfaces for heteromolecular condensation (in the absence of particles).

2. Nitrate Formation

The modes of formation of aerosol nitrates are less well understood than those leading to sulfate. Nitrate levels in Los Angeles are observed to peak sharply in the morning and then to increase slowly in air masses as they move over the eastern portions of the Basin. The rapid NO_3^- morning buildup appears to be unrelated to the gradual increase in NO_3^- eastward across the Basin later in the day. In the ACHEX study no systematic, useful relation could be established between NO_3^- levels and those of O_3, NO, NO_2, $SO_4^=$, relative humidity, or noncarbonate carbon (Hidy et al., 1975).

There is virtually no quantitative information available on the rates of conversion of NO_x to NO_3^- in the atmosphere. A rapid transient conversion exists in conjunction with the morning influx of NO_x, perhaps associated with the high humidity prevalent in the morning hours. The second NO_3^- formation process is slower than that in the morning and is roughly comparable in rate to SO_2 oxidation to $SO_4^=$.

Aerosol nitrates can be formed by homogeneous and heterogeneous pathways. Figure 19 summarizes many of these pathways. The low vapor pressure of sulfuric acid leads to rapid homogeneous nucleation at H_2SO_4 partial pressures in the range 10^{-8} to 10^{-10} torr. The hydration of sulfuric acid droplets is thermodynamically favored over a wide range of relative humidities. Thus, sulfuric acid formed in the gas phase can be expected to become rapidly incorporated into the particulate phase. Although nitric acid can be formed in the gas phase in several ways (to be discussed shortly). the vapor pressure of nitric acid is relatively high, and homogeneous nucleation of HNO_3 in a humid atmosphere is not expected to take place under normal atmospheric conditions (Kiang et al., 1973). Nitric acid does form certain stable complexes in sulfuric acid solutions (Gillespie et al., 1950), and Castleman (1974) suggested that HNO_3 may become incorporated in sulfuric acid droplets.* It appears that the production of aerosol nitrate must involve formation of a condensable species such as NH_4NO_3 in the gas phase, or the absorption of an NO_x species in a droplet followed by chemical stabilization.

The morning nitrate mechanism, generally associated with particles of diameter greater than 0.5 μm, probably involves absorption of NO_x species into droplets followed by chemical reaction in the drop. The afternoon mechanism, generally associated with particles of sizes less than 0.5μm, probably involves gas phase oxidation of NO_x in photochemical smog reactions followed by condensation of products such as NH_4NO_3.

We now consider both gas and liquid phase nitrate forming mechanisms. The objective is to identify clearly what is known and unknown concerning NO_3^- chemistry in urban aerosols.

---

*To assess the importance of this pathway for removal of HNO_3 from the gas phase, Castleman (1974) suggested measurement of HNO_3 vapor pressures over H_2SO_4-H_2O-HNO_3 solutions.

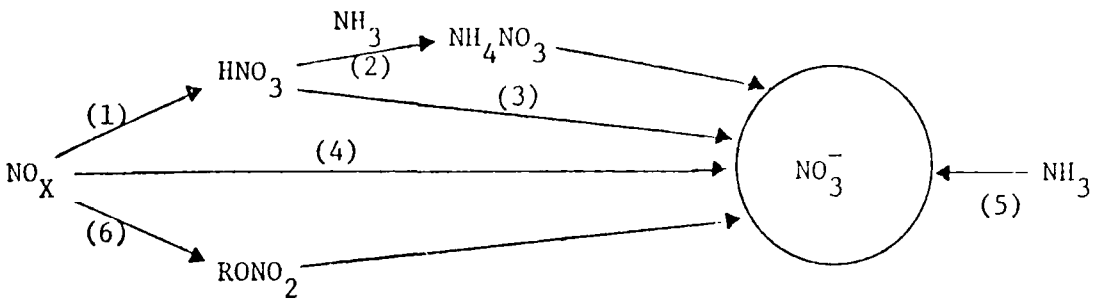

1. Gas-phase formation of HNO_3 from NO_x
2. Gas-phase formation of NH_4NO_3 followed by condensation of NH_4NO_3 on existing droplets
3. Absorption of HNO_3 in droplet
4. Direct absorption of NO_2 in droplet
5. Direct absorption of NH_3 in droplet
6. Formation of organic nitrates in the gas phase followed by condensation of the organic nitrates.

FIGURE 19. PATHWAYS FOR FORMATION OF NITRATE AEROSOLS

a. Nitrate Formation in the Gas Phase

The reaction paths for nitrate accumulation in the particulate phase via homogeneous steps all involve reactions of gaseous nitric acid. Table 20 lists the major gas phase reactions involving nitric acid. The major homogeneous sources of nitric acid in photochemical smog are Reactions 3 and 4 in Table 20. Based on the rate constants given in Table 20, the rates of formation of nitric acid by these two reactions can be estimated for typical atmospheric conditions. If we assume that $[NO_2]$= 0.1 ppm, $[H_2O]$= 10^4 ppm, $[N_2O_5]$= 10^{-3} ppm, and [OH]= 10^{-7} ppm, then the rates of formation of $HONO_2$ through Reactions 3 and 4 are

$$R_3 = 5 \times 10^{-5} \text{ ppm min}^{-1}$$
$$R_4 = 10^{-4} \text{ ppm min}^{-1}$$

Thus, it appears that Reaction 4 is the principal one for gaseous $HONO_2$ formation in photochemical smog. The rate of conversion of NO_2 to $HONO_2$ by Reaction 4 is of the order of 6 percent per hour.

The following reactions appear to be the principal ones involving ammonia in the nitrate system:

$NH_3 + HONO_2 \rightarrow NH_4NO_3$	2.8×10^{-2} ppm^{-1} min^{-1}	Calvert (1974)
$NH_3 + HNO_2 \rightarrow NH_4NO_2$	2.8×10^{-2} ppm^{-1} min^{-1}	Calvert (1974)

Countess and Heichlen (1973) measured the rate constant for the reaction

$$NH_3 + HCl \rightarrow NH_4Cl$$

Table 20

MAJOR HOMOGENEOUS REACTIONS INVOLVING NITRIC ACID IN PHOTOCHEMICAL SMOG

No.	Reaction	Rate Constant at 25°C, ppm^{-1} min^{-1}	Reference
1.	$NO_3 + NO_2 \rightarrow N_2O_5$	5.6×10^3	Garvin and Hampson (1974
2.	$N_2O_5 \rightarrow NO_3 + NO_2$	30 min^{-1}	Garvin and Hampson (1974
3.	$N_2O_5 + H_2O \rightarrow 2\ HONO_2$	5×10^{-6}	Garvin and Hampson (1974
4.	$OH + NO_2 \rightarrow HONO_2$	10^4	Garvin and Hampson (1974
5.	$OH + HNO_3 \rightarrow H_2O + NO_3$	190	Garvin and Hampson (1974
6.	$HO_2 + NO_3 \rightarrow HONO_2 + O_2$	2.5×10^3	Demerjian, Kerr, and Calvert (1974)
7.	$NO + HNO_3 \rightarrow HNO_2 + NO_2$	2.5×10^{-4}	Hecht, Seinfeld, and Dodge (1974)
8.	$HNO_2 + HNO_3 \rightarrow H_2O + 2\ NO_2$	0.2	Hecht, Seinfeld, and Dodge (1974)

as 2.8×10^{-2} ppm^{-1} min^{-1}. If the NH_3 - HONO reaction has a rate constant of this magnitude, and if NH_3 and HONO concentrations can be estimated as 1 pphm, Calvert (1974) estimated the homogeneous rate of NH_4NO_3 formation as 2.8×10^{-6} ppm min^{-1}.

b. Nitrate Formation in Solution

Little is known about liquid-phase nitrate formation in atmospheric aerosols. Liquid-phase mechanisms may be largely responsible for the morning nitrate peak observed in Los Angeles. In this subsection we discuss the possible chemistry leading to NO_3^- formation in aerosol droplets. Consider an idealized situation in which a droplet of pure water is exposed to an atmosphere containing NO, NO_2, SO_2, NH_3, O_3, and CO_2. An equilibrium situation will be established in the droplet as the result of the dissolution of the gases and subsequent reaction and ionization. In addition to the equilibria, sulfate and nitrate form irreversibly by

$$SO_3^= + \frac{1}{2} O_2 \rightarrow SO_4^=$$

$$NO_2^- + \frac{1}{2} O_2 \rightarrow NO_3^-$$

$$NO_2^- + O_3 \rightarrow NO_3^- + O_2$$

The equilibria in the SO_2-NH_3-CO_2-H_2O system as well as the kinetics of sulfate formation have been considered by Scott and Hobbs (1967) and were discussed in the previous section (see Table 19). An analogous study of NO-NO_2-NH_3-CO_2-H_2O equilibria and nitrate formation kinetics has not been carried out.

Table 21 presents four reactions and their equilibrium constants which occur subsequent to absorption of NO and NO_2 by a droplet. We note that NO_3^- can form as a result of the equilibrium established in Reaction 2 as well as by the irreversible oxidation reactions with dissolved O_2 and O_3. At this point the relative efficiencies of the nitrate-forming reactions are unknown.

No.	Reaction	Equilibrium Constant	Value at 25°C	Reference
1.	$(NO)_g + (NO_2)_g + H_2O \rightleftharpoons 2HNO_2$	$K_{1n} = \frac{[HNO_2]^2}{P_{NO}\ P_{NO_2}}$	122	--
2.	$2(NO_2)_g + H_2O \rightleftharpoons HNO_2 + H^+ + NO_3^-$	$K_{2n} = \frac{[HNO_2][H^+][NO_3^-]}{P^2_{NO_2}}$	4.3×10^5	(Pick, 1920)
3.	$HNO_2 \rightleftharpoons H^+ + NO_2^-$	$K_{3n} = \frac{[H^+][NO_2^-]}{[HNO_2]}$	4.5×10^{-4}	(Abegg)

3. The Generation of Organic Compounds of Low Volatility

The formation of photochemical aerosols during the irradiation of hydrocarbon-NO_x mixtures was first observed by Haagen-Smit in the early 1950s (Haagen-Smit and Fox, 1952). Since that time, a number of studies have been performed to determine the types of hydrocarbons that lead to aerosol formation when reacted with ozone or irradiated in the presence of NO_x. Table 22 presents a summary of several of these studies. Based on these studies, the following conclusions can be drawn concerning photochemical aerosol formation:

> Paraffins, olefins containing fewer than five carbon atoms, and benzene do not form aerosols.
> Five- and six-carbon monolefins form aerosols only if the hydrocarbon is branched.
> In general, only those olefins that produce a radical with six or more carbon atoms after rupture of the double bond form aerosols.
> Cyclic olefins and diolefins form significantly more aerosol than do alkenes that lead to radicals with the same number of carbon atoms.
> Terpenes form the most aerosol of the hydrocarbons studied.

In addition to the studies cited in Table 22, investigators examined the effect of adding SO_2 to hydrocarbon-O_3 or hydrocarbon-NO_x systems. We have already stated that SO_2 can be effectively oxidized by intermediates formed in an irradiated hydrocarbon-NO_x system. In many smog chamber studies, aerosol sulfate has formed in irradiated hydrocarbon-NO_x or hydrocarbon-O_3 systems (Prager et al., 1960; Stevenson et al., 1965; Schuck and Doyle, 1959; Schuck et al., 1960; Endow et al., 1963; Harkins and Nicksic,

Table 22

STUDIES REPORTING AEROSOL FORMATION FOR DIFFERENT HYDROCARBONS UPON REACTION WITH OZONE OR PHOTOLYSIS IN THE PRESENCE OF NO_x

Hydrocarbon	Reference*
Monolefins	
1-hexene	2, 6, 9
1-heptene	2, 5, 7, 8
2-methyl-1-hexene	7
2,4,4-trimethyl-1-pentene	1
1-octane	6
1-decene	6
1-dodecene	6
Cyclic olefins	
Cyclopentene	1, 3, 8
Cyclohexene	1, 3, 4, 5, 6, 7, 8, 9
α-pinene	3, 4, 5, 7, 8
Diolefins	
1,3-butadiene	1
1,5-hexadiene	1, 4, 8
1,6-heptadiene	7
1,7-octadiene	7, 8
1,6-octadiene	7
2-methyl-1,5-hexadiene	7
Cyclopentadiene	1
Aromatics	
Toluene	9
m-Xylene	9

* Numbers refer to the following references:

Number	Reference
1	Prager et al. (1960)
2	Stevenson et al. (1965)
3	Groblicki and Nebel (1971)
4	Ripperton et al. (1972)
5	Wilson et al. (1972)
6	Hidy and Burton (1974)
7	O'Brien et al. (1975)
8	Grosjean and Friedlander (1975)
9	Kocmod et al. (1975)

1965; Groblicki and Nebel, 1971; Wilson et al. 1972; Cox and Penkett, 1972; McNelis, 1974). In a recent study, Grosjean (1975) found that the formation of aerosol sulfate depends on the hydrocarbon type. Alkenes having less than seven carbon atoms, which do not form organic aerosols in irradiated NO_x systems, always produce sulfate aerosols when SO_2 is added. Alkenes with seven or more carbon atoms and C_1-C_4 diolefins form organic aerosols in the absence of SO_2 and both organic and sulfate aerosols in the presence of SO_2. For C_5+ diolefins and cyclic olefins, Grosjean found no significant sulfate formation, and the nature and yield of organic aerosols is unaffected when SO_2 is added. Grosjean's observations with respect to cyclohexene were, however, not substantiated by the study of Kocmond et al. (1975), in which a substantial increase in aerosol formation was observed in a system of cyclohexene-NO_x-SO_x over that in a system of cyclohexene-NO_x. Because the composition of the aerosol was not measured in the Kocmond et al. study, it cannot be established that there was any sulfate aerosol present, although it is highly probable there was.

Although photochemical aerosols have been known to exist for more than two decades, until recently no significant attempts were made to identify the composition of the aerosols, particularly the organic fraction. Using a gas chromatograph and mass spectrometer system, Wilson et al. (1972) analyzed the aerosol generated from cyclohexene and α-pinene in the presence of NO_2. They found that each identifiable constituent contained an organic acid functional group. Each of these species also contained a second functional group, either an aldehyde, an alcohol, a nitrate ester, or a ketone. O'Brien et al. (1975) analyzed the aerosol formed from the reaction of cyclohexene and 1,7-octadiene with ozone and found adipic acid to be a major component. Upon irradiation of cyclohexene and 1,7-octadiene, Grosjean (1975) found the following product distributions:

Reactant	Products	Percent of Total Organic Aerosol Mass
Cyclohexene	Adipic acid	55%
	Hexanoic acid nitrate	24
1,7-octadiene	Adipic acid	61
	Hexanoic acid nitrate	25

One would expect that if organic acids and their derivatives were present in the atmosphere, they would accumulate in the particulate phase because of their very low vapor pressures at ambient temperatures.

a. Vapor Pressures of Organic Aerosol Constituents

The primary reason for the condensation of the relatively high-molecular-weight organic acids and their derivatives is the extremely low vapor pressures of these species at ambient temperatures. Unfortunately, very little specific data are available on the vapor pressures of the organic species (discussed above) that have recently been identified. For example, of the major species identified by Grosjean and O'Brien et al., adipic acid is the only one for which vapor pressure data are available. Figure 20 shows the vapor pressure of adipic acid as a function of temperature. At 25°C, adipic acid in the pure state is a solid, although it probably exists in solution in aerosol particles. Now that commonly occurring organic aerosol species have been identified, vapor pressure determinations will be quite desirable for the purposes of predicting rates of heterogeneous condensation.

b. Reaction Mechanisms Leading to Organic Aerosol Constituents

As a result of recent identifications of several organic aerosol species in field and laboratory smog chamber studies, we can now postulate mechanisms that might account for the observed products.

It appears that the principal reaction responsible for the formation of organic aerosol precursors (the species that, once formed, condense into the particulate phase) is the ozone-olefin reaction. In Table 23 we summarize the classical Criegee mechanism for liquid phase ozone-olefin reactions, which has often been used to explain gas phase reactions in photochemical smog, and the new mechanism proposed by O'Neal and Blumstein (1973). The principal aspect of the Criegee mechanism is the decomposition of the molozonide intermediate into a carbonyl compound and a diradical, or a zwitterion. The zwitterion can then decompose or react with other species in the system. In the O'Neal and Blumstein mechanism, the molozonide is postulated to be in equilibrium with two diradicals. The diradicals can then participate in hydrogen abstraction reactions.

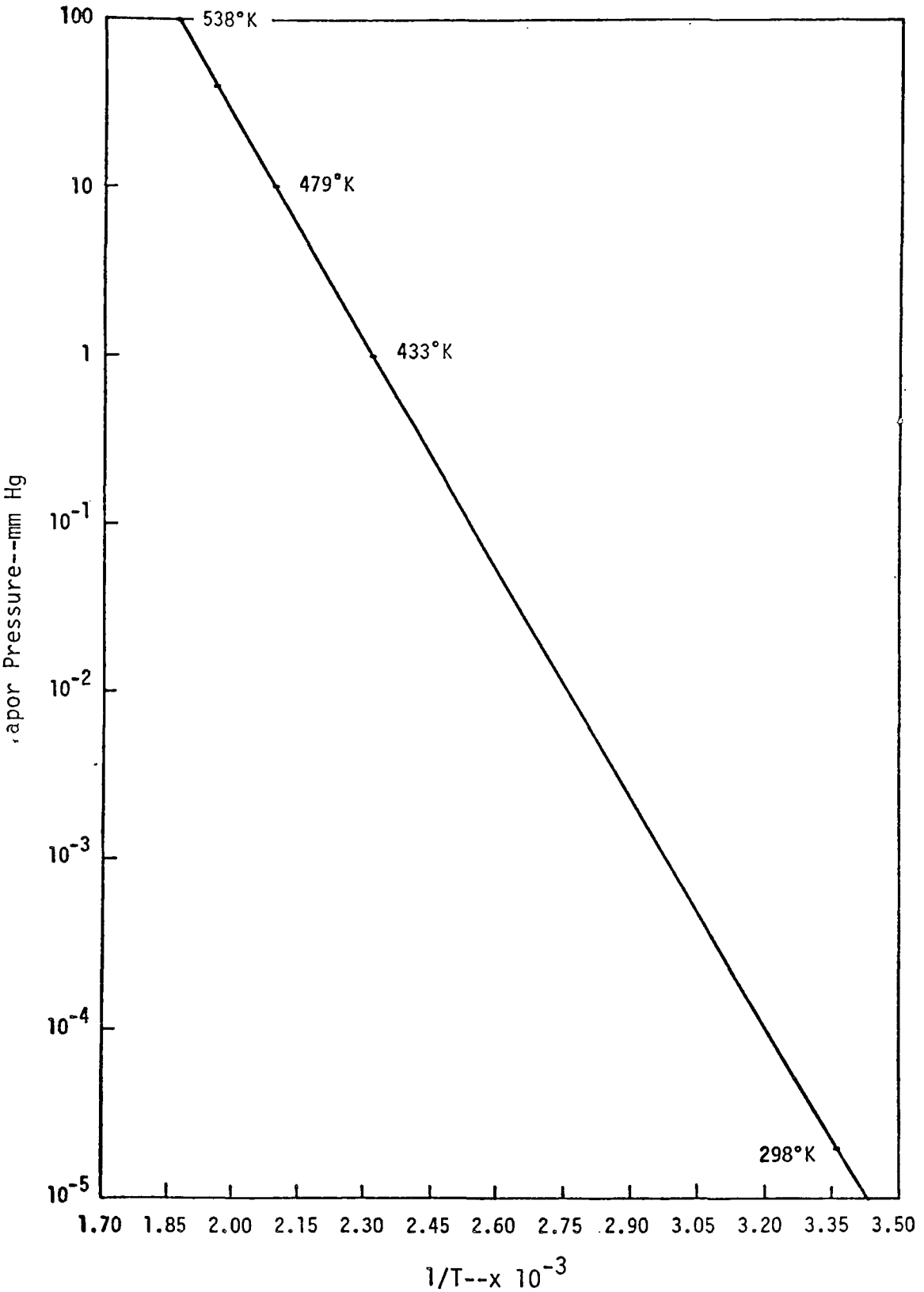

FIGURE 20. EXTRAPOLATION OF THE VAPOR PRESSURE OF ADIPIC ACID TO THE AMBIENT TEMPERATURE

Table 23

OZONE-OLEFIN REACTION MECHANISMS

Criegee mechanism

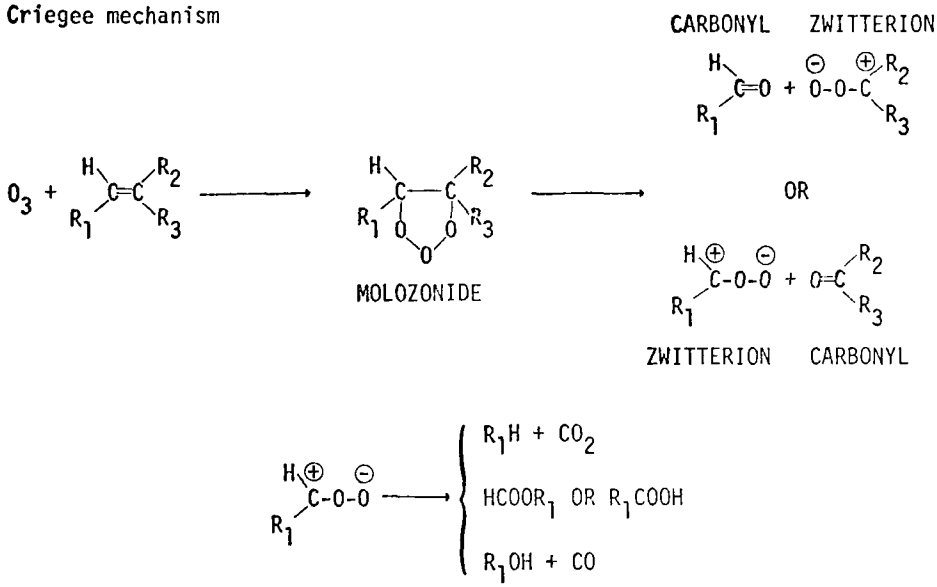

O'Neal and Blumstein mechanism

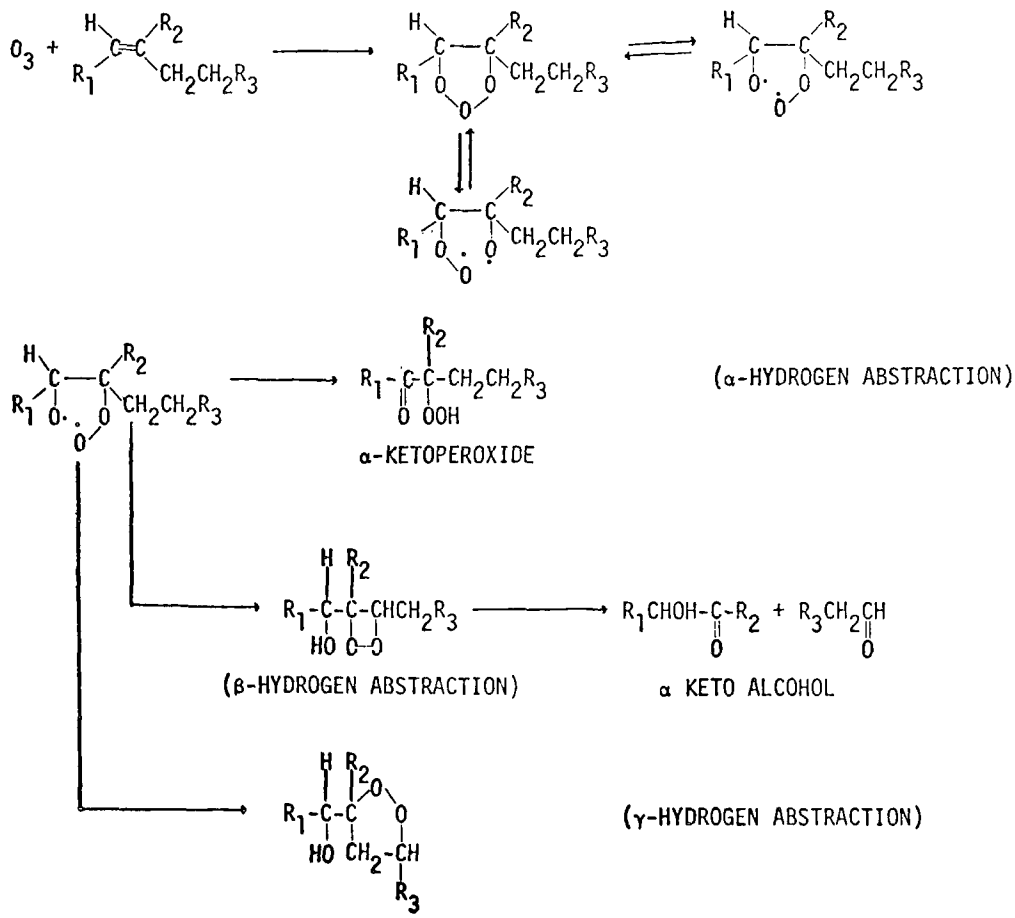

O'Neal and Blumstein estimated that the Criegee mechanism is more important for ethylene and propylene, that both the Criegee and hydrogen abstraction mechanisms are of equal importance for butenes, and that the latter mechanism is more important for alkenes with five or more carbon atoms.

Let us now consider possible mechanisms for accounting for observed organic aerosol species. The most effective aerosol generators have been found to be cyclic olefins and diolefins. Two olefins in these classes that have been studied recently in smog chamber experiments are cyclohexene and 1,7-octadiene. Table 24 summarizes the products observed in three such studies. The major products found in these smog chamber studies were difunctional aliphatic compounds. Thus, the desired mechanisms are those that will convert cyclic olefins and diolefins to difunctional aliphatic compounds. Although the reaction with ozone appears to be the major one responsible for aerosol formation, reactions with atomic oxygen and hydroxyl radicals can also be postulated. Table 25 presents mechanisms involving the reaction of cyclohexene with O, OH, and O_3. In this table, the species that have been identified in smog chamber studies are shown in boxes.

Table 24

ORGANIC AEROSOL CONSTITUENTS IDENTIFIED IN SMOG CHAMBER STUDIES

Cyclohexene		1,7-Octadiene
Wilson et al. (1972)	Grosjean (1975)	O'Brien et al. (1975), Grosjean (1975)
$CH_2OH - (CH_2)_3 - COOH$	$COOH - (CH_2)_4 - COOH$	$COOH - (CH_2)_4 - COOH$
$COH - (CH_2)_3 - COOH$	$COOH - (CH_2)_4 - CH_2ONO_2$	$COOH - (CH_2)_4 - CH_2ONO_2$
$CH_2ONO_2 - (CH_2)_3 - COOH$	$CH_2OH - (CH_2)_3 - CH_2OH$	
$CHO - (CH_2)_4 - COOH$		

4. The Role of Water in Photochemical Aerosols

There is strong evidence that the total photochemical aerosol mass is closely correlated with the liquid water content of the aerosol. Figure 21

Table 25

MECHANISMS FOR REACTIONS OF CYCLOHEXENE
LEADING TO DIFUNCTIONAL ALIPHATIC COMPOUNDS

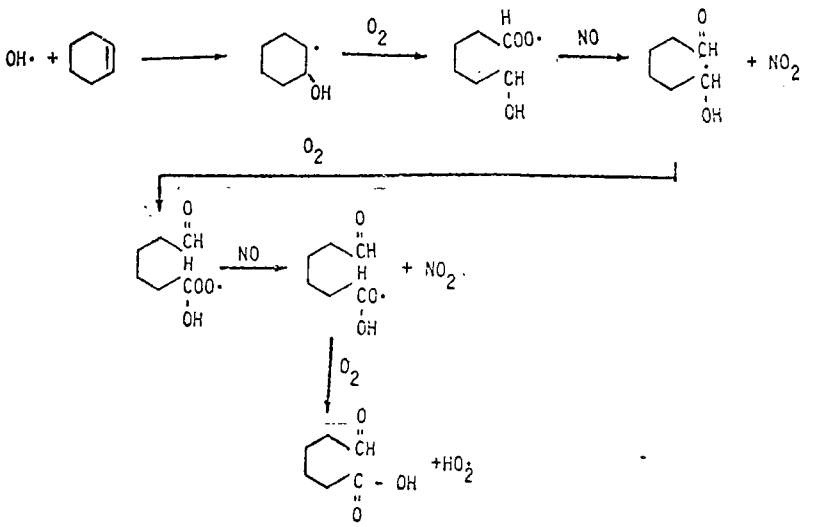

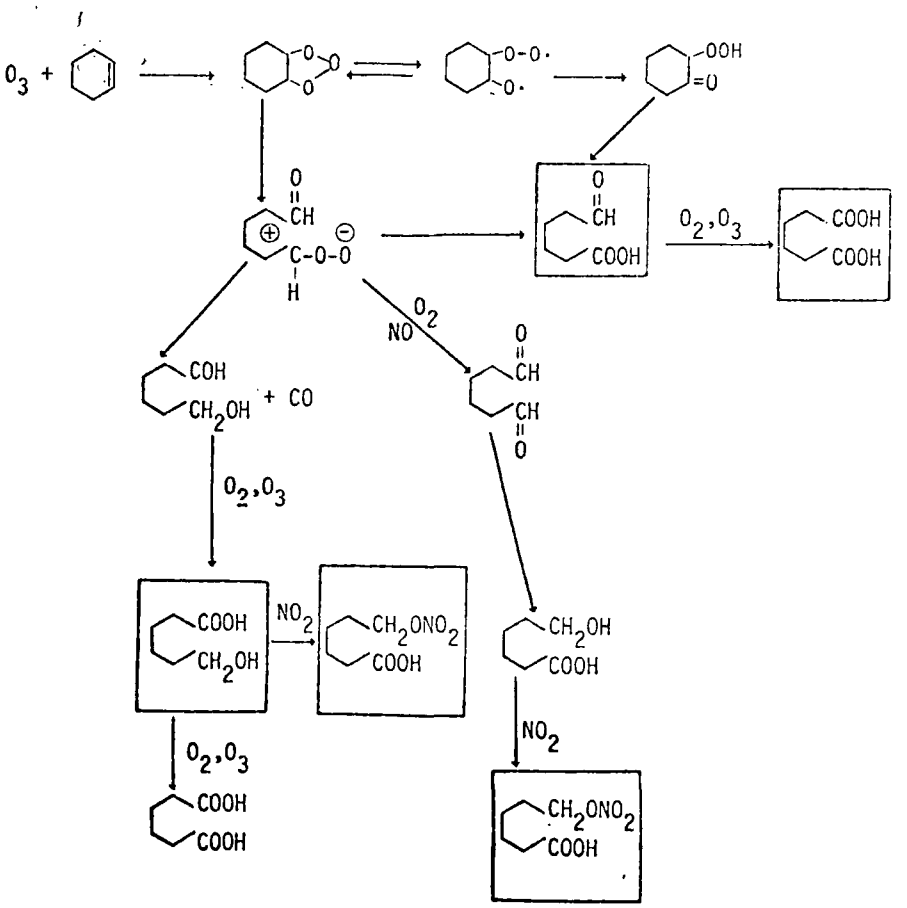

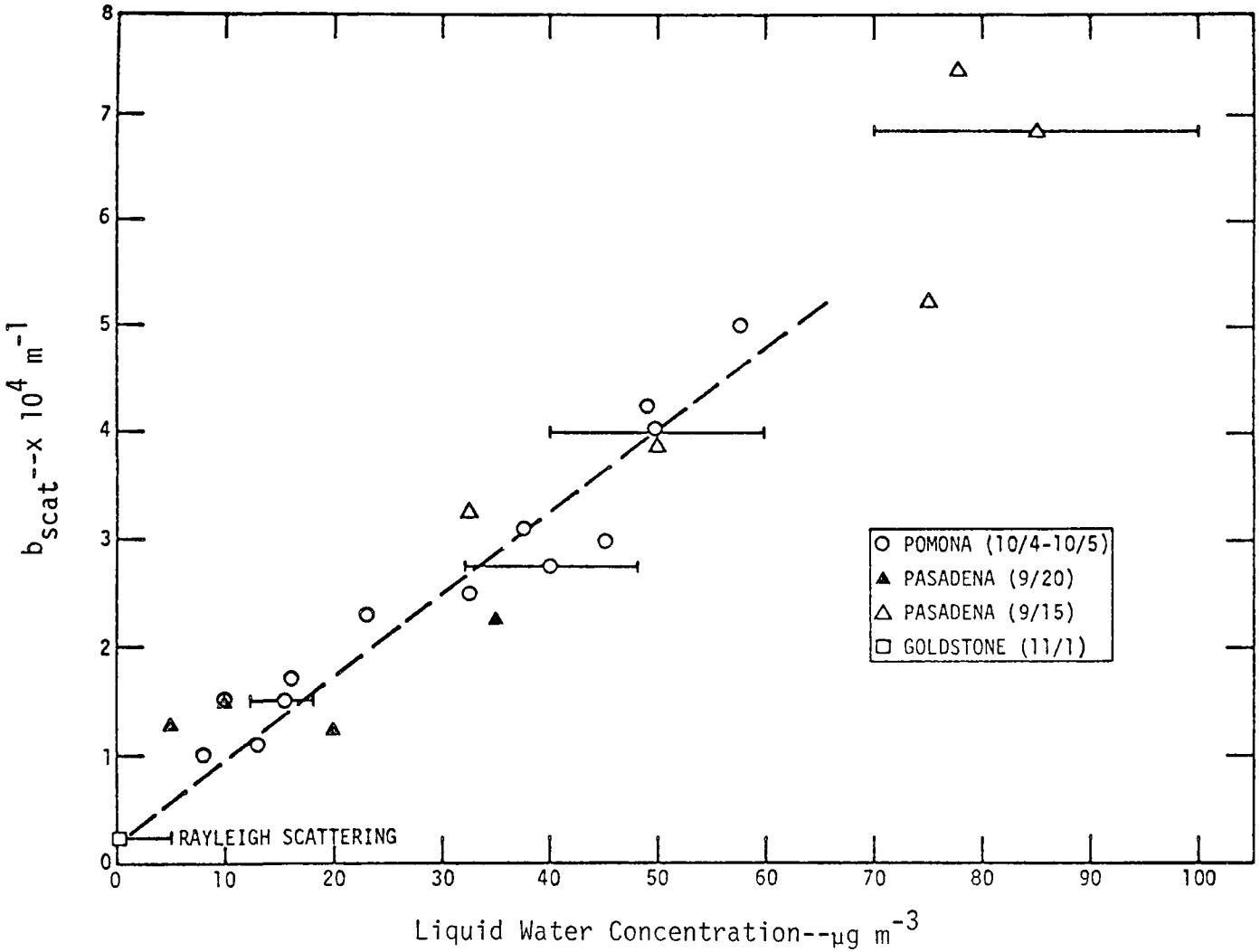

Source: Hidy et al. (1975).

FIGURE 21. THE LIGHT-SCATTERING COEFFICIENT AS A FUNCTION OF LIQUID WATER CONTENT

shows the light-scattering coefficient as a function of aerosol liquid water concentration at four locations during 1972. Figures 22 through 24 present the diurnal fluctuations of total aerosol mass and aerosol liquid water concentrations of Pomona and Pasadena. In these three figures, the data indicate that substantial changes in aerosol water content can occur despite only small changes in relative humidity. Measurements made during the 1972 ARB study indicate that changes in aerosol water content correspond closely with changes in the sulfur, nitrogen, and carbon content of the aerosol. The recent work of Ho (1975) during the 1972 ACHEX indicated that the aerosol liquid water content may display a diurnal variation closely linked with changes in aerosol mass and b_{scat} (as seen in Figures 22 through 24). Water is probably involved in sulfate and nitrate formation in the aerosol. At present, however, the mechanisms by which the water content of aerosols changes with time seem to be unknown and thus constitute a key area for future investigation.

D. SUMMARY

In this chapter, we have surveyed much of what is currently known regarding the chemistry of photochemical aerosols. In a description of urban aerosol dynamics, the prediction of the chemical composition of the aerosol requires knowledge of the details of both homogeneous and heterogeneous chemistry. The key features of such a prediction are the description of the rate of formation of condensible species and the composition of those species Compared with what is known about the physical processes that influence aerosol dynamics, our knowledge of the chemical processes is much less developed. From the review given in this chapter, the following major problem areas have emerged:

> Understanding of the homogeneous oxidation of SO_2 in photochemical smog--the important reactions and their rate constants.

> Determination of the probable route of formation of sulfate in photochemical aerosols--for example, homogeneous formation

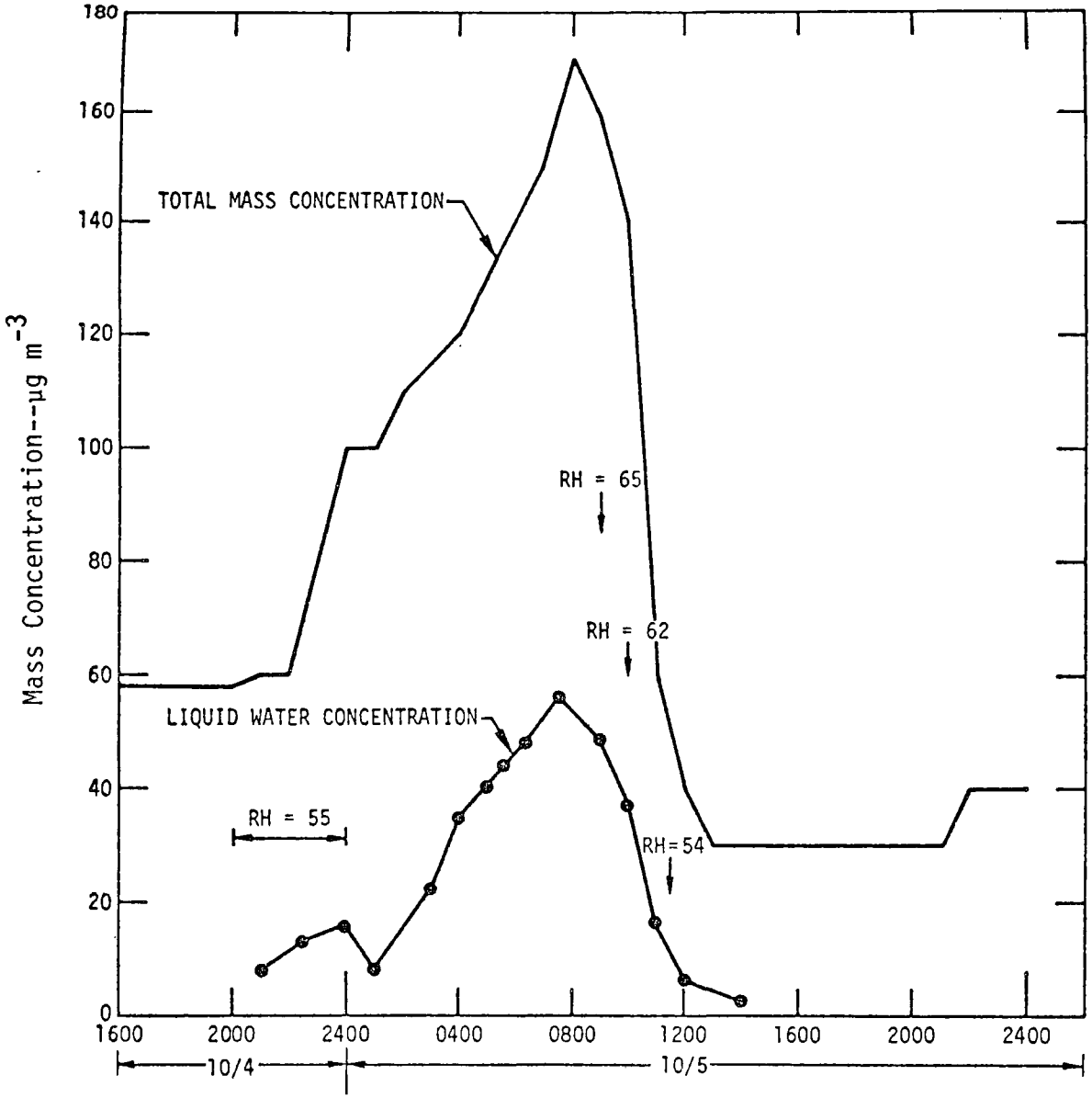

Source: Hidy et al. (1975).

FIGURE 22. DIURNAL PATTERNS OF WATEROMETER DATA FOR POMONA--4-5 OCTOBER 1972

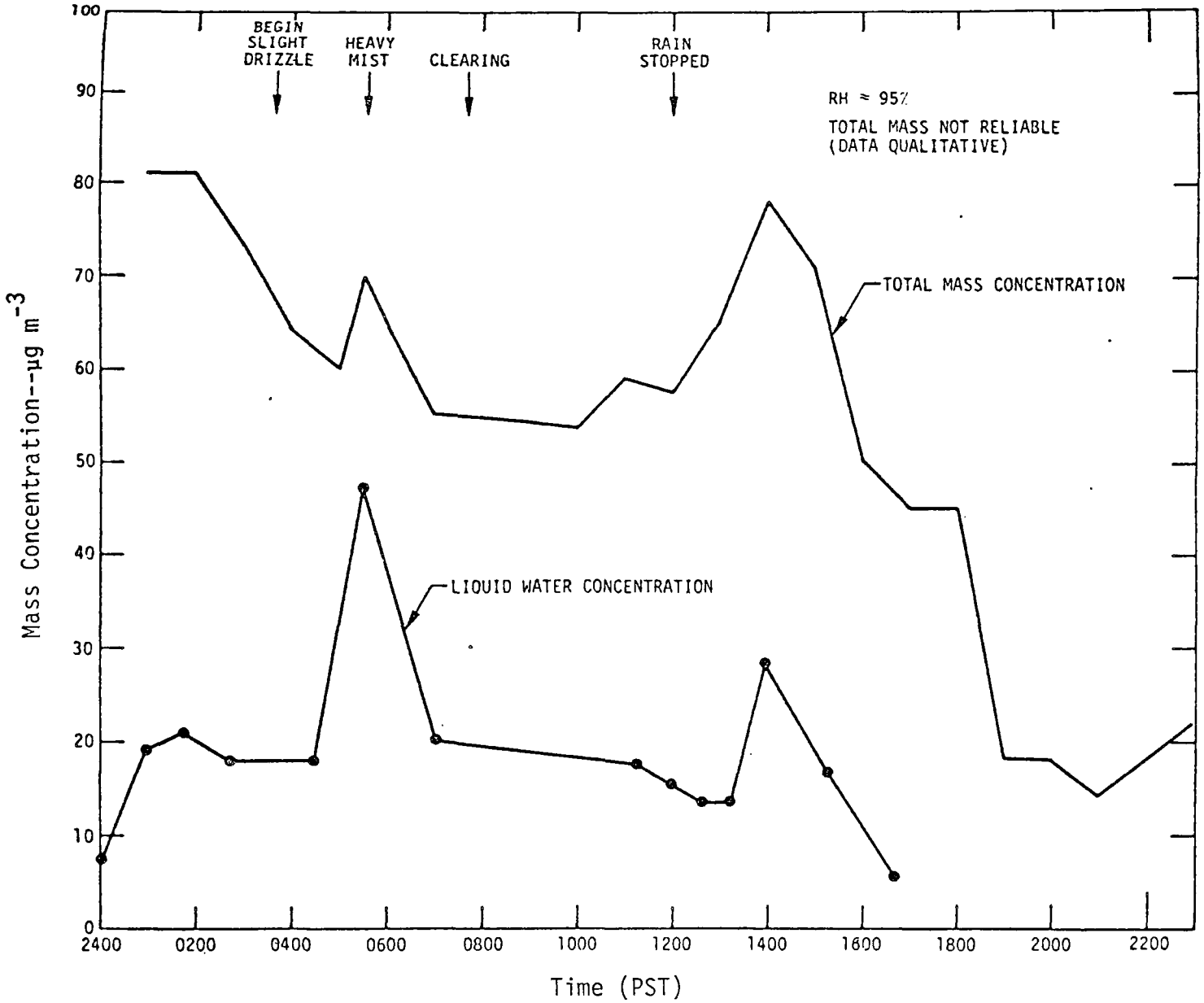

Source: Hidy et al. (1975).

FIGURE 23. DIURNAL PATTERNS OF WATEROMETER DATA FOR PASADENA--9 SEPTEMBER 1972

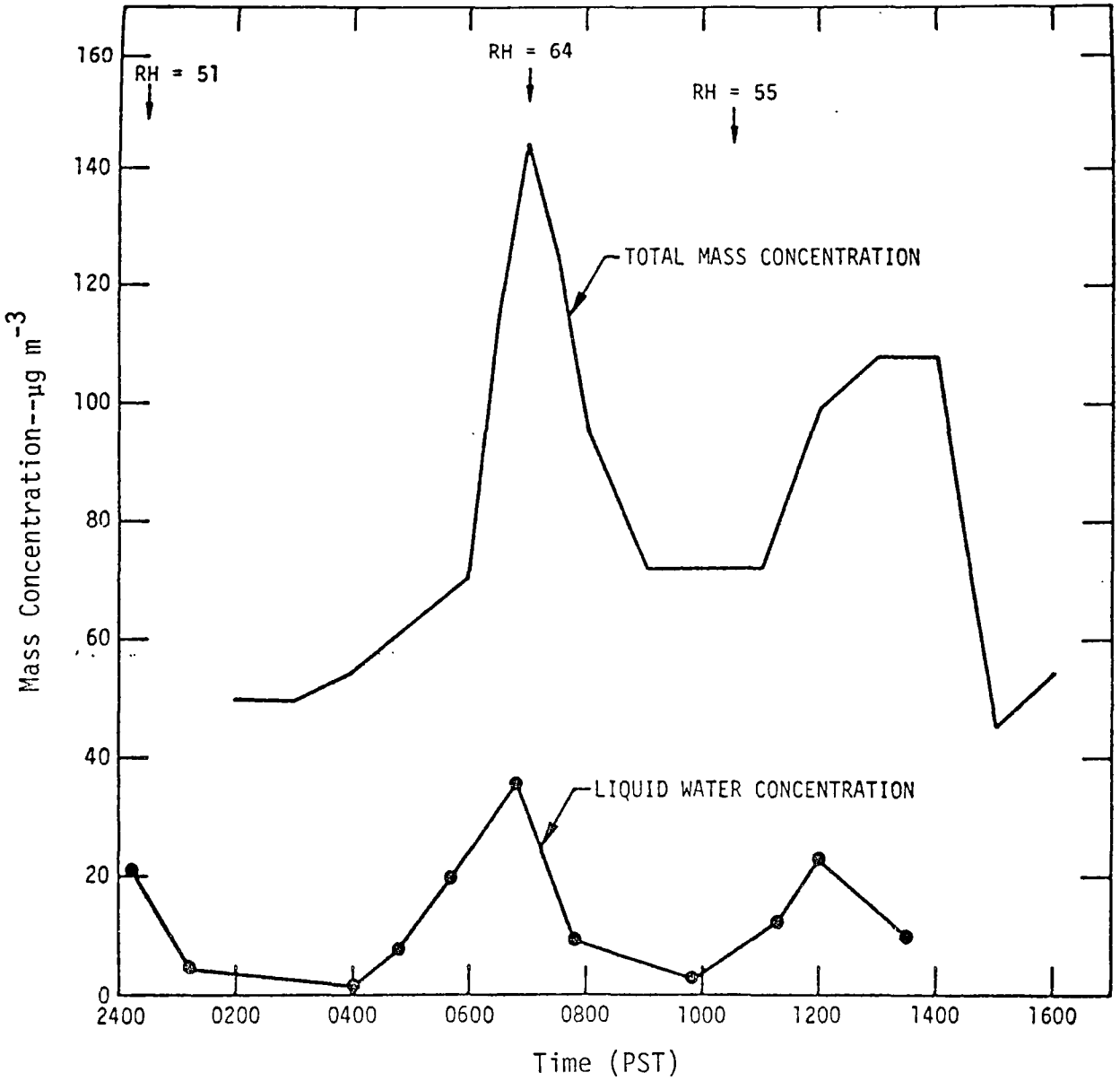

Source: Hidy et al. (1975).

FIGURE 24. DIURNAL PATTERNS OF WATEROMETER DATA FOR PASADENA--20 SEPTEMBER 1972

of H_2SO_4, followed by heterogeneous condensation, and heterogeneous formation of $SO_4^{=}$ in the presence of dissolved NH_3.

> Determination of the probable route of formation of nitrate in photochemical aerosols--for example, homogeneous formation of NO_3^-.

> Measurement of organic aerosol constituents.

> Determination of the vapor pressure of organic aerosol constituents.

> Determination of the mechanisms of formation of organic aerosol precursors in the laboratory.

> Elucidation of the mechanism of incorporation of liquid water in aerosols.

IV MATHEMATICAL MODELING OF THE DYNAMIC BEHAVIOR OF PHOTOCHEMICAL AEROSOLS

Our purpose in the previous chapters was to review the physical and chemical processes that govern the evolution of photochemical aerosols. In this chapter, we first discuss the status of emissions inventories for aerosols, then we derive the model equations, and finally we describe the approximations that might be made in developing a model.

A. THE STATUS OF AEROSOL EMISSIONS INVENTORIES

In Chapter III, we pointed out that the analysis of aerosol data for the Los Angeles basin indicates that roughly half of the aerosol mass can be attributed to gas-to-particle conversions. In Figure 25, we illustrate diagrammatically the need for a gaseous emissions inventory, as well as a primary emissions inventory, for the aerosol model. Table 26 presents references that can be used to compile an emissions inventory of natural and anthropogenic primary aerosols.

The existing emissions inventories for primary particulate matter are based on measurements made in the vicinity of the sources. On the subgrid scale, coagulation and sedimentation will modify the size distribution of the emissions. Hence,a microscale model will be necessary to account for these changes in the particle size distribution function.

The gaseous emissions inventory should include the principal secondary aerosols (such as reactive hydrocarbons, SO_2, and NO_x) as well as gases that play a role in transforming these gases to the particulate phase (such as ammonia). Although source data for emissions of gaseous pollutants have been compiled for application to photochemical smog models (Roth et al., 1974),

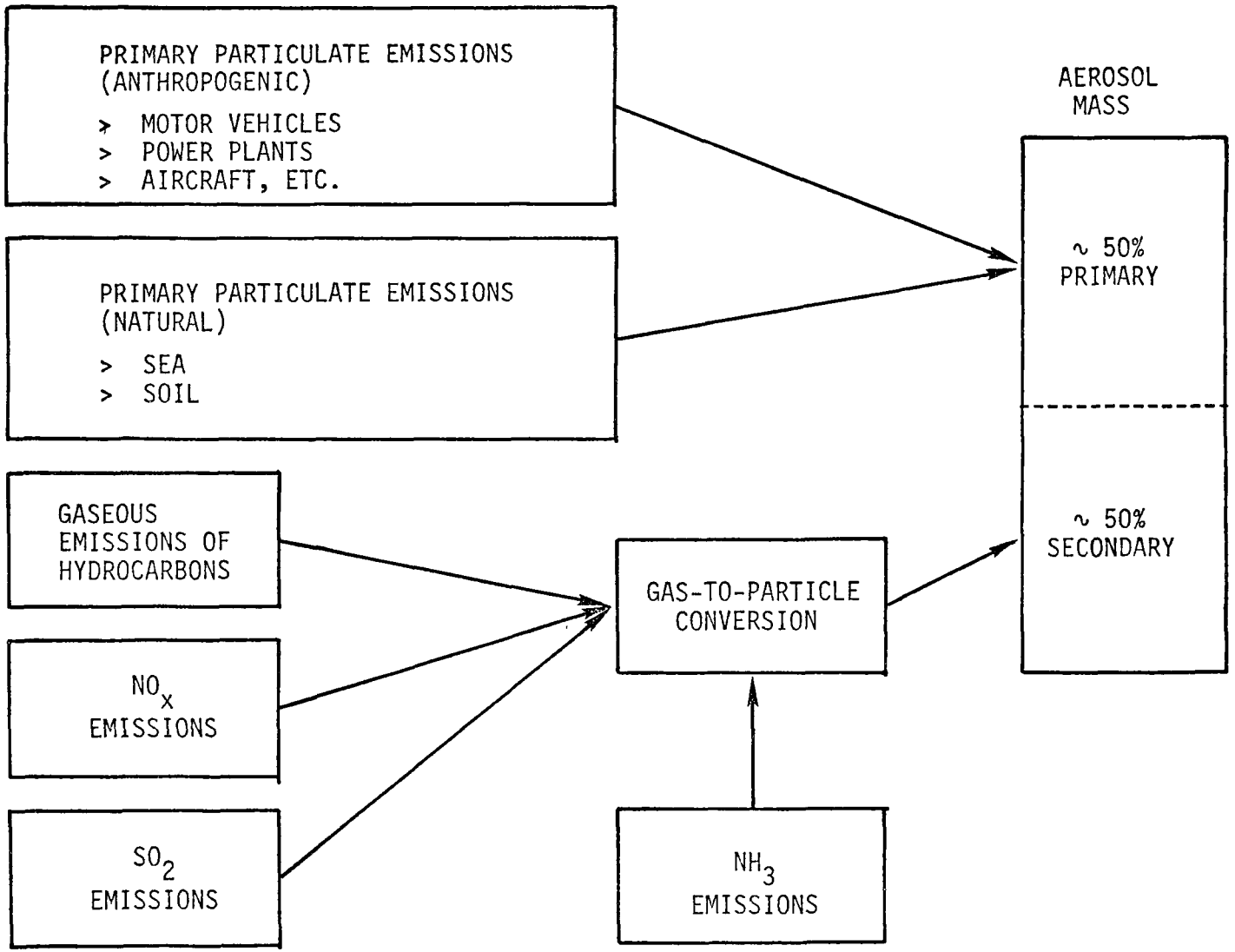

FIGURE 25. DIAGRAM OF THE RELATIONSHIP OF THE EMISSIONS INVENTORY TO THE AEROSOL MASS

Table 26

SOURCES OF DATA FOR AN AEROSOL EMISSIONS INVENTORY

Emission Source	Chemical	Size Distribution
Motor Vehicles	Miller et al. (1972) Gangley and Springer (1974) Hirschler et al. (1957) Cahill and Feeney (1974) Gatz (1974)	Whitby et al. (1969) Gartrell et al. (1974) Gangley and Springer (1974) Cahill and Feeney (1974) Ter Haar (1972) Ter Haar and Stephens (1971) White et al. (1973)
Power plants	Miller et al. (1972) Gatz (1974)	
Sea	Miller et al. (1972)	Gartrell et al. (1974) Woodcock (1953)
Soil	Gatz (1974) Miller et al. (1972)	Gartrell et al. (1974)

such inventories do not provide separate emissions data for individual hydrocarbons. The California Department of Transportation is currently compiling more extensive emissions inventories, and the EPA is sponsoring an inventory that includes differentiation by hydrocarbon type.

The spatial and temporal distributions of water vapor are also important factors in photochemical aerosol growth. During the summers of 1972 and 1973, the California Air Resources Board took three-dimensional measurements of temperature and relative humidity in the Los Angeles basin; these data are available for determining the distribution of water vapor in the basin.

B. THE BASIC EQUATIONS OF AN AEROSOL MODEL

To develop the general equation governing the dynamics of the aerosol in photochemical smog, we assume that the aerosol is composed of liquid droplets of composition (c_1, c_2, ..., c_K) (moles/volume) of the K species present in the aerosol. We then define $n(c_1,c_2,\ldots,c_K,\underset{\sim}{r},t)dc_1\ldots dc_K$ as the numbers of particles per unit volume of atmosphere at location $\underset{\sim}{r}$ and time t containing between c_i and $c_i + dc_i$ moles of species i, i = 1, 2, ..., K. We can refer to n as the <u>number density distribution function</u>. The total particle number density (cm^{-3}) at location $\underset{\sim}{r}$ at time t is

$$N_\infty(\underset{\sim}{r},t) = \int_0^\infty \cdots \int_0^\infty n(c_1,\ldots,c_K,\underset{\sim}{r},t)\, dc_1\ldots dc_K \quad . \tag{54}$$

It is convenient to introduce the particle volume v into the number density distribution function. Since the volume of a particle can be expressed in terms of the molar volumes, $\tilde{v}_i$, i = 1, 2, ..., K, and the species concentrations by

$$v = \sum_{i=1}^{K} c_i \tilde{v}_i \quad , \tag{55}$$

the particle volume v can replace one of the concentrations as an independent variable of n; that is, $n = n(c_1,\ldots,c_{K-1},v,\underset{\sim}{r},t)$.

If only the distribution of particles by volume is of interest, we can define $n_0(v,\underset{\sim}{r},t)dv$ as the number of particles per unit volume of atmosphere of volume v to v + dv at location $\underset{\sim}{r}$ at time t. The distribution function n_0 is related to n by

$$n_0(v,\underset{\sim}{r},t) = \int_0^\infty \cdots \int_0^\infty n(c_1,\ldots,c_{K-1},v,\underset{\sim}{r},t)\, dc_1 \ldots dc_{K-1} \quad . \qquad (56)$$

The total aerosol volume per unit volume of atmosphere ($\mu m^3\ cm^{-3}$) at location $\underset{\sim}{r}$ and time t is given by

$$V_\infty(\underset{\sim}{r},t) = \int_0^\infty v n_0(v,\underset{\sim}{r},t)\, dv \quad . \qquad (57)$$

Chu and Seinfeld (1975) derived the general equation governing $n(c_1,\ldots,c_{K-1},v,\underset{\sim}{r},t)$. This equation includes the effects of advection, heterogeneous condensation, coagulation, Brownian and turbulent diffusion, sedimentation, homogeneous nucleation, and heterogeneous chemical reaction. In deriving the equation, one must consider the processes that influence the total derivative of n in a unit volume of atmosphere. In particular, the total derivative of n is

$$\frac{Dn}{Dt} = \text{rate of homogeneous nucleation} + \text{rate of coagulation} + \text{rate of washout} + \text{rate of rainout} + \text{rate of Brownian diffusion.} \qquad (58)$$

Thus, the total derivative is equal to the net rate of all processes that serve to introduce or remove particles from a unit volume of atmosphere.* The total derivative of n can be expressed as

---

* Particle losses by impaction on surfaces and particle introduction from sources are accounted for in the boundary conditions on the equation for n.

$$\frac{Dn}{Dt} = \frac{\partial n}{\partial t} + \sum_{i=1}^{K-1} \frac{\partial}{\partial c_i}\left(\frac{\partial c_i}{\partial t} n\right) + \frac{\partial}{\partial v}\left(\frac{\partial v}{\partial t} n\right) + \sum_{i=1}^{3} \frac{\partial}{\partial r_i}\left(\frac{\partial r_i}{\partial t} n\right) \quad , \tag{59}$$

where

$\partial c_i/\partial t$ = rate of change of the concentration of species i in a particle. Changes in c_i will occur as a result of heterogeneous condensation and chemical reaction. We can represent these two rates by $I_i(c_1,\ldots,c_{K-1},\eta_i,v)$ and $R_i(c_1,\ldots,c_{K-1},v)$, respectively, where η_i is the gas phase concentration of species i.

$\partial v/\partial t$ = rate of change of the volume of a particle. Changes in v will occur as a result of heterogeneous condensation and chemical reaction. We can represent these two rates by $I_0(c_1,\ldots,c_{K-1},\eta_1,\ldots,\eta_L,v)$ and $R_0(c_1\ldots,c_{K-1},v)$, respectively.

$\partial r_i/\partial t$ = rate of change of the ith coordinate location of a particle due to advection. Thus, $\partial r_i/\partial t = u_i$, the ith component of the wind velocity. Note that $\partial r_3/\partial t$ may differ from u_3 because of sedimentation. If the settling velocity of a particle is $-u_s$, then $\partial r_3/\partial t = u_3 - u_s$. Henceforth, we consider u_3 to be the <u>net</u> vertical velocity.

Combining Eqs. (83) and (84), we can write

$$\frac{\partial n}{\partial t} + \sum_{i=1}^{K-1} \frac{\partial}{\partial c_i}\left[(I_i + R_i)n\right] + \frac{\partial}{\partial v}\left[(I_0 + R_0)n\right] + \sum_{i=1}^{3} \frac{\partial}{\partial r_i}(u_i n) \tag{60}$$

$$= S_{\substack{\text{homogeneous}\\ \text{nucleation}}} + S_{\text{coagulation}} + S_{\text{washout}} + S_{\text{rainout}} + S_{\substack{\text{Brownian}\\ \text{diffusion}}} \quad ,$$

where each S on the right-hand side represents the rate of change of n $[(\ell/\text{mole})^{K-1}\ \mu m^{-3}\ cm^{-3}\ sec^{-1}]$ as a result of the particular process.

The rate of homogeneous nucleation can be expressed as $S_h(c_1,\ldots,c_K,n_1,\ldots,n_L,v)$. We discussed the computation of this term in Chapter II. The rate of change of n due to coagulation is

$$S_{coag} = \frac{1}{2^K}\int_0^v \int_0^{c_1} \cdots \int_0^{c_{K-1}} \beta(v-\tilde{v},\tilde{v})\ n(c_1-\tilde{c}_1,\ldots c_{K-1}-\tilde{c}_{K-1},v-\tilde{v},\underset{\sim}{r},t)$$

$$\cdot\ n(\tilde{c}_1,\ldots,\tilde{c}_{K-1},\tilde{v},\underset{\sim}{r},t)\ d\tilde{c}_1\ldots d\tilde{c}_{K-1}\ d\tilde{v}$$

$$-\int_0^\infty \cdots \int_0^\infty \beta(v,\tilde{v})\ n(c_1,\ldots,c_{K-1},v,\underset{\sim}{r},t)$$

$$\cdot\ n(\tilde{c}_1,\ldots,\tilde{c}_{K-1},\tilde{v},\underset{\sim}{r},t)\ d\tilde{c}_1\ldots d\tilde{c}_{K-1}\ d\tilde{v} \qquad (61)$$

An expression for the rate of change of the number density distribution function due to washout can be developed by analogy to that for coagulation:

$$S_{washout} = -\int_0^\infty \cdots \int_0^\infty \gamma(v,v_r)\ n(c_1,\ldots,c_{K-1},v,\underset{\sim}{r},t)\ g_r(v_r,\underset{\sim}{r},t)\ dc_1\ldots dc_{K-1}\ dv_r \qquad (62)$$

where $\gamma(v,v_r)$ is a collision frequency factor equal to $(3/4\pi)^{2/3}\ \pi(v^{2/3} + v_r^{2/3})\ q_s(v_r)\ E_r(v,v_r)$ in the notation of Chapter II, and $g_p(v,\underset{\sim}{r},t)$ is the number density distribution function for raindrops at location $\underset{\sim}{r}$ and time t. Thus, the total number density of raindrops at $\underset{\sim}{r}$ at time t is given by

$$N_p(\underset{\sim}{r},t) = \int_0^\infty g_p(v,\underset{\sim}{r},t)\, dv \tag{63}$$

$S_{rainout}$ is a complicated function of particle size, composition, water vapor concentration, and turbulence within the cloud. Because this process is unimportant in the atmospheric layer closest to the ground for photochemical aerosols, we do not consider it further here.

Finally, the rate of change of n by Brownian diffusion is

$$S_{\substack{\text{Brownian}\\ \text{diffusion}}} = D(v) \sum_{i=1}^{3} \frac{\partial^2 n}{\partial r_i^2} \quad , \tag{64}$$

where D(v) is the Brownian diffusivity, a function only of particle size.

Equation (60), with Eqs. (61), (62), and (64), represents the complete conservation equation for the aerosol number density distribution function in a fluid. When the fluid is turbulent, the velocities in Eq. (60) contain random components. In addition, the gas concentrations $\eta_1, \ldots, \eta_L$ are random functions in a turbulent field. Consequently, n is itself a random function. In developing the conservation equation for n in a turbulent flow field, we follow the usual procedure of decomposing the wind velocities into mean and random components, $\overline{u}_i + u_i'$. Similarly, the gas phase concentrations and the number density distribution function can be expressed as the sum of mean and random components, $\eta_i = \overline{\eta}_i + \eta_i'$ and $n = \overline{n} + n'$. Because I_0 and I_i depend, in general, on the η_i, these two functions must be expressed as $I_0 = \overline{I}_0 + I_0'$ and $I_i = \overline{I}_i + I_i'$. Finally, we must also write $g_p = \overline{g}_p + g_p'$.

We wish to obtain an equation governing the mean value of the number density distribution function, $\overline{n}$, from Eq. (60). The desired equation can be obtained by substituting $u_i = \overline{u}_i + u_i'$, $n = \overline{n} + n'$, $g_p = \overline{g}_p + g_p'$, $I_0 = \overline{I}_0 + I_0'$, and $I_i = \overline{I}_i + I_i'$ into Eqs. (60) through (63) and then taking the mean value of the resulting equation. During this operation, a number of new dependent variables emerge that represent mean values of the product

of two fluctuating quantities: $\overline{u_i'n'}$, $\overline{I_0'n'}$, $\overline{I_i'n'}$, $\overline{n'n'}$, and $\overline{n'g_p'}$. The first of these variables is simply the turbulent flux of the number density distribution and can be expressed in terms of a turbulent eddy diffusivity, K_{ii}, as

$$\overline{u_i'n'} = -K_{ii} \frac{\partial \overline{n}}{\partial r_i} \quad . \tag{65}$$

There is virtually no theory available for treating the remaining second-order variables above. For example, $\overline{I_0'n'}$ represents the turbulent contribution to the change of $\overline{n}$ by heterogeneous condensation. We do not expect any of these second-order terms to be important in urban-scale aerosol simulation.

Thus, the final general dynamic equation governing the mean number density distribution function in the atmosphere is

$$\frac{\partial \overline{n}}{\partial t} + \sum_{i=1}^{3} \frac{\partial}{\partial r_i} (\overline{u}_i \overline{n}) + \sum_{i=1}^{K-1} \frac{\partial}{\partial c_i} \left[(\overline{I}_i + R_i)\overline{n}\right] + \frac{\partial}{\partial v} \left[(\overline{I}_0 + R_0)\overline{n}\right]$$

$$= \sum_{i=1}^{3} \frac{\partial}{\partial r_i} \left\{\left[K_{ii} + D(v)\right] \frac{\partial \overline{n}}{\partial r_i}\right\} + \overline{S}_h$$

$$+ \frac{1}{2^K} \int_0^v \int_0^{c_1} \cdots \int_0^{c_{K-1}} \beta(v-\tilde{v},\tilde{v})\ \overline{n}(c_1-\tilde{c}_1,\ldots,c_{K-1}-\tilde{c}_{K-1},v-\tilde{v},\underset{\sim}{r},t)$$

$$\cdot\ \overline{n}(\tilde{c}_1,\ldots,\tilde{c}_{K-1},\tilde{v},\underset{\sim}{r},t)\ d\tilde{c}_1 \ldots d\tilde{c}_{K-1}\ d\tilde{v}$$

$$- \int_0^\infty \cdots \int_0^\infty \beta(v,\tilde{v})\ \overline{n}(c_1\ldots,c_{K-1},v,\underset{\sim}{r},t)\ \overline{n}(\tilde{c}_1,\ldots,\tilde{c}_{K-1},\tilde{v},\underset{\sim}{r},t)\ d\tilde{c}_1 \ldots d\tilde{c}_{K-1}\ d\tilde{v}$$

$$- \int_0^\infty \cdots \int_0^\infty \gamma(v,\tilde{v})\ \overline{n}(c_1,\ldots,c_{K-1},v,\underset{\sim}{r},t)\ \overline{g}_r(\tilde{v},\underset{\sim}{r},t)\ d\tilde{v}\ dc_1 \ldots dc_{K-1} \quad .$$

C. APPLICATION OF THE GENERAL EQUATION TO PHOTOCHEMICAL AEROSOLS

With the appropriate input functions, Eq. (66) constitutes a general model capable of describing the dynamic behavior of urban aerosols. On the basis of the discussion in Chapter II, however, certain terms in Eq. (66) can be neglected when considering photochemical aerosols. We are interested primarily in the evolution of photochemical aerosols in the submicron size range over spatial and temporal scales comparable to those of the SAI gas phase photochemical pollutant model. The principal conclusions of Chapter II relative to Eq. (66) are the following:

> Brownian diffusion can be neglected relative to turbulent diffusion.

> Homogeneous nucleation is negligible compared with heterogeneous condensation.

> Sedimentation is important only for particles larger than 1 μm in diameter and can be neglected here.

> Coagulation is important in shaping the size distribution near sources. Turbulent coagulation and coagulation by differential sedimentation may be important for particles larger than 1 μm in diameter. In the 0.1 μm $\leq D_p \leq$ 1 μm range, however, coagulation can be neglected in urban-scale models.

> Washout is an infrequent phenomenon in the region of interest and can be neglected (if there was no rainfall during the time periods over which the model is exercised).

Thus, Eq. (66) becomes

$$\frac{\partial \bar{n}}{\partial t} + \sum_{i=1}^{3} \frac{\partial}{\partial r_i} (\bar{u}_i \bar{n}) + \sum_{i=1}^{K-1} \frac{\partial}{\partial c_i} \left[(\bar{I}_i + R_i)\bar{n} \right] + \frac{\partial}{\partial v} \left[(\bar{I}_0 + R_0)\bar{n} \right]$$

$$= \sum_{i=1}^{3} \frac{\partial}{\partial r_i} \left(K_{ii} \frac{\partial \bar{n}}{\partial r_i} \right) \quad . \tag{67}$$

Table 27 summarizes the significance of each term in Eq. (67).

Although most of the desired information concerning photochemical aerosols is embodied in the function $\bar{n}$, the effort involved in computing $\bar{n}$ may not be justified in view of the data avilable for validation. Routine monitoring of the size and chemical composition distribution of an urban aerosol is not generally possible. On one hand, optical analyzers (Charlson, 1969) and electrostatic devices (Whitby et al., 1972) measure the number of particles in a given size range without regard to composition. On the other hand, current methods of measuring chemical composition do not differentiate particles by sizes. In addition, the objectives of an aerosol model may not require the level of detail inherent in $\bar{n}$. For example, the prediction of visibility degradation requires only the total aerosol volume concentration in the size range 0.1 to 1.0 μm diameter. Therefore, in this section, we develop several models for urban aerosols, each involving a different degree of complexity. The models are most easily characterized by the function chosen to describe the aerosol population (see Table 28).

The first entry of Table 28 is the most general and detailed model, that based on computing $\bar{n}(c_1,\ldots,c_{K-1},v,\underset{\sim}{r},t)$ by Eq. (67). The equations that serve as the basis for computing the other functions in Table 28 are developed in the sections that follow.

1. Mean Number Density Distribution Function

In this subsection, we develop the general dynamic equation governing $\bar{n}_0(v,\underset{\sim}{r},t)$, the mean number density distribution function for particle size. Integrating Eq. (67) over all compositions, we obtain

$$\frac{\partial \bar{n}_0}{\partial t} + \sum_{i=1}^{3} \frac{\partial}{\partial r_i} (\bar{u}_i \bar{n}_0) + \int_0^\infty \cdots \int_0^\infty \sum_{i=1}^{K-1} \frac{\partial}{\partial c_i} \left[(\bar{I}_i + R_i)\bar{n} \right] dc_1 \ldots dc_{K-1}$$

$$+ \int_0^\infty \cdots \int_0^\infty \frac{\partial}{\partial v} \left[(\bar{I}_0 + R_0)\bar{n} \right] dc_1 \ldots dc_{K-1} = \sum_{i=1}^{3} \frac{\partial}{\partial r_i} \left(K_{ii} \frac{\partial \bar{n}_0}{\partial r_i} \right) \quad . \qquad (68)$$

Table 27

SIGNIFICANCE OF THE TERMS IN THE GENERAL DYNAMIC EQUATION [Eq. (67)]

Term	Comments
$\frac{\partial \bar{n}}{\partial t}$	Rate of accumulation of $\bar{n}$ at location $\underset{\sim}{r}$ at time t $\left[(\ell/\text{mole})^{K-1}\ \mu m^{-3}\ cm^{-3}\ sec^{-1}\right]$.
$\sum_{i=1}^{3} \frac{\partial}{\partial r_i} (\bar{u}_i \bar{n})$	Advection of $\bar{n}$. This term affects all particles equally (having neglected sedimentation) but drops out of the equation if an air parcel moving with the mean flow is considered.
$\sum_{i=1}^{K-1} \frac{\partial}{\partial c_i} \left[(\bar{I}_i + R_i)\bar{n}\right]$	Rate of change of the chemical composition of a particle resulting from heterogeneous condensation and chemical reaction.
$\frac{\partial}{\partial v} \left[(\bar{I}_0 + R_0)\bar{n}\right]$	Rate of change of the volume of a particle resulting from heterogeneous condensation and chemical reaction. This is the dominant volume growth term for photochemical aerosols.
$\sum_{i=1}^{3} \frac{\partial}{\partial r_i} \left(K_{ii} \frac{\partial \bar{n}}{\partial r_i}\right)$	Rate of change of $\bar{n}$ due to turbulent diffusion. This term affects all particles equally.

Table 28

LEVELS OF DETAIL IN THE REPRESENTATION OF AN URBAN AEROSOL POPULATION

Term Describing the Aerosol Population	Comments
$\bar{n}(c_1,\ldots,c_{K-1},v,\underset{\sim}{r},t)$	Mean number density distribution as a function of particle chemical composition, size, location, and time. The most detailed representation possible. Governed by Eq. (67).
$\bar{n}_0(v,\underset{\sim}{r},t)$	Mean number density distribution as a function of particle size, location, and time. Chemical composition not accounted for explicitly. Governed by Eq. (68).
$\bar{N}_\infty(\underset{\sim}{r},t)$	Total mean number density as a function of location and time. Governed by Eq. (75).
$\bar{V}_\infty(\underset{\sim}{r},t)$	Total mean aerosol volume per unit volume of gas as a function of location and time. Within the size range 0.1 μm to 1.0 μm diameter, this quantity can be related directly to the light-scattering coefficient and, hence, to visibility reduction. Governed by Eq. (76).

The integrand of the third term on the left-hand side represents the rate of change of $\bar{n}$ due to changes in the species concentration within a particle. These composition changes do not affect $\bar{n}_0$, and this term can be shown to equal zero.

The fourth term on the left-hand side of Eq. (68) represents the rate of change of $\bar{n}_0$ due to changes in the particle volume by heterogeneous condensation and chemical reaction. We recall that $\bar{I}_0 = \bar{I}_0(c_1,\ldots,c_{K-1},v,\bar{n}_1,\ldots,\bar{n}_L)$ and $R_0 = R_0(c_1,\ldots c_{K-1},v)$. Thus, the rate of change of particle volume by heterogeneous condensation depends on the concentrations of the species in the particle, as well as on those of the gaseous condensing species. Also, the rate of change of particle volume due to heterogeneous chemical reaction depends on the species concentrations in the particle. If we define

$$\tilde{I}_0(v,\bar{n}_1,\ldots\bar{n}_K,\underset{\sim}{r},t) = \frac{\int_0^\infty\cdots\int_0^\infty \bar{I}_0(c_1,\ldots,c_{K-1},v,\bar{n}_1,\ldots,\bar{n}_K)\bar{n}\,dc_1\ldots dc_{K-1}}{\bar{n}_0(v,\underset{\sim}{r},t)} \tag{69}$$

and

$$\tilde{R}_0(v,\underset{\sim}{r},t) = \frac{\int_0^\infty\cdots\int_0^\infty R_0(c_1,\ldots,c_{K-1},v)\bar{n}\,dc_1\ldots dc_{K-1}}{\bar{n}_0(v,\underset{\sim}{r},t)} \quad , \tag{70}$$

we can express Eq. (68) as

$$\frac{\partial\bar{n}_0}{\partial t} + \sum_{i=1}^{3}\frac{\partial}{\partial r_i}(\bar{u}_i\bar{n}_0) + \frac{\partial}{\partial v}\left[(\tilde{I}_0 + \tilde{R}_0)\bar{n}_0\right] = \sum_{i=1}^{3}\frac{\partial}{\partial r_i}\left(K_{ii}\frac{\partial\bar{n}_0}{\partial r_i}\right) \quad . \tag{71}$$

The sum $\tilde{I}_0 + \tilde{R}_0$ can be interpreted as the rate of change of the total particle volume due to heterogeneous condensation and chemical reaction; that is,

$$\frac{dv}{dt} = \tilde{I}_0 + \tilde{R}_0 \quad . \tag{72}$$

To compute $\tilde{I}_0$ and $\tilde{R}_0$ using Eqs. (69) and (70), we must know $\bar{n}$ and thus the detailed chemical composition distribution of the aerosol. Clearly, this calculation should be avoided if possible in using Eq. (71). It is desirable to use a growth relation that can be expressed only in terms of the particle volume and the concentrations of the gaseous condensing species. As discussed in Chapter II, Heisler and Friedlander (1974) developed empirical growth relations of this type. Because the changing chemical compositions of the particles are not accounted for, these growth relations are not capable of predicting an equilibrium particle size corresponding to the initial particle composition and the gas phase concentration. However, if the conditions of application of the model are similar to those of the experiments from which the growth relations were determined, the use of these relationships in atmospheric applications should be justified. If we represent the empirical growth law as

$$\frac{dv}{dt} = I_0^e(v,\bar{n}_1,\ldots,\bar{n}_L) \quad , \tag{73}$$

then Eq. (71) becomes

$$\frac{\partial \bar{n}_0}{\partial t} + \sum_{i=1}^{3} \frac{\partial}{\partial r_i} (\bar{u}_i \bar{n}_0) + \frac{\partial}{\partial v} \left[I_0^e \, \bar{n}_0 \right] = \sum_{i=1}^{3} \frac{\partial}{\partial r_i} \left(K_{ii} \frac{\partial \bar{n}_0}{\partial r_i} \right) \quad . \tag{74}$$

2. Total Mean Number Density

An equation governing the total mean number density $N_\infty(\underset{\sim}{r},t)$ can be obtained by integrating Eq. (71) over all volumes. The result is

$$\frac{\partial N_\infty}{\partial t} + \sum_{i=1}^{3} \frac{\partial}{\partial r_i} (\bar{u}_i N_\infty) = \sum_{i=1}^{3} \frac{\partial}{\partial r_i} \left(K_{ii} \frac{\partial N_\infty}{\partial r_i} \right) \quad . \tag{75}$$

We note that heterogeneous condensation does not affect the total number of particles; it affects only their size and composition distribution.

3. Total Mean Aerosol Volume

Recalling Eq. (57), we can derive an equation governing the total mean aerosol volume per unit volume of atmosphere $\bar{V}_\infty(\underset{\sim}{r},t)$, by multiplying Eq. (71) by v and then integrating over all v. The result is

$$\frac{\partial \bar{V}_\infty}{\partial t} + \sum_{i=1}^{3} \frac{\partial}{\partial r_i} (\bar{u}_i \bar{V}_\infty) + \int_0^\infty [\tilde{I}_0 + \tilde{R}_0]\bar{n}_0 \, dv = \sum_{i=1}^{3} \frac{\partial}{\partial r_i} \left(K_{ii} \frac{\partial \bar{V}_\infty}{\partial r_i} \right) \quad . \tag{76}$$

If we employ the growth law [Eq. (73)], then Eq. (76) becomes

$$\frac{\partial \bar{V}_\infty}{\partial t} + \sum_{i=1}^{3} \frac{\partial}{\partial r_i} (\bar{u}_i \bar{V}_\infty) + \int_0^\infty I_0^e(v,\bar{n}_1,\ldots,\bar{n}_K)\bar{n}_0 \, dv = \sum_{i=1}^{3} \frac{\partial}{\partial r_i} \left(K_{ii} \frac{\partial \bar{V}_\infty}{\partial r_i} \right) \quad . \tag{77}$$

Since we are most interested in the particle size (diameter) range of 0.1 to 1.0 μm, we would like to replace the integral in Eq. (77) with

$$\int_{v_*}^{v^*} I_0^e(v,\bar{n}_1,\ldots,\bar{n}_K)\bar{n}_0 \, dv \quad ,$$

where v_* and v^* are the volumes corresponding to $D_p \cong 0.1$ μm and 1.0 μm, respectively. To validate this approximation, we can estimate the quantity of material added by condensation in the size range of $v > v^*$. Assuming that $dv/dt \sim D_p$ for diffusional growth, and assuming a Junge distribution for particles above $D_p = 1.0$ μm, that is,

$$\bar{n}_0(v) \sim D_p^{-4} \quad ,$$

then the ratio of the mass converted on particles with $D_p > 1$ μm to the mass converted on particles with $0.1 \leq D_p \leq 1$ μm is

$$\frac{\left(\frac{dm}{dt}\right)v > v^*}{\left(\frac{dm}{dt}\right)v_* \leq v \leq v^*} = \frac{\int_1^\infty D_p^{-3}\, dD_p}{\int_{0.1}^1 D_p^{-3}\, dD_p} \quad ,$$

$$\cong 0.01 \quad .$$

One cannot obtain an equation for V_∞ that involves only V_∞ because of the volume dependence of the heterogeneous condensation growth law (since it is necessary to have $\bar{n}_0$ to compute $\bar{V}_\infty$). Eq. (77) is an alternative to Eq. (74), since $\bar{V}_\infty$ can always be obtained directly from $\bar{n}_0$ by using Eq. (57).

D. ALTERNATIVE FORMS OF AEROSOL MODELS

In this section, we consider certain aerosol model forms based on the functions summarized in Table 28. The mean number density distribution function $\bar{n}(c_1,\ldots,c_{K-1},v,\underset{\sim}{r},t)$ represents a complete description of the aerosol distribution. By reducing the number of variables on which $\bar{n}$ depends, one gains improvements in model simplicity at the cost of less detail in the aerosol distribution. We can distinguish the possible models based on $\bar{n}$ according to the spatial and chemical species dependence on the distribution. We consider the following cases:

> Spatial dependence
- Spatially homogeneous
- Vertically inhomogeneous
- Spatially inhomogeneous

> Species dependence
  - Chemically homogeneous
  - Two component
  - Multicomponent.

Table 29 lists the functional dependences of the nine combinations.

We note that a chemically homogeneous $\bar{n}$ may be different in principle than $\bar{n}_0$. Chemical homogeneity implies that the concentrations of the species in each particle do not vary with particle size, location, or time. Of course, in general, the composition of particles can vary with particle size, location, and time. In the equation governing $\bar{n}_0$ [Eq. (71)], $\bar{n}_0$ depends on the composition distribution through the definitions of $\tilde{I}_0$ and $\tilde{R}_0$. In practice, we have noted that $\tilde{I}_0 + \tilde{R}_0$ would be replaced by an empirical, concentration-independent growth law. Therefore, from the point of view of implementation, a model based on $\bar{n}$ would not differ from a model based on $\bar{n}_0$.

An approximation of the multicomponent nature of a real particle can be obtained by considering each droplet to consist of two species. How these species should be chosen depends upon the needs of the calculation. The following are two possible choices:

(1) c_1 = water
    c_2 = all species except water.
(2) c_1 = condensible species (secondary aerosol)
    c_2 = noncondensible species (primary aerosol).

Chu and Seinfeld (1975) developed an aerosol model based on the assumption of a two-component particle consisting of condensible and noncondensible species. From the point of view of compromising between computational feasibility and representation of as much of the detailed composition of a particle as possible, a model based on a particle of a few components should be considered in future work. As summarized in Table 29, simplifications in the spatial dependence of the aerosol distribution can be achieved.

Table 29

FUNCTIONAL DEPENDENCES OF THE MEAN NUMBER DENSITY DISTRIBUTION FUNCTION

Species Dependence	Spatial Dependence: Spatially Homogeneous	Spatial Dependence: Vertically Inhomogeneous	Spatial Dependence: Spatially Inhomogeneous
Chemically homogeneous	$\bar{n}(v,t)$	$\bar{n}(v,z,t)$	$\bar{n}(v,x,y,z,t)$
Two component	$\bar{n}(c,v,t)$	$\bar{n}(c,v,z,t)$	$\bar{n}(c,v,x,y,z,t)$
Multicomponent	$\bar{n}(c_1,\ldots,c_{K-1},v,t)$	$\bar{n}(c_1,\ldots,c_{K-1},v,z,t)$	$\bar{n}(c_1,\ldots,c_{K-1},v,x,y,z,t)$

There are two alternative forms of dynamic urban air pollution models: (1) models based on the solution of the conservation equations on a fixed grid and (2) those based on the solution of the conservation equations with respect to a moving coordinate frame that follows a surface wind trajectory (see, for example, Seinfeld et al., 1972). As normally applied, trajectory models are based on the solution of the governing conservation equations in a vertical column of air, having a fixed area and a variable height (to accommodate inversion base height changes), that moves through the airshed at the local mean surface wind velocity. Horizontal turbulent mixing across the boundaries of the parcel is neglected, as are the effects of the variations of wind speed and direction with height on the pollutant concentrations in the parcel. Liu and Seinfeld (1974) have delineated the conditions under which such a model is valid. The most serious assumption limiting the validity of the model is the lack of consideration of the changes of wind speed and direction with height, although it appears that for typical conditions in the Los Angeles airshed this assumption may not be seriously in error.

Grid models generally require more computer storage than trajectory models. However, the two model types cannot be compared with respect to computing time because grid models predict the variables of interest at all locations as a function of time, whereas trajectory models predict the variable only along a given wind path.

The entries in Table 29, based on spatial distribution, correspond, respectively, to a trajectory model with no vertical gradients, a trajectory model with vertical gradients, and a full three-dimensional grid model. One possibility not shown is that of a two-dimensional, vertically homogeneous grid model, for example, $\overline{n}(v,x,y,t)$ in the chemically homogeneous case.

The most important process in governing the size and composition distribution of photochemical aerosols is heterogeneous condensation. As discussed in Chapter III, the principal secondary species in a "typical" photochemical aerosol are sulfate, nitrate, organic carbon, and water. The key problem in developing a mathematical model of urban aerosol dynamics is the representation

of the condensation growth process. The degree of detail required in this representation depends on the degree of detail in the functional dependence of the density function computed in the model. We have already discussed the type of growth relation needed for a model based on $\overline{n}_0(v,\underset{\sim}{r},t)$, for example. Because only a few studies have been carried out to determine condensation growth relations for photochemical aerosols, validated expressions for use in urban models do not now exist. Although we derived a complete growth relation for a spherical droplet consisting of K species in Chapter II, insufficient knowledge of the initial composition and of the composition of the condensing species have prevented the application of this relationship to atmospheric photochemical aerosols. Such calculations will need to be carried out in developing appropriate growth relations. For initial model development, certain simplifications of the treatment of particle growth may be possible by reducing the number of variables on which the growth rate depends.

The rate of condensation depends, in general, on both the aerosol and gas phase compositions. Let us consider first how the gaseous condensing species can be treated in an aerosol model. First, the potential condensing species must be identified, for example, H_2SO_4, HNO_3, NH_3, and organic species. For the aerosol model, these species, say K of them, are the only ones of interest in the calculation. Therefore, it would be necessary in a gas phase model to predict the concentrations of these species as a function of location and time. If the amount of the gaseous species that transfers to the particulate phase is small compared with that which remains in the gas phase, then the gas phase model calculation can be done independently of the aerosol calculation. For the intermediate case in which roughly comparable amounts of the condensible species are in the gas and aerosol phases, it is necessary to account for the condensation loss in the gas phase model, thus coupling the two models.

Let us now consider how the condensation process is treated. The major distinction in describing the condensation process rests on whether the chemical composition of the particle is accounted for. As we have demonstrated

in Chapter II, if the composition of the particle is explicitly included in the condensation growth law, then it is possible, in principle, for the particle to reach an equilibrium size at a particular gas phase concentration. In addition, if the growth is rapid in comparison to the rate of change of the gas phase concentrations, then the particle size and composition will attain a pseudo-steady state at any time when the particle size and composition are in equilibrium with the local gas phase concentration. The "steady state" size and composition can be determined by solving the following equations:

$$\left.\begin{aligned} \frac{dv}{dt} &= 0 \\ \frac{dc_i}{dt} &= 0 \end{aligned}\right\} \quad i = 1, 2, \ldots, K-1 \quad .$$

Applying the steady-state concept, Chu and Seinfeld (1975) found that the time required for particles to attain an equilibrium size and composition was on the order of minutes.

Growth relations based on the assumption that the concentrations of species in the aerosol are independent of time predict that a continuous volume increases as long as the particle is exposed to the gas. Relationships of this type are required if the particle chemical composition is not included in the model.

E. SUMMARY

In this chapter, we have discussed the modeling of photochemical aerosols and the simplifications that can be made in a model. In general, the specification of the spatial and species dependence of the number density distribution function exhibit trade-offs in the description of the aerosol properties and the computational complexity of the model. Modeling the condensational

growth of the aerosol particles represents the major problem in developing the urban aerosol model. If the growth relationship includes the time-dependent composition of the particle, a key simplification in the model can be made if one assumes that the particles reach equilibrium with the gas phase concentration on a time scale that is short compared with the time scale for changes in the gas phase composition. Another assumption that we have used to obtain empirical growth relations is that of the independence of the composition of the aerosol with respect to time. The determination of the utility of each of these approximations awaits development and testing.

V RECOMMENDATIONS FOR FUTURE RESEARCH

In the preceding chapters, we have delineated the current state of understanding of the evolution of photochemical aerosols and have cited areas in which further research is needed. In this chapter, we briefly summarize those areas of research that will provide additional information about the nature of photochemical aerosols and the physical and chemical processes that are responsible for the evolution of the aerosol size distribution. Such information--particularly classification of the important processes involved in gas-to-particle conversion--is essential to the development of dynamic models. We recommend that the following research be undertaken to delineate the form of the growth relationship in the aerosol model:

> Determination of the dependence of the rate of volume growth on particle diameter. In Chapter II, we showed that the rate at which the volume of an aerosol particle increases would be proportional (1) to D_p if the process were diffusion limited, (2) to D_p^2 if the growth were limited by surface-catalyzed reactions, or (3) to D_p^3 if the growth were limited by volume-catalyzed heterogeneous reactions. The rate constants measured for heterogeneous reactions involving SO_2 and NO_x indicate diffusion-limited particle growth. However, further studies, similar to those reported by Heisler and Friedlander (1974), should be undertaken to provide experimental evidence for diffusion-limited or heterogeneous-reaction-limited growth.

> Consideration of the use of growth relationships that treat the composition of the aerosol particles as independent of time. One of the most important questions that must be

addressed in aerosol modeling is whether a growth relationship that predicts unlimited growth of a particle (concentration independent of time) can replace the rigorous theoretical expression that predicts an equilibrium size depending on the gas phase concentration of the species being converted. If the empirically derived growth relationships can be employed in the modeling of urban aerosols, then a significant simplification can be achieved by separating the chemistry from the dynamics of the aerosol growth.

> Investigation of the behavior of the peak in the submicron volume distribution in photochemical aerosols. Evidence from the ACHEX study indicates that the mode in the submicron volume distribution is not consistently centered about 0.25 μm as was previously thought. Since the growth of this mode is apparently a result of gas-to-particle conversion, an investigation of the development of this mode with time can provide information about the process by which mass is converted from the gas phase to the particulate phase. The spatial variation of the mode may reflect the variation of the chemical composition of the aerosol and the atmosphere.

> Examination of the distribution of chemical species in individual aerosol particles. A closer examination of aerosol particles present in photochemical smog should be made to determine whether particles are composed of an agglomeration of chemical species or whether each particles consists of only a limited number of species.

> Investigation of the thermodynamic state of aerosol particles. It is generally assumed that the aerosol particles of interest are droplets rather than solid particles. Further studies should be made to determine the validity of this assumption.

> Examination of the relation of the distribution of sulfate, nitrate, and hydrocarbons to that of the gaseous pollutants. In particular, the distribution of O_3, NH_3, and H_2O gases, which are known to play an important role in the stabilization or transformation of sulfur-, nitrogen-, and carbon-containing compounds should be compared with the distribution of the aerosol species. The availability of the ACHEX data, the data from the Three-Dimensional Gradient Study sponsored by the State of California Air Resources Board, and the improvement of ammonia emissions inventories provide an excellent opportunity to investigate the role of ozone, ammonia, and water vapor in aerosol chemistry.

> Further investigation of the role of liquid water in the evolution of aerosols. During the 1972 ACHEX study, the measurements of water content in aerosols indicated larger quantities of liquid water present than would be expected from the water vapor present in the air. The paths by which water is adsorbed into aerosol particles must be studied, since water represents a substantial fraction of the aerosol mass. In particular, many of the constituents of photochemical aerosols are hygroscopic or deliquescent, and the size of the aerosol particles may be very sensitive to the water vapor concentration in the surrounding air.

> Determination of the important reactions in the homogeneous oxidation of SO_2 and the rate constants of these reactions.

> Determination of the route by which sulfate is incorporated into aerosols. It is possible that H_2SO_4 or $(NH_4)_2SO_4$ can form homogeneously after the diffusion of SO_2 or SO_3 to the particle. The importance of each of these routes and the contribution of catalytic conversion should be determined.

> Determination of the routes by which nitrate is formed in aerosols.

> Determination of the organic compounds present in aerosols
Although organic compounds comprise the largest fraction of photochemical aerosols and although most of these substances are known to result from gas-to-particle conversion, knowledge of the organic compounds present in aerosols and of their spatial and temporal distributions is inadequate. In particular, to determine the paths by which organic compounds are converted to the particulate phase, one must elucidate the distribution of these compounds with respect to size and the chemical species that are present with them.

> Measurement of the vapor pressures of these organic compounds at room temperature.

> Improvement and extension of aerosol emissions inventories to include both primary and secondary emissions. Existing primary particulate emissions inventories specify tailpipe emissions and locally measured size distributions. However, these sources do not represent the sources that will be used as input to the model. Because of the limited spatial resolution of the model (for example, the SAI airshed model uses two mile by two mile grid squares), the size distribution of the primary aerosol emissions defined on the basis of the grid size of the model will differ from that measured at the sources because coagulation, sedimentation, and other physical processes modify the size distribution and number density. The emissions inventory for gaseous pollutants should be extended to include emissions of NH_3 and to differentiate the emissions of individual hydrocarbons, particularly olefins.

> Investigation of the spatial distribution of aerosols and water vapor in the Los Angeles basin. The three-dimensional data obtained by the California Air Resources Board should be studied to establish initial conditions on the vertical distribution of pollutants in the Los Angeles basin. Furthermore, the spatial and temporal distributions of water vapor in the basin can be obtained from these data; they should permit parameterization of the distribution of water vapor in the aerosol model.

> Formulation of a dynamic aerosol model and its integration into the airshed model. Clearly, much information is required before the process by which the distribution of aerosols in the urban atmosphere changes can be fully understood. However, the information required to initialize and verify simple models is now available, and an effort should be made to develop such models, as discussed in Chapter IV.

REFERENCES

Abegg, Handbuch Organic Chem., Vol. 3, No. III, page 144.

Appel, B. R., J. J. Wesolowski, and G. M. Hidy (1974), "Analysis of the Sulfate and Nitrate Data from the Aerosol Characterization Study," AIHL Report No. 166, Air and Industrial Hygiene Laboratory, Berkeley, California.

Badcock, C. C., H. W. Sidebottom, and J. C. Calvert (1971), J. Amer. Chem. Soc., Vol. 93, p. 3115.

Blifford, I. H., Jr., and L. Ringer (1969), "The Size and Number Distribution of Aerosols in the Continental Troposphere," J. Atmos. Sci., Vol. 26, pp. 716-726.

Blumenthal, D. L., et al. (1974), "Three-Dimensional Pollutant Gradient Study--1972-1973 Program," Meteorology Research, Incorporated, Altadena, California.

Boreskov, G. K., and V. V. Illiaronov (1940), J. Phys. Chem., Moscow, Vol. 14, p. 1428.

Bufalini, J. J. (1971), Environ. Sci. and Technol., Vol. 5, p. 685.

Cadle, R. D. (1966), Air Pollution Handbook, Vol. III, P. L. Magill, ed. (McGraw-Hill Book Company, New York).

Cahill, T. A., and P. J. Feeney (1974), "Contribution of Freeway Traffic to Airborne Particulate Matter," U.C. Davis Crocker Nuclear Laboratory, ARB R 502 7406.

Calvert, J. G. (1974), "Modes of Formation of the Salts of Sulfur and Nitrogen in an NO_x-SO_2-Hydrocarbon-Polluted Atmosphere," paper presented at the Conference of Atmospheric Salts and Gases of Sulfur and Nitrogen in Association with Photochemical Oxidant, University of California, Irvine, (January 1974) to appear in a final report to State of California Air Resources Board.

Castleman, A. W., Jr., R. E. Davis, H. R. Munkelwitz, I. N. Tang, and W. P. Wood, paper in "Symposium on Chemical Kinetics Data for the Lower and Upper Atmosphere," Airlie House, Virginia (September 1974).

Castleman, A. W., Jr. (1974), "Nucleation Processes and Aerosol Chemistry," Space Science Rev.

Chamberlain, A. C. (1967), "Radioactive Aerosols and Vapors," Contemporary Phys., Vol. 8, pp. 561-581.

Charlson, R. J. (1969), "Atmospheric Visibility Related to Aerosol Mass Concentration: A Review," Environ. Sci. Technol., Vol. 3, pp. 913-918.

Charlson, R. J. et al. (1969), "Monitoring of Atmospheric Aerosol Parameters with the Integrating Nephelometer," J. Air Poll. Contr. Assoc., Vol. 19, pp. 937-942.

Charlson, R. J., N. C. Ahlquist, and H. Horvath (1968), "On the Generality of Correlation of Atmospheric Aerosol Mass Concentration and Light Scatter," Atmos. Environ., Vol. 2, pp. 455-464.

Chu, K. J., and J. H. Seinfeld (1975), Atmos. Environ. (in press).

Colucci, J. M., C. R. Begeman, and K. Kumler (1969), "Lead Concentrations in Detroit, New York, and Los Angeles Air," J. Air Poll. Contr. Assoc., Vol. 19, p. 255 (April 1969).

Countess, R. F., and J. Heichlen (1973), J. Phys. Chem., Vol. 77, p. 444.

Cox, R. A., and S. A. Penkett (1971), Nature, Vol. 229, p. 486.

Cox, R. A. and S. A. Penkett (1972), "Aerosol Formation from Sulfur Dioxide in the Presence of Ozone and Olefinic Hydrocarbons," J. of the Chemical Society, Faraday Transactions I, Part 9, Vol. 68, p. 1735.

Craig, N. L., A. B. Harlser, and T. Novakov (1974), "Determination of the Chemical States of Sulfur in Ambient Pollution Aerosols by X-ray Photoelectron Spectroscopy," Atmos. Environ., Vol. 8, pp. 15-22.

Dainton, F. S. and K. J. Ivin (1950), Trans. Faraday Soc., Vol. 46, p. 374.

Daubendiek and Calvert (1973), "Photochemical Study Involving SO_2, O_2, SO_3, and O_3," presented at the 165th National Meeting of the American Chemical Society, Dallas, Texas (April, 1973).

Davis, D. D., W. A. Payne, and L. J. Stief (1974), Science, Vol. 179, p. 280.

Davis, D. D. (1974), "Absolute Rate Constants for Elementary Reactions of Atmospheric Importance: Results from the University of Maryland Gas Kinetics Laboratory," Chemistry Department, University of Maryland, College Park, Maryland.

Demerjian, K. L., J. A. Kerr, and J. G. Calvert (1974), Advances in Environmental Sciences and Technology, J. N. Pitts and R. L. Metcalf eds., Vol. 4, pp. 1-262 (John Wiley and Sons, New York).

dePenda, R. G., K. Olzyna, and J. Heidelen (1973), J. Chem. Phys., Vol. 77, p. 438.

Doyle, G. J. (1961), "Self-Nucleation in the Sulfuric Acid-Water System," J. Chem. Phys., Vol. 35, pp. 795-799.

Dreisbach, R. R., ed. (1959), "Physical Properties of Chemical Compounds, II," Adv. in Chem., Vol. 22, pp. 110-217.

Endow, N., G. J. Doyle, and J. L. Jones (1963), "The Nature of Some Model Photochemical Aerosols," JAPCA, Vol. 13, p. 4.

Friedlander, S. K. (1973), "Chemical Element Balances and Identification of Air Pollution Sources," Environ. Sci. Technol., Vol. 7, pp. 235-340.

_____ (1964), "The Similarity Theory of the Particle Size Distribution of the Atmospheric Aerosols," Aerosols, Phys. Chemistry and Appl., K. Spurny, ed., pp. 115-130, Czechoslovak Academy of Science, Prague.

Friend, J. P. (1966), Tellus, Vol. 18, p. 465.

Fuchs, N. A. (1964), Mechanics of Aerosols (Pergamon Press, New York).

Fukuta, N., and L. A. Walter (1970), "Kinetics of Hydrometeor Growth from a Vapor-Spherical Mode," J. Atmos. Sci., Vol. 27, pp. 1160-1172.

Gangley, J. T., and G. S. Springer (1974), Environ. Sci. and Technol., Vol. 8, pp. 340-347.

Gartrell, G., Jr., and S. K. Friedlander (1974), "Relating Particulate Pollution to Sources: The 1972 California Aerosol Characterization Study," submitted for publication.

Garvin, D., and R. F. Hampson (1974), "Chemical Kinetics Data Survey VII: Tables of Rate and Photochemical Data for Modeling of the Stratosphere," NBSIR 74-430, National Bureau of Standards, Washington, D. C.

Gatz, D. P. (1974), "St. Louis Air Pollution: Estimates of Aerosol Source Coefficients and Elemental Emission Rates," Proc. Symposium on Atmos. Diffusion and Air Pollution, Santa Barbara, California, pp. 109-114.

Gerhard, E. R., and H. F. Johnstone (1955), Ind. Eng. Chem., Vol. 47, p. 972.

Gillespie, J., et al. (1950), J. Chem. Soc., p. 2504.

Goetz, A., and R. F. Pueschel (1967), Atmos. Environ., Vol. 1, p. 287.

Gordon, S., and W. A. Niloc (1975), Inter. J. Chemical Kinetics, Symposium No. 7, p. 289.

Groblicki, P. J. and G. J. Nebel (1971), "The Photochemical Formation of Aerosols in Urban Atmospheres," Chemical Reactions in Urban Atmospheres (C.S. Tuesday, ed.), American Elsevier, New York, pp. 241-267.

Grosjean, D. (1975), "The Role of Ozone in the Formation of Organic Aerosols," California Institute of Technology, Pasadena, California, first draft.

Grosjean, D., and S. K. Friedlander (1975), "The Nature and Formation of Secondary Aerosol Organics. I. Cyclic Olefins and Diolefins as Possible Hydrocarbon Precursors," in preparation.

Haagen-Smit, A. J. (1952), Ind. Eng. Chem., Vol. 44, pp. 1342-1346.

Hall, T. C., Jr. (1953), Ph.D. Thesis, University of California, Los Angeles.

Harkins, J., and S. W. Nicksic (1965), "Studies on the Role of Sulfur Dioxide on Visibility Reduction," JAPCA, Vol. 15, No. 5, p. 218.

Hecht, T. A., J. H. Seinfeld, and M. C. Dodge (1974), "Growth Mechanisms for Urban Aerosol Particles," California Institute of Technology, Pasadena, California.

Heisler, S. L. (1975), Ph.D. Thesis, California Institute of Technology, Pasadena, California.

Heisler, S. L., and S. K. Friedlander (1974), "Growth Mechanisms for Urban Aerosol Particles," California Institute of Technology, Pasadena, California.

Hidy, G. M. (1973a), "Theory of Formation and Properties of Photochemical Aerosols," Summer Institute, Battelle Seattle Research Center.

_____ (1973b), "Removal Process of Gaseous and Particulate Pollutants," Chem. of the Lower Atmos., S. I. Rasool, ed. (Plenum Press, New York).

_____ (1972), "Characterization of Aerosols in California (ACHEX)", Interim Report for Phase I, Air Resources Board, State of California.

Hidy, G. M., and C. S. Burton (1974), "Atmospheric Aerosol Formation by Chemical Reactions," Symp. on Chemical Kinetics Data for the Lower and Upper Atmosphere, Warrenton, Virginia (September 16-18).

Hidy, G. M., and J. R. Brock (1970), The Dynamics of Aerocolloidal Systems (Pergamon Press, New York).

Hidy, G. M., and S. K. Friedlander (1971), "The Nature of the Los Angeles Aerosol," Proc. Second IUAPPA Clean Air Congress (Academic Press, New York).

Hidy, G. M., et al. (1975), "Characterization of Aerosols in California (ACHEX)," Final Report, Air Resources Board, State of California.

Hirschler, D. A., L. F. Gilbert, F. W. Lamb, and L. M. Niebylski (1957), Ind. Eng. Chem., Vol. 49. p. 1131.

Ho, W. W. (1975), "Measurement of Liquid Water Content in Atmospheric Aerosols," to be published.

Holworth, G. C. (1959), "Atmospheric Contamination at Remote California Coastal Sites," J. Meteorol., Vol. 16, p. 68 (February 1959).

Husar, R. B., (1971), "Coagulation of Knudsen Aerosols," University of Minnesota

Husar, R. B., K. T. Whitby, and B.Y.H. Liu (1972), "Physical Mechanisms Governing the Dynamics of Los Angeles Smog Aerosol," Aerosols and Atmospheric Chemistry, pp. 271-284 (Academic Press, New York).

International Critical Tables (1928), Vol. IV, p. 464 (McGraw-Hill Book Company, New York).

Jaffee, S., and F. S. Klein (1966), Trans. Faraday Soc., Vol. 62, p. 2150.

Katz, M. and S. B. Gale (1970), "Mechanism of Photooxidation of Sulfur Dioxide in the Atmosphere," Proc. Second IUAPPA Clean Air Congress, Washington, D.C. (December 1970), pp. 336-343 (Academic Press, New York).

Kiang, C. S., D. Stauffer, V. A. Mohnen, J. Bricard, and D. Vigla (1973), "Heteromolecular Nucleation Theory Applied to Gas-to-Particle Conversion," Atmospheric Environment, Vol. 7, p. 1.

Kocmond, W. C., D. B. Kittelson, J. Y. Yang, and K. L. Demerjian (1975), "Study of Aerosol Formation in Photochemical Air Pollution," Calspan Corporation, Buffalo, New York (March 1975).

Lamb, H. (1932), Hydrodynamics, 6th ed. (Cambridge) University Press, pp. 590-597.

Landahl, H. D. (1959), Bull. Math. Biophys., Vol. 12, pp. 43-56.

Langer, G. (1965), "Particle Deposition and Reentrainment from Coniferous Trees, Part II," Kolloid Z., Vol. 204, pp. 119-124.

Langmuir, I., and K. Blodgett (1946), U.S. Army TR 5418.

Levy, A., E. L. Merryman, and W. T. Reid (1970), Environ. Sci. Technol. Vol. 4, p. 653.

Liu, M. K., and J. H. Seinfeld (1974), "A Comparison of the Grid and Trajectory Models of Urban Air Pollution," presented at the Symposium on Atmospheric Diffusion and Air Pollution, Santa Barbara, California (September 9-13).

Ludwig, J. H., G. B. Morgan, and T. B. McMullen (1970), "Trends in Urban Air Quality," Trans. Amer. Geophys. Union, Vol. 51, p. 468 (May 1970).

Lundgren, D. A. (1969), "Atmospheric Aerosol Composition and Concentration as a Function of Particle Size and of Time," presented at the 62nd Annual Meeting, Air Pollution Control Association, New York (June 1969).

McNelis, D. N. (1974), "Aerosol Formation from Gas-Phase Reactions of Ozone and Olefin in the Presence of Sulful Dioxide," National Environmental Research Center, Las Vegas, Nevada.

Meszaros, A. (1969), "Vertical Profile of Large and Giant Particles in the Lower Troposphere," Proc. 7th Intl. Conf. Condensation and Ice Nuclei, Prague-Vienna, pp. 364-368.

Miller, J. M., and R. G. dePena (1971), "The Rate of Sulfate Ion Formation in Water Droplets in Atmospheres with Differential Partial Pressures of SO_2," in Proc. of the Second IUAPPA Clean Air Congress, Washington, D.C. (December 1970), pp. 375-378 (Academic Press, New York).

Miller, M. S., S. K. Friedlander, and G. M. Hidy (1972), "A Chemical Element Balance for the Pasadena Aerosol," in Aerosols and Atmospheric Chemistry, G. M. Hidy, ed., pp. 301-311 (Academic Press, New York).

Mirabel, P. and J. L. Katz (1974), J. Chem. Phys., Vol. 60, p. 1138.

Mulcahy, F. R., J. R. Stephen, and J. C. Ward (1967), J. Phys. Chem., Vol. 71, p. 2124.

O'Brien, R. J., J. R. Holmes, and A. H. Bockian (1975), "Organic Photochemical Aerosol I. Environmental Chamber Experiments," Environ. Sci. Technol. (in press).

Okuda, S., T. N. Rao, and J. G. Calvert (1969), J. Phys. Chem., Vol. 73, p. 4412

Olszyna, K. J., and J. Hircklen (1972), "The Reaction of Ozone with Ammonia," Adv. in Chem., Vol. 113, p. 191.

O'Neal, H. E., and C. Blumstein (1973), Int. J. Chem. Kinet., Vol. 5, p. 397.

Payne, W. A., L. J. Stief, and D. D. Davis (1973), "A Kinetics Study of the Reaction of HO_2 with SO_2 and NO," Journal of the American Chemical Society, Vol. 95, p. 7614.

Penkett, S. A. (1972), Nature Phys. Sci., Vol. 240, p. 75.

Penzhorn et al. (1973), Chemisphere, Vol. 3, p. 111.

Pick (1920), Z. Elektrochem, Vol. 26, p. 182.

Prager, M. J., E. R. Stephens, and W. E. Scott (1960), "Aerosol Formation from Gaseous Air Pollutants," Industrial and Engineering Chemistry, Vol. 52, p. 521.

Quon, J. E., R. P. Siegel, and H. M. Mulburg (1971), "Particle Formation from Photolysis of Sulfur Dioxide in Air," Proc. Second IUAPPA Clean Air Congress, Washington, D.C. (December 1970), pp. 330-335 (Academic Press, New York).

Rao, T. N., S. S. Collier, and J. G. Calvert (1969), J. Phys. Chem., Vol. 73, p. 4412.

Reiss, H. (1950), J. Chem. Phys., Vol. 18, pp. 840-848.

Renzetti, N. A., and G. J. Doyle (1960), Int. J. Air Pollution, Vol. 2, p. 327.

_____ (1959), "The Chemical Nature of the Particulate in Irradiated Automobile Exhaust," J. Air Poll. Contr. Assoc., Vol. 8, pp. 293-296.

Ripperton, L. A., H. E. Jeffries, and O. White (1972), "Formation of Aerosols by Reaction of Ozone with Selected Hydrocarbons," Photochemical Smog and Ozone Reactions, American Chemical Society, Washington, D.C., pp. 219-231.

Roberts, P. T. (1975), Ph.D. Thesis, California Institute of Technology, Pasadena, California.

Roberts, P. T., and S. K. Friedlander (1974), "Conversion of SO_2 to Ambient Particulate Sulfates in the Los Angeles Atmosphere," presented at the Conference on Health Consequences of Environmental Controls: Impact of Mobile Emissions Controls, Durham, North Carolina (April 17-19).

Rosinski, J., and C. T. Nagamoto (1965), "Particle Deposition on and Reentrainment from Coniferous Trees," Part I., Kolloid Z., Vol. 24, pp. 111-119.

Roth, P. M., P.J.W. Roberts, M. K. Liu, S. D. Reynolds, and J. H. Seinfeld (1974), "Mathematical Modeling of Photochemical Air Pollution: II. A Model and Inventory of Pollutant Emissions," Atmos. Environ., Vol. 8, pp. 97-130.

Saffman, P. G., and J. S. Turner (1956), "On the Collision of Drops in Turbulent Clouds," J. Fluid Mech., Vol. 1, pp. 16-30.

Samuels, H. J., et al. (1973), "Visibility, Light Scattering and Mass Concentration of Particulate Matter," Report of the California Tri-City Aerosol Sampling Project, Air Resources Board, State of California.

Schuetzle, D., D. R. Cronn, and A. L. Crittenden (1973), 172nd National ACS Meeting, Symposium on Surface and Colloid Chemistry in Air Pollution Control, Chicago, Illinois (August 27).

Schuck, E. A., G. J. Doyle, and N. Endow (1960), "A Progress Report on the Photochemistry of Polluted Atmospheres," Report No. 31, Air Pollution Foundation, San Marino, California.

Schuck, E. A., and G. J. Doyle (1959), "Photooxidation of Hydrocarbons in Mixtures Containing Oxides of Nitrogen and Sulfur Dioxide," Report No. 29, Air Pollution Foundation, San Marino, California.

Scott, W. D., and P. V. Hobbs (1967), "The Formation of Sulfate in Water Droplets," J. Atmos. Sci., Vol. 24, pp. 54-57.

Seinfeld, J. H., S. D. Reynolds, and P. M. Roth (1972), "Simulation of Urban Air Pollution," Advances in Chemistry Series 113, American Chemical Society, pp. 58-100.

Sidebottom, H. W., et al. (1972), Environ. Sci. and Technol., Vol. 6, p. 72.

_____ (1971), J. Amer. Chem. Soc., Vol. 93, p. 3121.

Slinn, W.G.N., and J. M. Hales (1970), "Thermophoretic Influences," in "Precipitation Scavenging," AEC Symposium Series No. 22, U.S. Atomic Energy Commission, Oak Ridge, Tennessee, pp. 411-424.

Slinn, W.G.N. (1967), "Precipitation Scavenging of Submicron Particles. Part A--Theory," in Proc. USAEC Meteorological Information Meeting, AECL-2797, 527-520, Chalk River Laboratories, Chalk River, Ontario.

Smith, J. P., and P. Urone (1974), Environ. Sci. Technol., Vol. 8, p. 742.

Stauffer, D., V. A. Mohnen, and C. S. Kiang (1973), "Heteromolecular Condensation Theory Applied to Gas-to-Particle Conversion," J. Aerosol Sci., Vol. 4, pp. 461-471.

Stevenson, H.J.R., D. E. Sanderson, and P. O. Altshuller (1965), "Formation of Photochemical Aerosols," Int. J. Air Water Poll., Vol. 9, p. 367.

Task Group on Lung Dynamics (1966), Health Physics, Vol. 12, pp. 173-207.

Ter Haar, G. L. (1972), "Composition, Size, and Control of Automobile Exhaust Particulates," JAPCA, Vol. 22, p. 39.

Ter Haar, G. L., and R. E. Stephens (1971), "The Effects of Automobile Exhaust Particulates on Visibility," paper presented at the 12th Conference on Methods in Air Pollution and Industrial Hygiene Studies, Los Angeles, California (April 1971).

Theilke, J. F., et al. (1972), "Multiwavelength Nephelometer Measurements in Los Angeles Smog Aerosol: II. Correlation with Size Distributions, Volume Concentrations," in Aerosols and Atmospheric Chemistry, G. M. Hidy, ed., pp. 325-332 (Academic Press, New York).

Urone, P., and W. H. Schroeder (1971), Proc. of the Second International Clean Air Congress, H. M. Englund and W. T. Berry, ed., pp. 370-372 (Academic Press. New York).

_____ (1969), "SO_2 in the Atmosphere: A Wealth of Monitoring Data but Few Reaction Rate Studies," Environ. Sci. and Technol., Vol. 3, pp. 436-445.

Urone, P., H. Lutsep, G. M. Noyes, and J. F. Parcher (1971), Proc. of the Second International Clean Air Congress, H. M. Englund and W. T. Berry, eds., pp. 370-72 (Academic Press, New York, New York).

_____ (1968), Environ. Sci. Technol., Vol. 2, p. 611.

U.S. Public Health Service (1968), "Air Quality Data from the National Air Sampling Networks, 1966," APTD 68-9, National Air Pollution Control Administration, Raleigh, North Carolina.

Weickmann, H. (1955), "Recent Measurements of the Vertical Distribution of Aitken Nuclei," in "Artificial Stimulation of Rain," Proc. First Conf. Phys. of Clouds and Precipitation Particles, H. Weickmann and W. S. Smith, eds., pp. 81-88 (Pergamon Press, New York).

Whitby, K. T., R. B. Husar, and B.Y.H. Liu (1972), "The Minnesota Aerosol-Analyzing System Used in the Los Angeles Smog Project," J. Colloids Interface Sci., Vol. 39, pp. 136-164.

Whitby, K. T., R. B. Husar, A. R. McFarland, and M. Tomaides (1969), "Generation and Decay of Small Ions," Particle Laboratory Publication No. 137, Department of Mechanical Engineering, University of Minnesota.

White, W. H., R. B. Husar, and S. K. Friedlander (1973), "A Study of Los Angèles Smog Aerosol Dynamics by Air Trajectory Analyses," presented at the June 1973 Annual Meeting, APCA, Chicago, Illinois.

Wilson, W. E., Jr., and A. Levy (1972), J. Air Poll. Contr. Assoc., Vol. 22, p. 27

_____ (1970), J. Air Poll. Contr. Assoc., Vol. 20, p. 385.

Wilson, W. E., Jr., A. Levy, and D. B. Wimmer (1972), J. Air Poll. Contr. Assoc., Vol. 22, p. 27.

Wilson, W. E., Jr., E. L. Merryman, A. Levy, and H. R. Taliaferro (1971). "Aerosol Formation in Photochemical Smog. I. Effect of Stirring." JAPCA, Vol. 21, No. 3, p. 128.

Wood, W. P., A. W. Castleman, Jr., and I. N. Tang (1974), "Mechanisms of Aerosol Formation for SO_2," Paper 74-153 67th Annual Meeting APCA, Denver, Colorado (June 9-13, 1974).

Woodcock, A. H. (1953), "Salt Nuclei in Marine Air as a Function of Altitude and Wind Force," J. Meteorology, Vol. 10, pp. 362-371.

TECHNICAL REPORT DATA
(Please read Instructions on the reverse before completing)

1. REPORT NO. EPA-600/4-76-016 d	2.	3. RECIPIENT'S ACCESSION NO.
4. TITLE AND SUBTITLE CONTINUED RESEARCH IN MESOSCALE AIR POLLUTION SIMULATION MODELING. VOLUME IV. Examination of the Feasibility of Modeling Photochemical Aerosol Dynamics		5. REPORT DATE May 1976
		6. PERFORMING ORGANIZATION CODE
7. AUTHOR(S) T. N. JERSKEY AND J. H. SEINFELD		8. PERFORMING ORGANIZATION REPORT NO. EF75-26
9. PERFORMING ORGANIZATION NAME AND ADDRESS SYSTEMS APPLICATIONS, INC. 950 NORTHGATE DRIVE SAN RAFAEL, CALIFORNIA 94903		10. PROGRAM ELEMENT NO. 1AA009
		11. CONTRACT/GRANT NO. 68-02-1237
12. SPONSORING AGENCY NAME AND ADDRESS ENVIRONMENTAL SCIENCES RESEARCH LABORATORY OFFICE OF RESEARCH AND DEVELOPMENT U.S. ENVIRONMENTAL PROTECTION AGENCY RESEARCH TRIANGLE PARK, N.C. 27711		13. TYPE OF REPORT AND PERIOD COVERED FINAL REPORT 6/74-6/75
		14. SPONSORING AGENCY CODE EPA-ORD

15. SUPPLEMENTARY NOTES

16. ABSTRACT

A mathematical model of the dynamics of photochemical aerosols should include emissions of primary particulates and gaseous precursors of secondary aerosols, homogeneous nucleation, heterogeneous condensation, heterogeneous chemical reaction, coagulation, advection, diffusion, settling, and deposition on surfaces. This report discusses the theory of each of these processes and assesses the relative importance of each in shaping the volume distribution of photochemical aerosols. The authors conclude that in Los Angeles photochemical smog heterogeneous condensation is the principal mechanism for changes of the volume distribution in the accumulation size range, though homogeneous nucleation can be important under certain conditions for forming very small particles (less than 100 Å diameter). Coagulation must be considered in reshaping the size distribution of emissions and in reducing the number of particles formed by homogeneous nucleation. An in-depth assessment is also presented of the pathways for the formation of aerosol material from the gas phase via homogeneous and heterogeneous chemistry. Finally, the equations governing the evolution of the photochemical aerosol are derived and simplified on the basis of order-of-magnitude calculations of the individual terms, and various equations for different properties of the aerosol are derived and discussed.

17. KEY WORDS AND DOCUMENT ANALYSIS

a. DESCRIPTORS	b. IDENTIFIERS/OPEN ENDED TERMS	c. COSATI Field/Group
*Air Pollution *Mathematical Models *Photochemical Reactions *Aerosols		13B 12A 07E 07D

18. DISTRIBUTION STATEMENT RELEASE TO PUBLIC	19. SECURITY CLASS *(This Report)* UNCLASSIFIED	21. NO. OF PAGES 156
	20. SECURITY CLASS *(This page)* UNCLASSIFIED	22. PRICE

EPA Form 2220-1 (9-73)